HOLOGRAPHIC CORRECTION OF ABERRATED TELESCOPES

by

Geoff Andersen

Thesis submitted for the degree of

Doctor of Philosophy

in

The University of Adelaide

(Department of Physics and Mathematical Physics)

January, 1996

This work contains no material which has been accepted for the award of any other degree or diploma in any university or other tertiary institution and, to the best of my knowledge and belief, contains no material previously published or written by another person, except where due reference has been made in the text.

I give consent to this copy of my thesis, when deposited in the University Library, being available for loan and photocopying.

SIGNED:

DATE: 31/1/96

Supervisors: Prof. J. Munch and Dr. P. Veitch

I never cared much for moonlit skies,
I never wink back at fireflies,
But now that the stars are in your eyes,
I'm beginning to see the light.

I never went in for afterglow,
Or candlelight on the mistletoe,
But now when you turn the lamp down low,
I'm beginning to see the light.

Used to ramble thru the park,
Shadow boxing in the dark,
Then you came and caused a spark,
That's a four alarm fire now.

I never made love by lantern shine,
I never saw rainbows in my wine,
But now that your lips are touching mine,
I'm beginning to see the light.

Duke Ellington

Acknowledgements

Throughout the course of my research I have come to owe a debt of thanks to many people who have provided advice (some helpful, some unwarranted) and generally helped me when things got difficult.

Firstly, my family, and especially my parents, who ensured I had at least one proper meal a week and proved to be a limitless source of encouragement and support.

To my two supervisors Jepser Munch and Peter Veitch. Jesper took a chance in taking me on for this project. He has pushed me into constantly improving my results, and I believe that this shows in the success of this work. He is a dedicated supervisor and an inexhaustible supply of advice and new ideas. Peter, who became my co-supervisor late in my studies, was invaluable and could always be relied on to give straight answers and constructive criticism whenever I needed it.

To everyone in the Lab, especially Peter Foster, Blair Middlemiss and Petar Atanackovic and lastly to the ARC for showing imagination in providing this novel project with a large grant.

Abstract

Astronomical imaging and lidar studies require large, high quality telescopes for maximum image resolution and light gathering ability. One of the major costs involved in producing such telescopes is the fabrication of the perfect primary optic (most often a mirror) and correcting for any changes in shape which may occur over a period of time. Holographic correction of poor quality mirrors is a technology which attempts to reduce these costs.

Throughout the course of this thesis I will be detailing the work I have carried out into the holographic correction of aberrated telescopes. The basic concept involves recording a demagnified image hologram of the mirror surface and then using this hologram as an optical element to remove the wavefront distortions introduced by the aberrated mirror on focused starlight. In this way, diffraction limited performance can be achieved with a poor-quality primary, over a limited bandwidth.

One of the major difficulties, up until now, has been that the methods of recording these holograms have required a distant light source, resulting in a telescope which is very large. In order to reduce costs for both ground and space based applications, a compact design is needed. This research has been aimed at producing an inexpensive, compact telescope which uses commonplace optical components with a view to simplicity and scalability. Included are theoretical and experimental results which demonstrate near-diffraction limited performance from a telescope constructed from a large diameter, heavily aberrated, spherical primary. Also included in this report is a discussion of alternative designs and new possibilities for this technology.

List of Symbols

Throughout this thesis, several symbols will be used consistently to signify specific physical quantities. For the readers convenience, these are listed below. note that in most optical texts a particular sign convention is adopted to indicate ray direction and object/image position. In this thesis, the ray directions and the position of the object and image planes will be largely self-evident, so all of the quantities will take their absolute values, with direction stated explicitly if necessary.

D ... Diameter/Aperture ($= 2\rho$)

f ... Focal length

F ... F-number ($= f/D$)

n ... Refractive index

R ... Radius of curvature

W ... Wavefront error

x ... Off-axis object distance (perpendicular to the optical axis)

x' ... Off-axis image distance (perpendicular to the optical axis)

y ... On-axis object distance (along the optical axis)

y' ... On-axis image distance (along the optical axis)

z ... Sag (depth of conic surface along the optical axis)

η_e ... Diffraction efficiency

λ ... Wavelength

λ' ... Reconstruction wavelength

ρ ... Semi-diameter (as a subscript denotes the edge or marginal ray)

Contents

Errata

1. Page 17, Line 5: For " ... which is the object wave modulated by fringes with a spatial frequency of $\sin\theta/\lambda$." read "which gives a sinusoidal grating with a spatial frequency of $\lambda/2\sin(\theta/2)$."

2. Page 59, Line 1: For $f = 0.6$mm read $f = 0.6$m.

3. Page 78, Caption for Figure 3.20 (a): Text should read "Lenses L1 & L2 are chromatic doublets and L3 is the simple lens...".

4. Page 106, Line 21: For 0.3m read 0.12m.

5. Page 118, Line 15: Text should read "... recording angle of 2θ between the beams."

6. Page 156, Caption should read: "Off-axis correction of a refractor. The dotted rays show the recording of the hologram, H, using an off-axis beacon located to the left of the aberrated lens. The solid rays show the reconstruction and correction of the aberrations by an object wave from infinity, imaged at plane I. A cylindrical lens (c.l.) is used to compensate for the astigmatism. Secondary lenses I_1 and I_2 produce identical, accurately superimposed images of the primary lens at H.

7. Page 162-167: Where Figures 1 to 8 are mentioned in the text, these correspond to Figures F8 to F15 on the subsequent pages.

Chapter 1

Introduction

1.1 Introduction

This thesis describes research conducted into the holographic correction of aberrations in large optical elements. This chapter will outline the motivation for the research as well as provide a brief summary of the field of precision imaging and a discussion of the previous work carried out into holographic aberration correction.

1.2 Background

Large conic mirrors are often required for lidar and astronomy. The larger the mirror, the better the instrument's light gathering capability and resolution.

Lidar is an acronym for Light Detection and Ranging. Direct detection lidar is a method of measuring the range of an object by using the time-in-flight analysis of a reflected light signal. Heterodyne detection can be used to measure velocity of distant objects by studying the Doppler frequency shift in the return signal. Lidar is often used for atmospheric studies in order to measure the wind velocity profile in a column forward of the detector [38, 25]. Due to the low reflectivity of the atmosphere at visible wavelengths the return signal is typically very weak, so a large mirror area is required to gather as much light as possible. For direct detection studies, the primary receiver must be of sufficient quality to minimise the focal spot size on the detector and hence maximise the signal to noise ratio (SNR). Heterodyne

detection requires the phase matching of the return signal with the local oscillator to be preserved over the entire aperture. This places even greater constraints on the mirror surface quality. In astronomy, where images of distant objects are sought, the requirements on the quality of the imaging elements are also very stringent.

The construction of large, high quality mirrors is expensive and time consuming but the demand is high - with a doubling in the total mirror area available to the world's astronomers, on average, every 12 years [91]. Even with new technologies, the cost of mirror fabrication still increases as the cube of the aperture. There are many reasons for this.

Large mirrors are made thick to increase their stiffness but tend to sag under their own weight. Furthermore, as the orientation of a telescope changes, the gravitational stresses on the mirror can change, giving a corresponding change in figure. Telescope mirrors are also susceptible to changes in shape due to thermal expansion. Using materials such as ULE or Zerodur, with minimal coefficients of thermal expansion, eliminates these changes in shape but the fabrication costs increase due to the expense of these materials [41]. One technique currently used to overcome many of these problems is active optics.

Active optics involves using actuators, placed behind a thin primary, to adjust for changes in the shape of a perfect mirror or mirror segments to minimise the image size of stars in the field of view [42]. An example is the Keck telescope where 36, 1.5m hexagonal mirror segments are kept in alignment by small actuators on the rear of the segments [65]. This technique can reduce the effects of thermal expansion, sag or gravitational stresses, but there is still the cost in producing the high quality mirror segments in the first place.

New designs using lighter, monolithic meniscus mirrors with actuator supports to keep the mirror in the correct shape have been very successful, but the mounting costs are formidable. Very high quality, well supported 8m mirrors are currently in the $10 million dollar class, weigh typically 10 or more tonnes, and in addition require multi-million dollar handling fixtures and coating facilities [80].

An alternative to solid primaries is to use mirrors made from spinning shallow baths of mercury [10, 40, 78]. These mirrors can be manufactured relatively cheaply

but they can only look directly upwards. Research is being carried out to increase their accessible region of sky to as much as 45° to the vertical using fixed and deformable secondary optics [54, 9, 11, 53, 62]. This technology is fast becoming attractive as more researchers look for alternatives to expensive telescopes. Liquid mirror telescopes require an acceleration, however, and although several space telescope designs have been suggested [8], such an instrument may be prohibitively expensive.

Fabrication is not the only problem faced by manufacturers of high quality mirrors. Testing of the final product requires extremely sensitive interferometers which must be aligned precisely in order to detect any figuring errors. Measurements of this type can quite easily go wrong as demonstrated with the Hubble Space Telescope. The mirror was made too spherical and the error was not detected due to a positioning error of a null-corrector in the test optics [1, 73].

Atmospheric turbulence causes the twinkling of stars by distorting the wavefront from the incoming star-light so that it is no longer a plane wave. This results in images which change rapidly over short periods of time [92, 17, 18, 59]. The aperture radius over which the incoming wave can be thought of as essentially undistorted is called the Fried parameter ($r_\circ$) [26, 27, 28]. From this we can define a "seeing angle", $\theta = \lambda/r_\circ$ which represents the maximum angular resolution for a given Fried parameter. Since $r_\circ \propto \lambda^{6/5}$ it poses less of a problem at infra-red wavelengths than in the visible region where, typically, $r_\circ \sim 10$cm (*i.e.* $\theta \sim 1.5''$). For a telescope with an aperture, D, greater than the Fried parameter, the instantaneous image consists of speckles of size λ/D. With a long exposure, the random motion of many of these speckles averages out to give a image size of $\lambda/r_\circ$ [26, 58]. Thus for telescopes with larger diameters there is no improvement in the resolution achievable in long exposures but more light can be gathered, allowing fainter objects to be detected. One solution to this problem is to decrease the amount of turbulent atmosphere between the observer and the object. By putting the telescope on top of a mountain, $r_\circ$ can be as much as 20-30cm ($\theta \sim 0.75''-0.5''$) at optical wavelengths and diffraction limited imaging is possible for $\lambda > 3\mu$m [4]. For diffraction limited performance from a large aperture telescope operating in the visible part of the spectrum, however,

the time-varying turbulent aberration function must be somehow removed from the stellar images, or the telescope placed in space.

There are two common ways of improving the astronomical image distorted by the atmosphere: speckle interferometry and adaptive optics. Speckle interferometry is a method by which a diffraction limited telescope is used to accumulate many very short exposures of a star (usually a few microseconds each). These images are digitally combined to produce the smallest possible image. This technique works very well for point-like objects but is fairly unusable for single objects covering any extent of field. A further problem is the large integrating time required to build up an image of faint objects.

Adaptive optics involves using deformable tertiary mirrors to minimise the image spot size of a guide star in the field of view of the telescope, thereby improving the image as a whole and removing the effects of atmospheric turbulence [3, 42, 74, 43, 2]. The guide stars used can be either bright natural stars or man-made "stars" created by focussing a laser in the upper atmosphere. The popularity of this technique is increasing but so far the results are best in the infra-red as less correction is required (r_o is larger) and more bright natural sources are available than in the visible. Added to this is the problem of the small field of view correction provided by single man-made laser guide stars; the so-called anisoplanatic angle problem [88, 19]. Once again, however, a large, high quality primary is required to collect the light initially.

Ground based sites have many other limitations. Populous centres anywhere in the vicinity of telescopes increase atmospheric turbulence and are sources of light pollution and vibrations. Added to this is the problem of man-made aerosols and pollutants which increase scattering and extinction of stellar light, making fainter and finer details harder to detect. Air-glow and zodiacal light (as well as aurorae in some latitudes) are a natural source of light pollution. Atmospheric absorption at various wavelengths limits ground-based astronomical imaging in the infrared and makes it all but impossible in the ultra-violet [84]. These problems can be reduced or eliminated with a telescope situated in space or on the surface of the moon.

A space or moon-based telescope permits observations at any wavelength, in many cases uninterrupted over a 24hr period [35]. Unfortunately, the cost involved

is very large. For the Hubble Space Telescope, the cost of initial fabrication and deployment was US$2 billion. Operating, repair and maintenance costs have since doubled this [21]. Several designs for the next- generation space telescope [61] have been suggested but the cost of these are too large for current research budgets. As for lunar-based telescopes, they are still in the design phase, with the first 1 & 2m aperture prototypes planned for initial operation in the late 1990s at the earliest. Larger 4 & 16m diameter telescopes are planned for the next century [89].

A large reduction in the cost of constructing ground and space based telescopes would occur if there were some way of using large, cheap imperfect mirrors and correcting, *in situ*, the inherent aberrations as well as thermal expansion and gravitational stresses. One possible solution is to use holographic correction of large, inexpensive, low-quality mirrors [63, 64]. The principle is simply to record the aberrations holographically and then use the hologram to remove these aberrations from the image of a star. This concept does not aim to correct for atmospheric aberrations, but can reduce the cost of the fabrication, mounting, housing and maintenance of the primary. It is also a most promising method of developing a large lunar or space based telescope within a realistic budget. Holographic correction could be used for ground based telescopes in conjunction with existing adaptive optics schemes as well as having applications in lidar and other imaging systems unrelated to astronomy.

1.3 Holography

A hologram is a recording of both the phase and amplitude of a wavefront relative to a reference wave. In most cases this reference wave is a diffraction limited plane-wave but in general it can be a reproducible beam of any type. The first hologram was made by Dennis Gabor in 1948 [30, 31] in an attempt to improve the resolution of electron microscopes. The Gabor hologram is an in-line hologram and has limited practical uses due to diffracted orders superimposing over one-another. In 1962 Leith and Upatnieks [50] demonstrated a method of separating the images using an off-axis or simple two-beam hologram. A more refined method was demonstrated

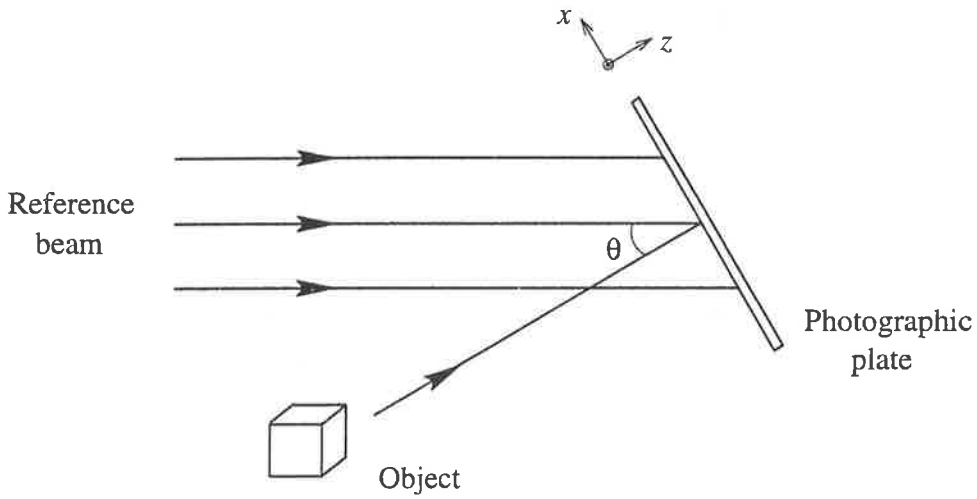

Figure 1.1: Reflected light from the object is incident normal to the plate which makes an angle of θ to the path-matched, plane wave reference beam.

by the same authors in 1964 [51]. It is this type of hologram which is generally used today.

To record a hologram of an object, coherent light is split into two beams. One of these beams illuminates an object and the other is spatially filtered and collimated to produce the reference beam. The interference pattern can be recorded with a photographic emulsion aligned along a plane where the reflected light from the object and the reference beam intersect. This is the hologram.

Consider two waves incident on the holographic recording media with the reference wave at an angle of θ to the object wave (Figure 1.1). We can describe the complex amplitude of the object and reference waves at any point (x, y) on the plate by $O(x, y)$ and $R(x, y)$, respectively [37].

$$O(x,y) = o(x,y)e^{-i\phi(x,y)} \tag{1.1}$$

$$R(x,y) = re^{ikx\sin\theta} \tag{1.2}$$

where r and $o(x, y)$ are the scalar amplitudes of the two waves at the plate and $k = 2\pi/\lambda$ is the wavenumber. Notice that since the reference beam has been taken to be a plane wave, for simplicity, its amplitude does not have an (x, y) dependence.

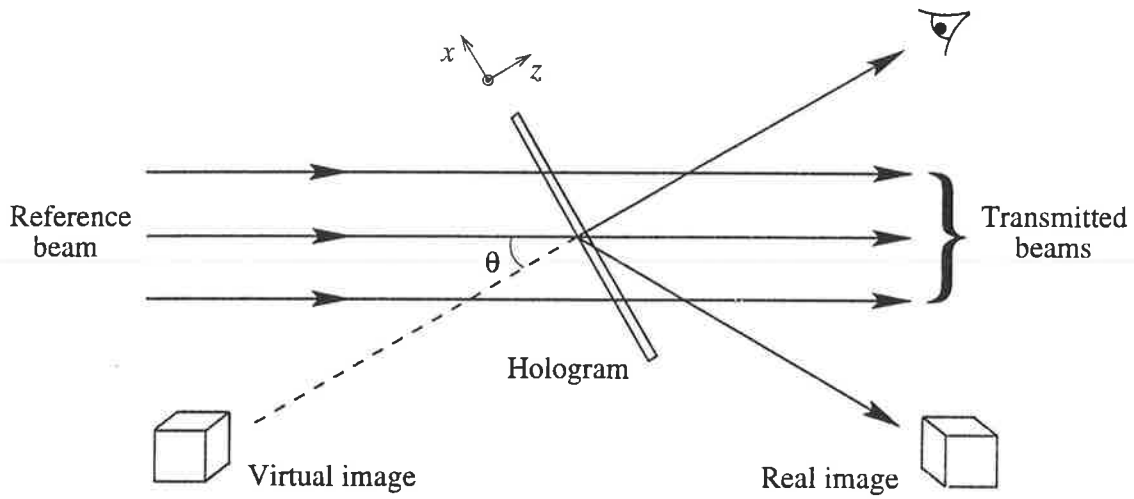

Figure 1.2: When the original reference beam is used to reconstruct the hologram we get several diffracted beams. The original reference beam continues with some attenuation along the same path as a zero diffracted order. A third beam is created at the plate which is a reconstruction of the object wave and, as such, produces a virtual image of the object. The fourth beam is a phase conjugate object beam which produces a real image of the object at an angle $-\theta$ to the reference beam.

The total intensity across the plate is $I(x,y)$;

$$\begin{aligned} I(x,y) &= [R(x,y)+O(x,y)][R(x,y)+O(x,y)]^* && (1.3)\\ &= |R(x,y)|^2+|O(x,y)|^2+R(x,y)O(x,y)^*+O(x,y)R(x,y)^* && (1.4)\\ &= r^2+o(x,y)^2+2ro(x,y)\cos[kx\sin\theta+\phi(x,y)] && (1.5) \end{aligned}$$

which is the object wave modulated by fringes with a spatial frequency of $\sin\theta/\lambda$. We can define the transmittance of the plate to be;

$$T(x,y) = t + \alpha I(x,y) \qquad (1.6)$$

where t is the average background transmittance and α represents the exposure and film sensitivity/processing. We can reconstruct the object wave with the original reference wave which will give us a transmitted wave intensity, $W(x,y)$ (Figure 1.2):

$$
\begin{aligned}
W(x,y) &= R(x,y)T(x,y) && (1.7)\\
&= R(x,y)[t+\alpha I(x,y)] && (1.8)\\
&= (t+\alpha r^2)re^{ikx\sin\theta} + \alpha r o(x,y)^2 e^{ikx\sin\theta} \\
&\quad + \alpha r^2 o(x,y)e^{-i\phi(x,y)} + \alpha r^2 o(x,y)e^{i\phi(x,y)}e^{2ikx\sin\theta} && (1.9)
\end{aligned}
$$

The first term in this equation is just the reference beam attenuated as it passes through the hologram and the second term is the zero diffracted order from the grating, collinear with the reference beam. The third term is, except for a scale factor, the initial object wave. If we were to view this light we would see a virtual image of the object, *indistinguishable from the original object*, since this wave is identical in phase to the original object beam. The fourth term represents the phase conjugate of the object wave at an angle of 2θ to the plate and will form a real image of the object at the same distance from the plate. A more comprehensive discussion of holographic grating theory is given by Kogelnik [46].

Although I have shown that the reference wave can be used to reconstruct the object wave, the reverse is also true, with the object wave capable of reconstructing the reference wave. Further, the reference beam was taken to be a plane wave for simplicity. In practice, however, the reference beam can have any form at all, but the condition that one of the beams be present in its original form, to perfectly reconstruct the other, will still hold. If both the object and reference beams are incident on the hologram after processing, the diffracted wavefront of one beam will interfere with the undiffracted wavefront of the other. These beams should be identical, so any change in the way the two wavefronts overlap will show up as fringes which modulate the transmitted beams. If the plate has been returned to exactly the same position it was in when the exposure was taken, and the reconstructing beams have not changed then there will be a single bright fringe seen over both transmitted beams. This "zero fringe" is desirable as it indicates that the environment is stable and that there has been no change in the emulsion during processing.

The hologram discussed above is a two beam transmission hologram. Although this was the type of hologram used in the course of my studies, there are several other ways to record a hologram. In a reflection (or Lippmann) hologram, the

object and reference beams are incident on the plate from different sides. Since the interference fringes produced between two plane waves are orientated parallel to the angular bisector, the fringes in this case are planes which lie in the emulsion. This type of hologram can give higher efficiency in a thick enough emulsion. A subset of this type of hologram is known as a Denisyuk hologram, in which a reference beam passes through the emulsion to the object which reflects the object wave back towards the plate. There are other types of holograms, such as evanescent wave and rainbow holograms, though they are not important in this discussion.

1.4 Holographic Correction of Aberrations

The first experiments to test the idea of using a hologram for the correction of optical wavefront aberrations were made by Kogelnik [45] and Leith and Upatnieks [52]. In Kogelnik's experiment a plane wave passed through a transparency with writing on it and then a warped glass plate (an aberrator) which distorted the wavefront (Figure 1.3). The hologram was recorded using this beam and a plane wave reference beam. The hologram was then reconstructed using a conjugate reference beam. The diffracted beam (the phase conjugate of the object wave) then passed back through the warped glass where all the wavefront distortions were removed. Following this, the original unaberrated wavefront was recovered along with a real image of the transparency. Leith and Upatnieks used a similar set-up but with a diffuser instead of an aberrated plate. These experiments demonstrated the possibility of image transmission through an aberrative element.

Further experiments by Gaskil [32] and Goodman *et al.* [33, 34] had the same concept but with the reference wave passing through the aberrator as well. In this fashion the two wavefronts were similarly distorted by the aberrator. The hologram records the difference between the two waves, so the aberration function cancelled out at the hologram, leaving the only the object wave recorded against the reference wave. When reconstructed with an unaberrated reference beam, an unaberrated object beam can be produced. These experiments were aimed at transmission of information through the atmosphere which can be thought of as a thick aberrator.

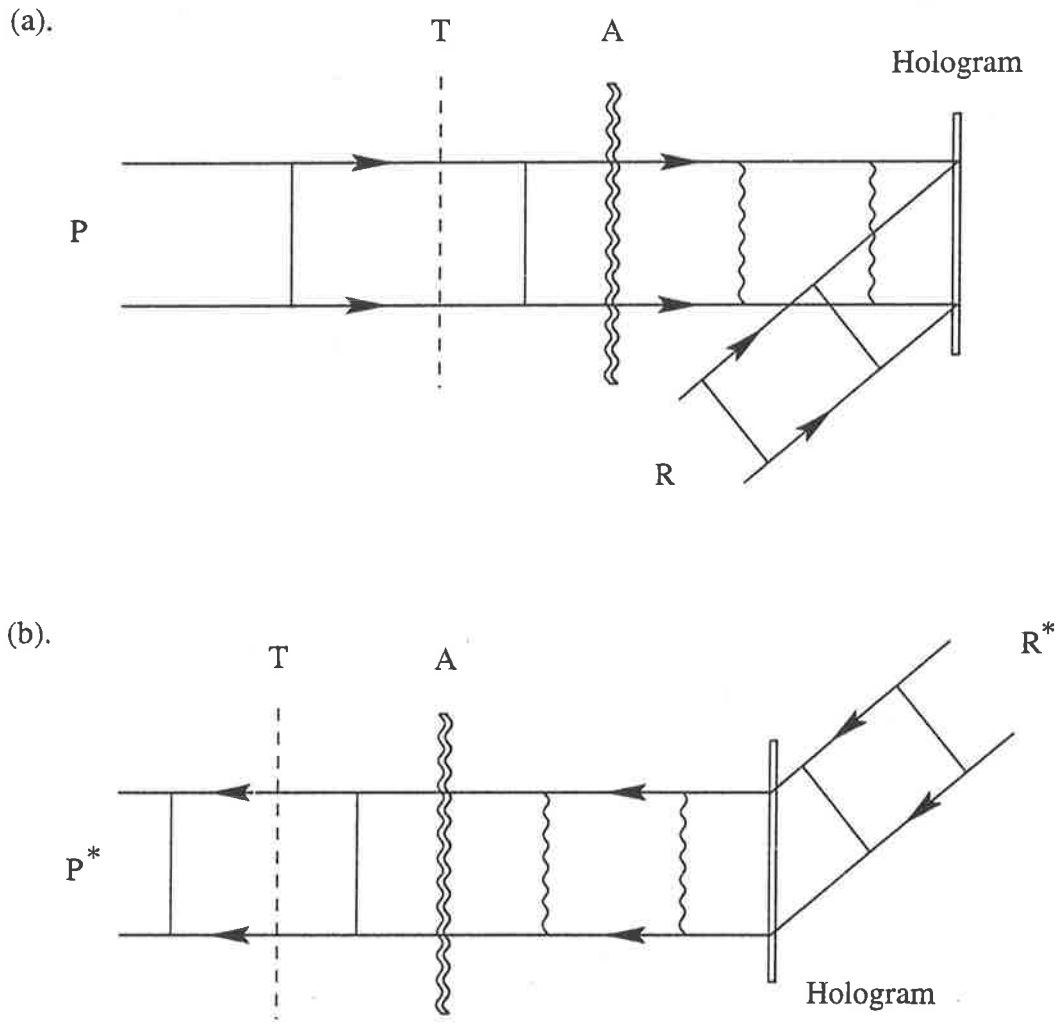

Figure 1.3: (a). A plane wave (P) passes through a transparency (T) and then through a distorting plate (A). The aberrated wavefront then interferes with a plane wave reference beam (R) to form a hologram. (b). The conjugate reference beam (R^*) is used to reconstruct the hologram, and the conjugate of the object beam is formed.

This type of correction suffers from a limited field of view similar to the anisoplanatic angle problem in adaptive optics, and will be discussed in more detail later in this thesis.

The first suggestion that holographic correction could be applied to an imaging device was made by Upatnieks *et al.* [85]. The idea was an extension to that shown that shown in Figure 1.3 except that there was no aberrating element as such, but instead, a single good-quality lens with spherical aberration. It was this aberration that was to be removed using holographic correction. The recording and replay schemes are shown in Figure 1.4. The experimental results showed that the resultant lens/hologram combination could be used to produce images free of spherical aberration. This is important because where it had previously been demonstrated that object information could be projected through aberrative elements, in this case the imaging optics themselves were corrected for a wavefront error they introduced. In this set-up, however, the telescopic transport optics could only be used with a unit magnification of the beam, so the hologram had to be as large as the optic to be corrected. Also, since the optics inverted the phase of the wavefront, the aberration to be corrected had to be rotationally symmetric about the optical axis.

The previous experiments were two-way correction schemes, in which the phase-conjugate of the reference beam was used to reconstruct a phase-conjugate of the aberrated object beam. This beam then passed through the aberrator to remove the wavefront distortions. In 1968, Kogelnik and Pennington [47] demonstrated a method of one-way aberration correction and image transmission (Figure 1.5). A plane wave was passed through an aberrator (a diffuser) and then a hologram was recorded with this as the object wave. To ensure that the hologram could resolve the aberrating elements, the diffuser was imaged onto the holographic plate and an image hologram was formed [12, 14]. This type of hologram is free of speckle at the image plane, giving an even illumination over the entire aperture. The image could also be demagnified which meant that the hologram no longer had to be as large as the distorting element. After writing the hologram, a beam with information on it was passed through the same aberrator and then onto the hologram. The reconstructed reference beam is aberration-free but *with the object information retained.*

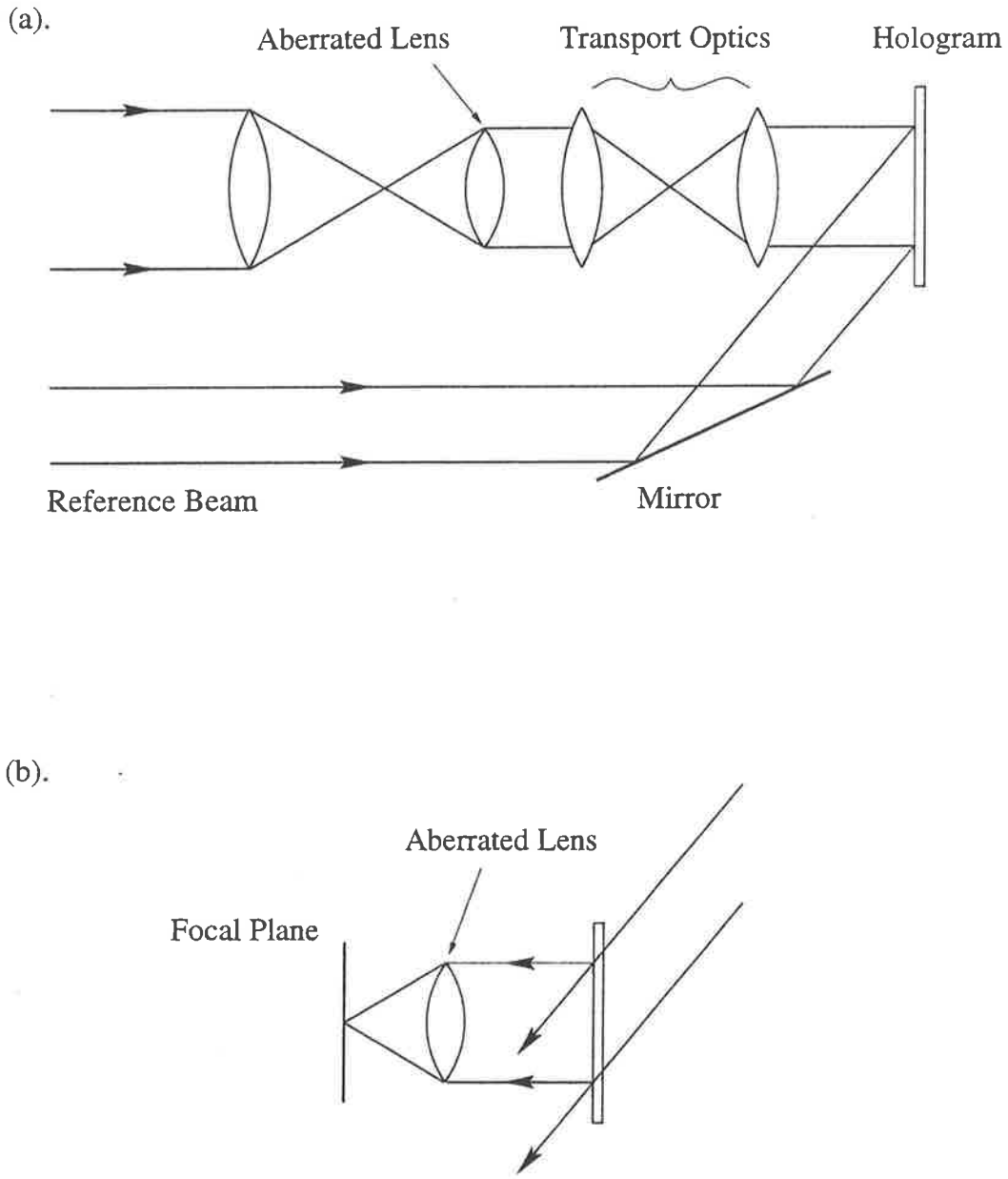

Figure 1.4: (a). Recording: A plane wave is focussed through the spherically aberrated lens and re-collimated by high quality lenses to form a hologram with a plane wave reference beam. (b). Reconstruction: The transport optics are removed and light from a scene (acting as a phase conjugate of the reference beam) passes through the aberrated lens to reconstruct the hologram. The image information from the scene is retained, and the focussed image is free of spherical aberration.

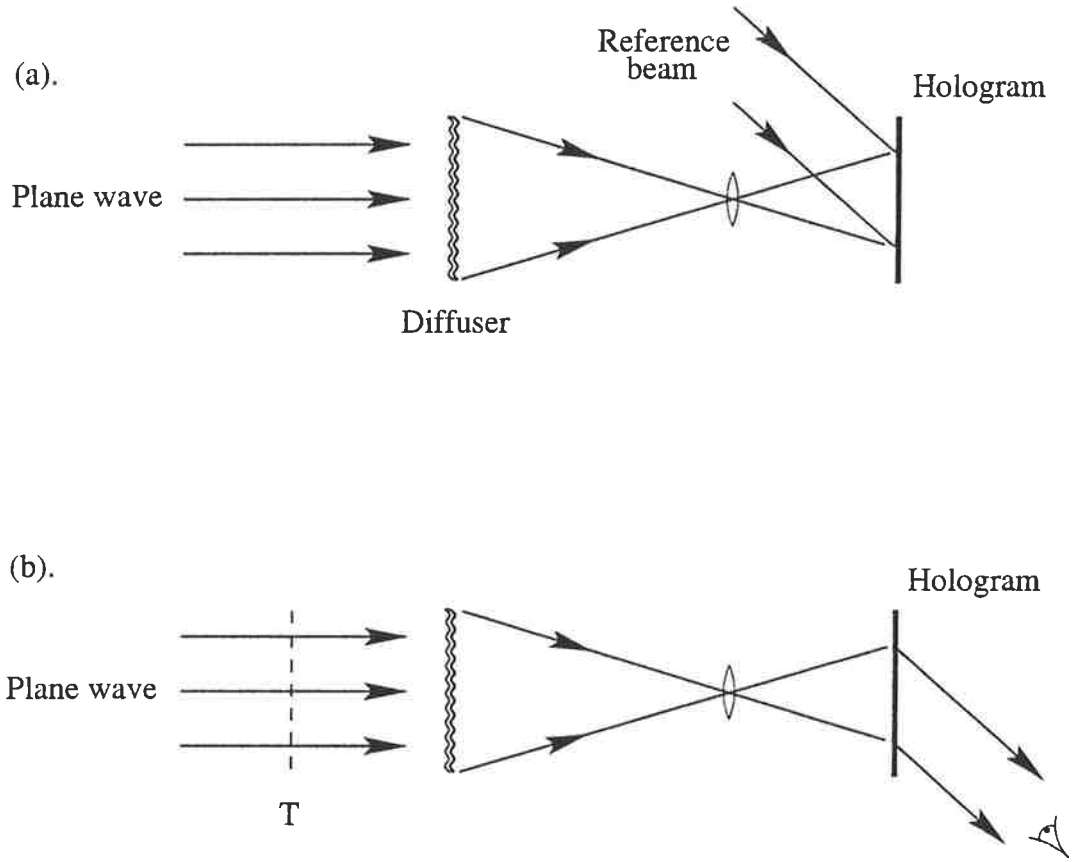

Figure 1.5: (a). Recording: A plane wave passes through the diffuser which is imaged onto the plate and a hologram is made with a plane wave reference beam. (b). Reconstruction: The original plane wave passes through a transparency, T, and then follows the same path as before to reconstruct the reference beam. This reference beam will contain object information about the transparency.

In this case a plane wave passes through the diffuser/aberrator with a spatially varying amplitude transmittance, $A(x,y)$, given by;

$$A(x,y) = a(x,y)e^{i\tau(x,y)} \tag{1.10}$$

At the plane of the hologram, the object wave has the same form but with a magnification factor provided by the imaging lens. The hologram is formed between this wave and a plane wave reference beam, $R(x,y)$, as before, giving a total intensity across the plate, $I(x,y)$;

$$I(x,y) = R^2 + A^2 + R^*.A + R.A^* \tag{1.11}$$

If we reconstruct this hologram with an identical object wave, we will generate the reference wave as expected. If however, the plane wave passes through a transparency, $T(x,y)$, before entering the diffuser, the resultant object wave reconstructing the hologram will be $O(x,y) = A(x,y)T(x,y)$. Reconstructing the hologram;

$$\begin{aligned} W(x,y) &= I(x,y)A(x,y)T(x,y) && (1.12)\\ &= R^2.A.T + A^2.A.T + R^*.A^2.T + R.A^*.A.T && (1.13) \end{aligned}$$

The last term in this equation is just $T(x,y)$ - the information imprinted on the plane wave. This means that image information can be transmitted through the aberrating element *without significant loss of fidelity.* It is this effect which forms the basis of the holographic correction. An important point to note, is that for a thin aberrator, the imaging requirement ensures that a ray incident on the aberrator from any just about angle will pass through the point on the hologram which will provide the necessary phase correction. This gives the system a useful field of view.

In other experiments, aberration correction has been achieved with computer generated holograms [54], liquid crystals [44], corner-cube arrays [15], four-wave mixing [90], and stimulated Brillouin scattering (SBS). Various other schemes have also been proposed for one-way [23, 49] and two-way [81, 20] imaging through random media.

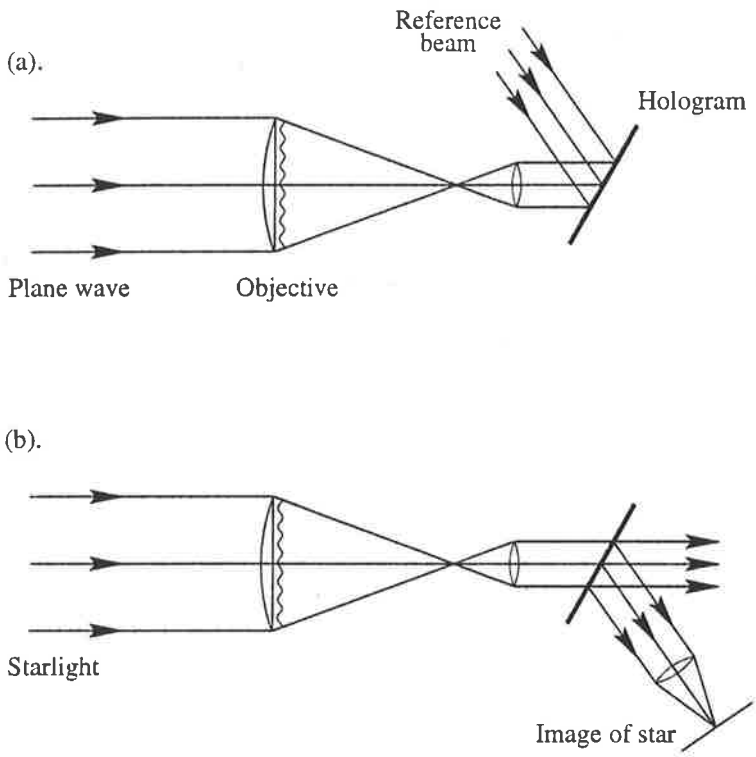

Figure 1.6: (a). A plane wave passes through the objective which has been randomly aberrated by the addition of a plate of distorted glass. An eyepiece lens collimates the light and images the distortions onto a plate where the hologram is made. (b). Starlight is used as the reconstructing plane wave.

1.5 Holographic Correction In Telescopes

In 1989 & 1990, Munch *et al.* [63, 64] demonstrated complete holographic correction of an aberrated telescope primary. The basic correction scheme is shown in Figure 1.6. A collimated beam of light (point source at infinity) passes through an aberrated objective lens and a secondary (eyepiece) lens collimates this light to produce a demagnified image of the primary lens onto the plane of the hologram. A plane wave reference beam is used to make the hologram.

To reconstruct the hologram, light from an object at infinity passes through the lens and is aberrated as before, continuing on through the same optical system as the object wave used to write the hologram. This beam will perfectly reconstruct the reference beam. As with the experiments carried out by Kogelnik and Penning-

ton [47], any optical information imprinted on the incoming beam will remain on the reconstructed reference beam, and thus an unaberrated image of the star can be formed using the diffracted beam. In this way, perfect imaging has been made possible with an aberrated primary. Since these two papers detail the extent of research in the field to date it is important to review the results in more detail.

The first experiments [63] were carried out on a high quality lens ($D = 50$mm, $f = 0.6$m) which was aberrated by the addition of a poor quality 3mm thick piece of glass. The uncorrected telescope produced a beam with a wavefront error of $\sim 4\lambda$ which was corrected to better than $\lambda/10$ with a 0.8° field of view. Once again, it is the use of the imaging eyepiece that has given this telescope such a large field of view and produces a small hologram capable of correcting a large aperture.

A recording source (beacon) located a finite distance from the objective (43 lens diameters) rather than at infinity gave similar results and showed that a beacon at infinity (a collimated wavefront) was not necessary for correction. In another experiment, a lens with a wavefront error of 10λ was corrected to $\lambda/10$ at the recording wavelength of 588nm which reduced to 0.4λ at a reconstructing wavelength of 632.8nm. The quality of the reconstructed image is reduced at other wavelengths since the magnitude of the aberrations have been recorded as a phase difference at the recording wavelength.

In their second paper, Munch *et al.* [64] demonstrated the operation of a broadband device using a more heavily aberrated objective (19λ) with the same dimensions as before. The objective was a good quality lens with a low-quality piece of glass placed in front to provide the aberrations. At the recording wavelength, the wavefront error was corrected to $\lambda/10$. The emphasis of this paper, however, was on the broadband operation of the refractor. The correction at wavelengths other than the recording wavelength was expected to be poorer, and the angle at which the corrected beam diffracts from the hologram is wavelength dependent. To overcome the dispersion in broadband operation, the diffracted light was reflected off a diffraction grating with the same spatial frequency as the holographic grating. The recording wavelength was 633nm and the performance of the corrected telescope was evaluated using resolution test charts. Before correction, the unaberrated lens

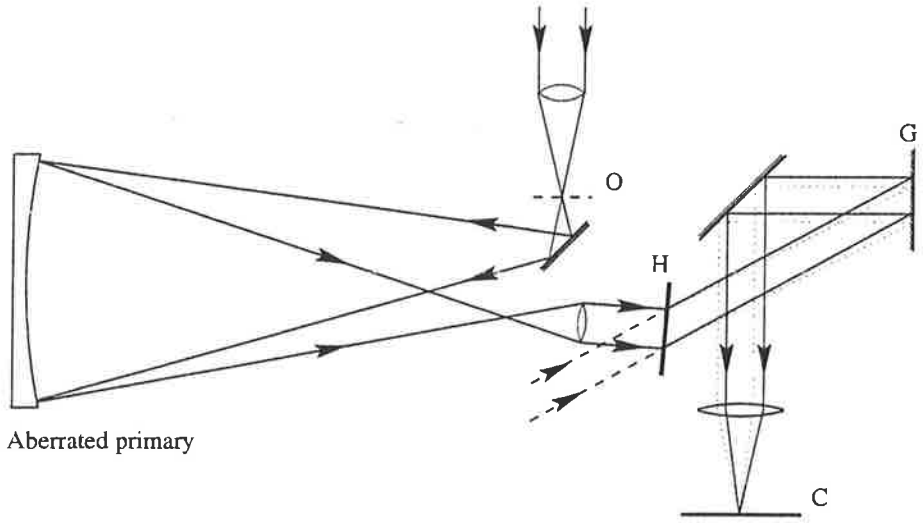

Figure 1.7: A plane wave is focussed and illuminates the aberrated primary from close to the center of curvature with a small off-axis angle. The light is then collimated and the mirror is imaged onto the plate (H) where a hologram is formed with a reference beam (dashed). On reconstruction a broadband source is used to illuminate an object placed at O. The hologram diffracts different wavelengths at different angles (solid & dotted) and they are recombined by the use of a reflective grating (G) and a lens. A focussed image is formed at the camera (C).

had a white-light resolution of 15μm and when the distorter was added, this was reduced to $\sim$ 0.3mm.

At the recording wavelength, the resolution was improved to 17.5μm, and over a bandwidth of $\Delta\lambda$ = 40nm the resolution was also a diffraction limited 12.4μm[1]. The white light imaging ($\Delta\lambda$ = 300nm) was a dramatic improvement over the uncorrected image.

As well as considering refractive primary optic, Munch et al. also demonstrated the correction of a mirror. Reflecting primaries are more useful for telescopes, since they do not suffer from chromatic aberration and are lighter and cheaper to manufacture. The experiments involved a poor-quality membrane spherical mirror (D = 0.4m, R = 2.6m) corrected with the one-to-one imaging arrangement as shown in Figure 1.7. The uncorrected mirror imaged a 10μm pinhole to a 10mm

[1]Although the numbers differ, both cases represent diffraction limited resolution, since the minimum resolvable feature is 1.6 times larger with coherent illumination than for incoherent illumination [7] p521.

spot. Once again, a reflective grating was used for the dispersion correction. At the recording wavelength, the corrected primary had a resolution of 15.6μm, with similar results over a bandwidth of $\Delta\lambda = 40$nm. Reconstruction over a bandwidth of $\Delta\lambda = 75$nm gave a resolution of 63μm and in white light the minimum resolvable features were 31μm in size.

These two papers demonstrated the possibility of using holographic correction of aberrated telescope optics to give perfect performance over a useful bandwidth. The recording arrangements, however, required that the recording beacon be a large distance away, thus putting limits on the uses of such telescopes. A more practical design would utilise a beacon located much closer to the primary.

In his honours thesis, Fotheringham [24] investigated the concept of a proximal beacon. The important experiments involved the recording of a image hologram of a poor-quality spherical mirror ($D = 0.33$m, $f = 0.6$m) from the centre of curvature using a plane wave reference beam (Figure 1.8). The processed hologram was moved to the focal plane where a phase conjugate plane wave reconstructed a phase conjugate of the aberrated object wave. Using an imaging lens of half the focal length, the object wave could be played back onto the surface of the mirror. The reflected light should have had most of the mirror aberrations removed to form an unaberrated, collimated beam. The experimental results showed the presence of a large amount of residual wavefront aberration, thought to be due to the slight off-axis angle used on recording, as well as the distortions present in the holographic substrate.

Although not demonstrated to be completely successful, the idea of recording the hologram from the centre of curvature and then moving it to the focal plane for reconstruction seemed sound enough. A first order theoretical analysis [24] showed that although the geometries of the two situations differ, enough of a similarity exists for the reconstructed wave to adequately correct for some of the surface aberrations.

1.6 The Scope of This Work

The research reported in this thesis concerns the development of compact holographic correction schemes involving beacons located as close as possible to the

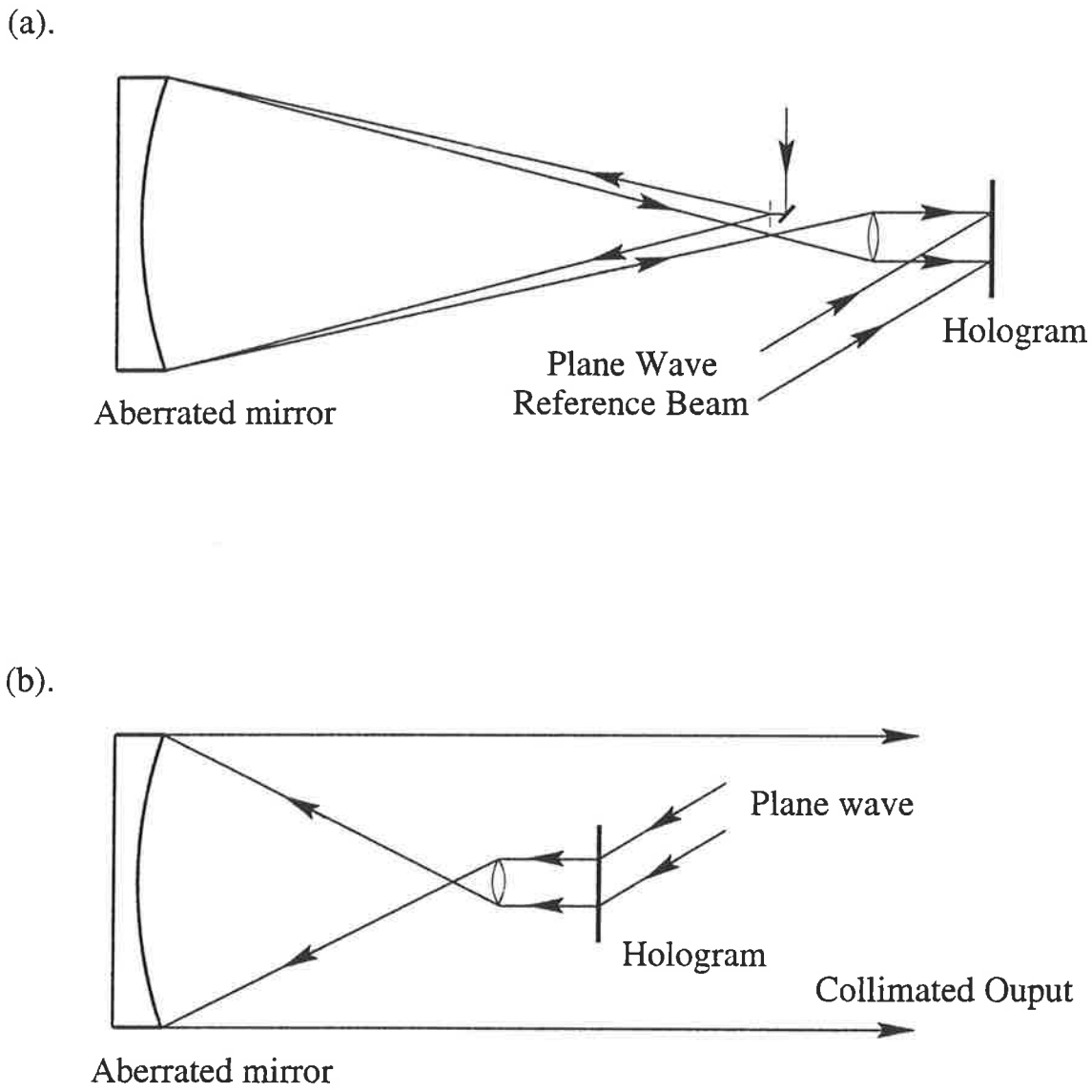

Figure 1.8: (a). Recording: A spatial filter illuminates the mirror from the centre of curvature and the reflected light is collimated and used to form an image hologram of the mirror. (b). Reconstruction: The hologram is moved to the focal plane where a plane wave (the phase conjugate reference beam) is used to reconstruct the phase conjugate object wave. This wave reflects off the mirror to give a collimated beam.

primary mirror. The compactness is considered absolutely essential for most space and ground-based applications, while the simplicity is important in reducing the costs of an final design.

In the following chapters I will introduce a theory of holographic correction which can be used to analyze most schemes and aid in selection of more suitable designs. A summary of Seidel aberration theory and an exact calculation of spherical aberration will also be presented.

Two specific designs have been investigated in detail, with both using conventional, inexpensive optical components as well as being suited to a simple increase in scale. The first is an off-axis recording scheme where the beacon is placed at the radius of curvature from the mirror, but at the edge of the aperture. This scheme will be shown to be successful in removing the aberrations of the mirror, leaving it with the spherical aberration expected from a perfect spherical surface focussing light from infinity. Several methods of removing this aberration in the correction process will be discussed.

The second design is an on-axis correction scheme. The beacon is placed on-axis at the centre of curvature of the spherical mirror. In this scheme, spherical aberration was introduced in the recording of the hologram. The residual wavefront error of the corrected telescope mirror is believed to be limited only by the quality of the test optics available. The simplicity and scalability of this design means that this design should result in similar performance for mirrors of much larger diameters.

Chapter 2

Aberration Theory

2.1 Introduction

In designing a compact, holographically corrected telescope, there are many possible positions for the proximal beacon. In any scheme there will be the surface aberrations of the primary itself, as well as aberrations introduced from the recording and reconstruction optical geometries. The two problems are quite different and each must be considered in order to evaluate the merits of any possible design. In this chapter a general description of aberrations will be presented which can be applied to a specific design in order to predict the performance.

2.2 Correction of Mirror Surface Aberrations

To record the hologram of an aberrated mirror, reflected light is used to form an image of the surface. The interference pattern formed between this object beam and a path-matched reference wave is recorded on film. The "height" of a bump is recorded as a phase difference between the ray reflecting off the actual surface (the object beam) and one reflecting off an unaberrated, reference surface (Figure 2.1).

In order to maintain the fidelity of the diffracted beam, the reconstructing wavefront must be identical to the original object beam used to record the hologram. The image formed at the plate on recording must also match the image on the plate on reconstruction. These conditions include a matching of phase, magnification,

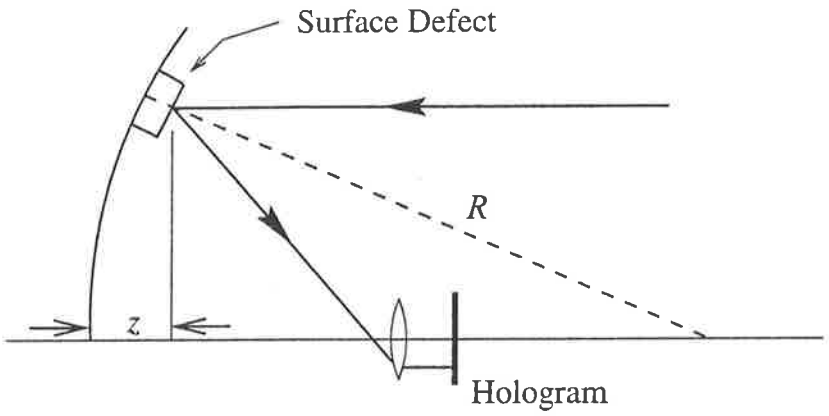

Figure 2.1: A ray shown reflecting off a bump on the mirror surface (greatly exaggerated) and passing through the imaging lens onto the hologram. The "height" of the bump is determined by the phase shift between this ray and a reference ray at the hologram.

wavelength, orientation, angle of incidence to the holographic plate and beam divergence. For example, an image hologram recorded of one mirror will not correct for the aberrations of a different mirror imaged to an identical magnification, since the location and size of the phase errors across each aperture may be very different.

In the experiments to follow, the imaging conditions (*e.g.* magnification, position, orientation, angle of incidence and beam divergence) are all kept constant. More detail concerning these factors will follow later. For now, all that matters is that the only difference between the recording and reconstructing object beams is the magnitude of the phase errors which are a direct result of the recording and reconstructing geometries. In the case of a single reflecting primary, the differences in the angle at which light reflects off a particular point on the mirror surface will give rise to slightly different phase shifts for a given aberration.

We now need to find an expression for the phase shift introduced by a bump. Figure 2.2 shows a ray from the recording beacon striking a bump on the spherical mirror surface at an angle α to the normal (a ray from the centre of curvature). The path difference between this ray, and one which would have reflected off an unaberrated mirror is;

$$a + b = 2h \cos \alpha \tag{2.1}$$

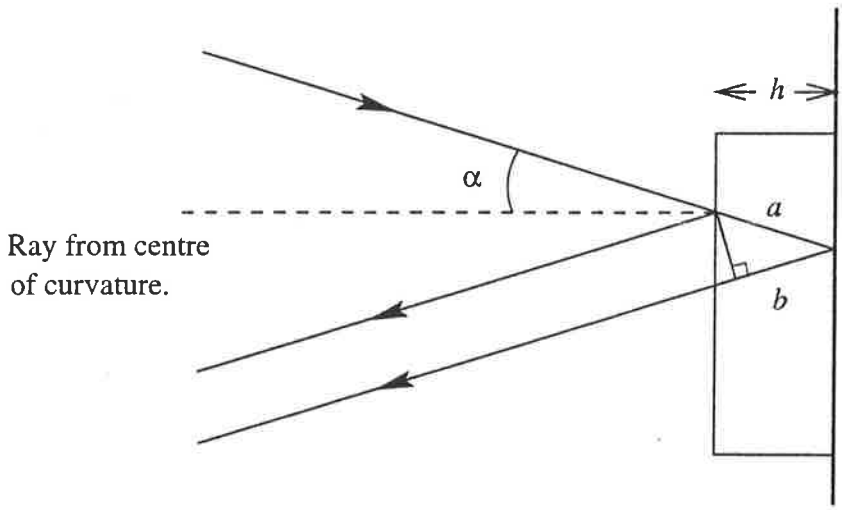

Figure 2.2: Recording: A ray from the beacon strikes a point on the bump at an angle of α to the normal and is reflected. The path difference between the ray from the top of the bump and one which would have reflected off the unaberrated mirror surface is $a + b$. On reconstruction the angle to the bump at the same point is β.

On reconstruction, a ray to the same point will make an angle β to the mirror normal. The recording and replay geometries may differ so the optical path difference in this case is

$$a' + b' = 2h \cos \beta \tag{2.2}$$

To find the optical phase difference, we need to divide by the wavelength used. Thus on recording at wavelength λ;

$$OPD_1 = \frac{2h \cos \alpha}{\lambda} \tag{2.3}$$

and on reconstruction at some different wavelength, λ';

$$OPD_2 = \frac{2h \cos \beta}{\lambda'} \tag{2.4}$$

The difference between these two values will show the residual phase error left behind when the hologram of the bump is reconstructed with a ray coming in from a different angle and at a different wavelength. We now define a relative phase

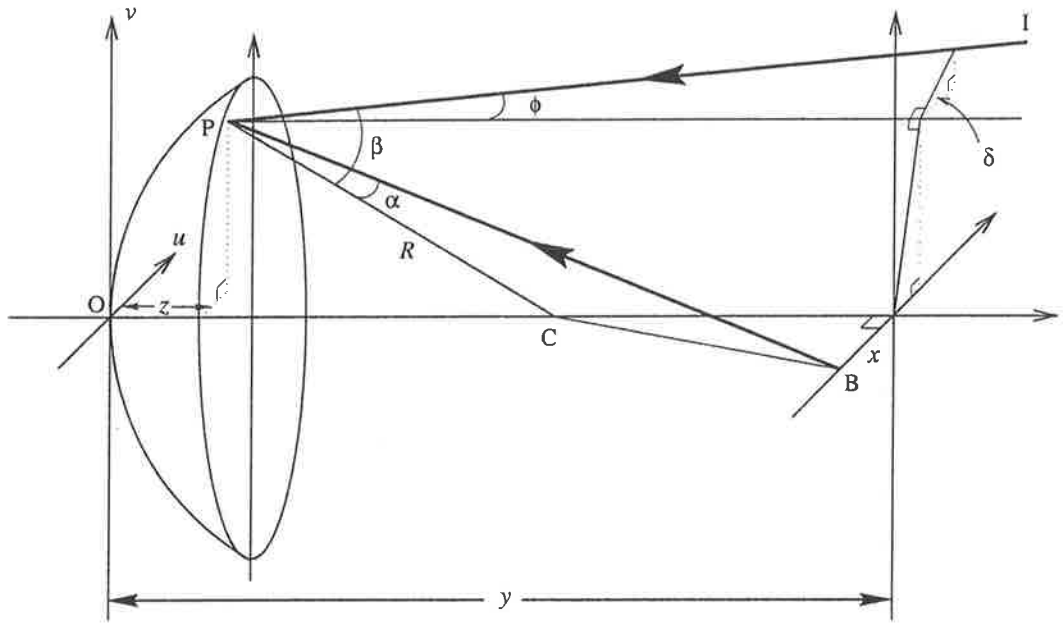

Figure 2.3: Recording: A ray from the beacon located at $B(x, 0, y)$ strikes the mirror at $P(u, v, z(u, v))$ making an angle α to the normal (a ray from the centre of curvature, C). Reconstruction: A ray from infinity (I) at a field angle φ, and polar angle δ relative to the optical axis of the mirror, strikes the same point P at an angle β to the normal.

factor Δ which represents the relative phase difference between the recorded and reconstructed height of a bump.

$$\Delta = \frac{OPD_1 - OPD_2}{OPD_2} = \frac{\lambda'}{\lambda}\frac{\cos\alpha}{\cos\beta} - 1 \tag{2.5}$$

We now consider a spherical mirror which is illuminated by a beacon situated at some finite distance y, on-axis, and x, off-axis (Figure 2.3). To calculate the relative phase difference on recording we need to find $\cos\alpha$ for a ray striking any position (u, v) on this mirror[1].

By using the geometry shown in Figure 2.3 we can now find an expression for $\cos\alpha$. The basic expressions are presented here, with a more complete derivation

[1]It is not necessary for us to know what happens to the ray after reflection, though it is assumed that the ray from a point on the mirror makes it through imaging optics to the unique image point on the hologram.

provided in Appendix B.

$$\cos\alpha = \frac{xu + Ry + Rz - yz}{R\sqrt{x^2 + 2xu + y^2 + 2Rz - 2yz}} \tag{2.6}$$

where the spherical sag, z, is given by

$$z = R - \sqrt{R^2 - u^2 - v^2} \tag{2.7}$$

On reconstruction, a general ray from any off-axis (field) angle ϕ and direction (polar) angle δ will make an angle β to the mirror normal (Figure 2.3).

$$\cos\beta = \frac{\cos\phi}{R}(R - z) - \frac{\sin o}{R}[u\cos\delta + v\sin\delta] \tag{2.8}$$

Substituting Eqs. 2.6 and 2.8 into Eq. 2.5. we get;

$$\Delta = \frac{\lambda'\,(xu + Ry + Rz - yz)}{\lambda\,((R - z)\cos\phi - [u\cos\delta + v\sin\delta]\sin o)\,\sqrt{x^2 + 2xu + y^2 + 2Rz - 2yz}} - 1 \tag{2.9}$$

We can now define a "Correction Factor" which is the inverse of the relative phase difference (Δ^{-1}). This represents the factor by which the height of a bump is reduced from recording to reconstruction. This general formula can be used to determine the effectiveness of different recording and reconstructing schemes in correcting spherical mirrors. For most of the work in this thesis, the case of on-axis reconstruction at the recording wavelength ($\phi = 0, \delta = 0$ & $\lambda = \lambda'$) will be considered, which greatly simplifies this equation.

Since the correction factor is determined by the magnitude of the angular difference between the recording and reconstructing rays to a point on the mirror, the speed of the mirror (F-number) will be critical. The effect of mirror speed on the correction factor will be investigated individually for each of the recording schemes in this thesis.

The theory above is concerned only with an aberrator having a uniquely defined aberrating surface. If the aberrator has an extended depth, the wavefront deformation no longer occurs in a single plane, but over a finite path. Such an object is known as a "thick aberrator". With a thin aberrator, such as a mirror, the optics

which image the thin aberrator onto the film ensure that any ray which strikes a particular point on the aberrator always ends up at the corresponding image point on the hologram, where a unique phase error is recorded (Figure 2.4(a)). With a thick aberrator, rays from different field points can take very different paths through the aberrator (Figure 2.4(b)). A lens can no longer image a single plane in which the required phase error is recorded, so the different rays will not receive the required phase correction at the hologram. As a result, field of view is lost in such a system. An example of a thick aberrator would be a thick lens made from a very inhomogeneous glass or with two aberrated surfaces. A reflecting telescope with an aberrated primary *and* secondary mirrors is another example, as is a turbulent atmosphere. In adaptive optics, the use of a guide star to correct for atmospheric turbulence faces this same field of view limitation. My work has concentrated on the correction of a single reflective primary, which is a thin aberrator, so this problem should not arise.

2.3 Geometrical Aberrations

2.3.1 Third Order Aberrations

Holograms record the light of an object beam with respect to a reference wavefront. Not only will the surface aberrations be recorded, but so will any aberrations which arise from the geometry of the recording set-up. These aberrations, often called the Seidel aberrations, will be present in most optical systems, even if the optical elements themselves are diffraction limited. Correcting for the mirror aberrations relies on the same aberrations being present in the same scale and orientation on replay so that the original diffraction limited reference beam is reconstructed. Any difference between the object wave on writing and reading of the hologram will be passed on to the reconstructed reference wave. With the geometrical aberrations, the situation is exactly the same.

Seidel aberrations can be derived from simple ray theory [56, 57]. Figure 2.5 shows a ray incident on a spherical mirror from a point (x, y) and reflecting off a point (r, θ) on the mirror surface to the image point (x', y'). The total third order

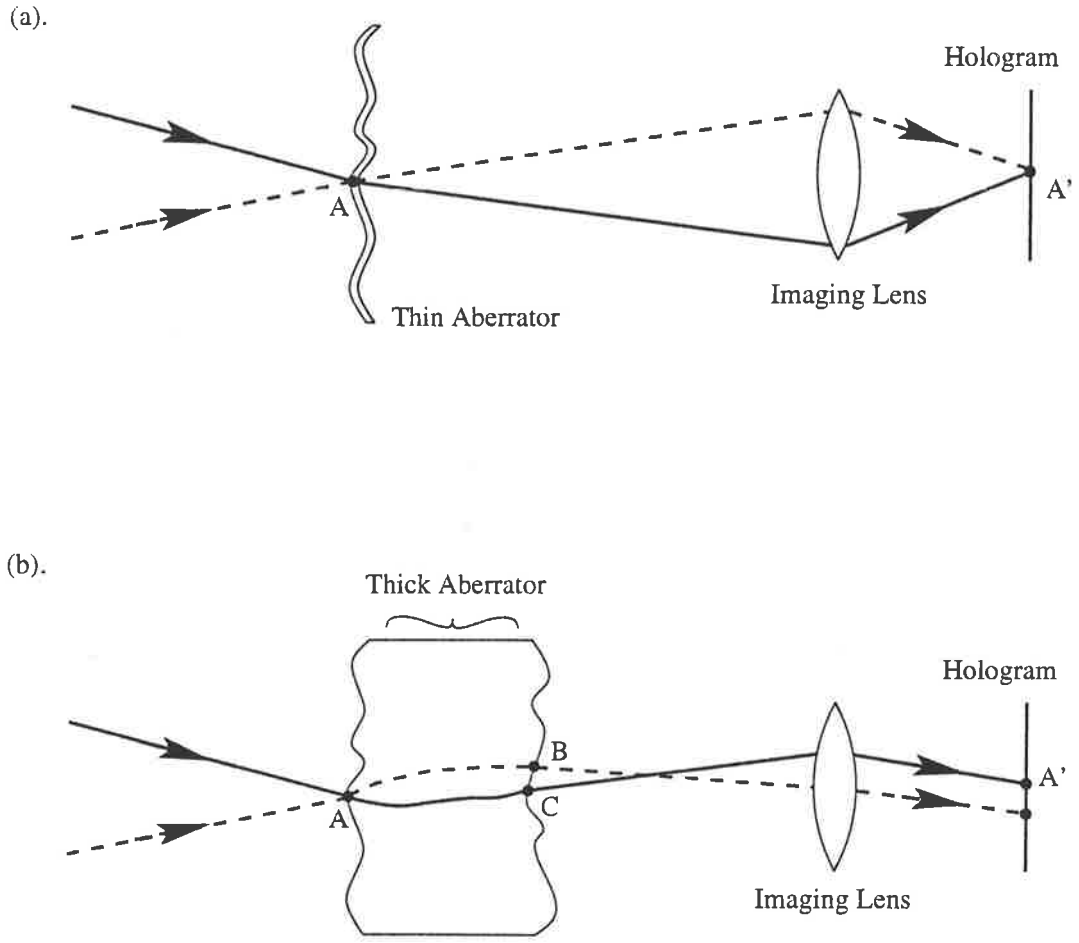

Figure 2.4: Rays from a pair of adjacent points are shown, one dashed and one solid. The hologram was recorded with the solid ray which in both cases passed through the aberrator at point A and was then imaged onto the hologram to point A′. On reconstruction, the original ray and another ray from a different field position strike the point A on the aberrator. (a). Thin Aberrator: Both rays strike A and are imaged by the lens onto the same point, A′ where the correct phase shift is recorded. (b). Thick Aberrator: In this case, the two rays will continue on from A to different points, B and C, on the other side of the aberrator. Only the recording ray can pass through the image point, A′, with the other ray striking a different point on the hologram.

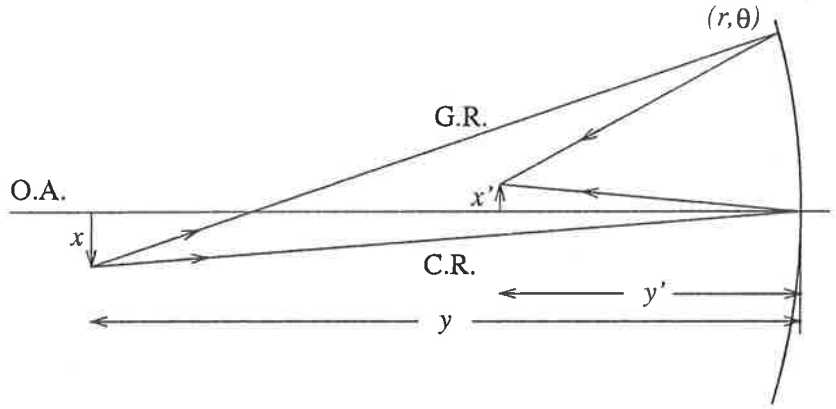

Figure 2.5: A ray from a point (x, y) off-axis has a corresponding image point (x', y') off-axis after reflection off a spherical mirror of radius of curvature, R. The aberration of a general ray (GR) reflecting off a point on the mirror with polar coords (r, θ) in the plane of the exit pupil, is calculated with respect to the chief ray (CR) passing through the centre of the exit pupil.

phase aberration in this situation is $\Phi(r, \theta)$;

$$\Phi(\rho, \theta) = A_s r^4 + A_c x' r^3 \cos\theta + A_a x'^2 r^2 \cos^2\theta + A_d x'^2 r^2 + A_p x'^3 r \cos\theta \qquad (2.10)$$

where A_s, A_c, A_a, A_d and A_p represent the coefficients for the terms spherical aberration, coma, astigmatism, distortion/tilt and Petzval curvature (curvature of field or defocus) respectively and are as follows;

$$A_s = \frac{1}{4R}\left(\frac{y'}{L}\right)^4 \left(\frac{1}{R} + \frac{1}{y}\right)^2 \qquad (2.11)$$

$$A_c = 4kA_s \qquad (2.12)$$

$$A_a = 4k^2 A_s \qquad (2.13)$$

$$A_d = 2k^2 A_s - \frac{1}{2RL^2} \qquad (2.14)$$

$$A_p = 4k^3 A_s - \frac{d}{RL^2} \qquad (2.15)$$

$$k = \frac{L - R - y'}{R + y'} \qquad (2.16)$$

where L is the distance of the Gaussian image from the plane of the exit pupil. For a reflection, L, R and y' are positive when measured to the left of the exit pupil

and negative when situated to the right. In most cases the aperture stop will be located at the mirror (along with the entrance and exit pupils) and hence $L = y'$. The object distance, y, will be positive when to the right of the mirror and the quantities, r, x and x' are all positive when above the optical axis.

The presence of each of these aberrations will have a particular effect on the appearance of a wavefront. The wavefront forms of the aberrations given in Eq. 2.10 are shown in Figures 2.6 & 2.7 along with the pattern observed from interference with a plane wave reference beam. The magnitude of many of these aberrations can be partially reduced by the addition of another. In the case of spherical aberration, the wavefront error can be off-set by the addition of a small amount of curvature of field to produce *balanced* spherical aberration.

2.3.2 Higher Order Aberrations

For large off-axis angles, or fast (small F-number) systems, the third order Seidel aberrations give an incomplete description of the wavefront aberrations. In this case higher order terms must be considered. A convenient way of expressing these terms is by using Zernike polynomials [7, 5, 86, 57].

Any circular wavefront function, $W(\rho, \theta)$, can be expressed as a linear combination of Zernike polynomials according to the following equation;

$$W(\rho,\theta) = \sum_{n=0}^{k} \sum_{m=0}^{n} A_{nm} R_n^{n-2m} \left\{ \begin{array}{c} \sin \\ \cos \end{array} \right\} (n-2m)\,\theta \tag{2.17}$$

where

$$R_n^{n-2m} = \rho^n, \rho^{n-2}, \cdots, \rho^{|l|} \tag{2.18}$$

A_{nm} is the weight of the particular term, $n \geq l$ and $n - l$ is always even.

For a higher order analysis of off-axis designs, an optical design program can be used to evaluate these terms. I used a program called Zemax (Focus Software) which can evaluate the coefficients of the first 36 Zernike polynomials. For on-axis designs, where spherical aberration is the only higher order aberration, it is simpler to derive the higher order expression directly.

(a).

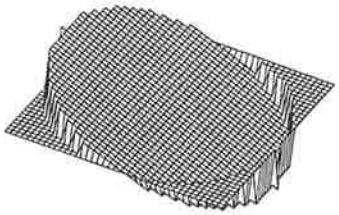

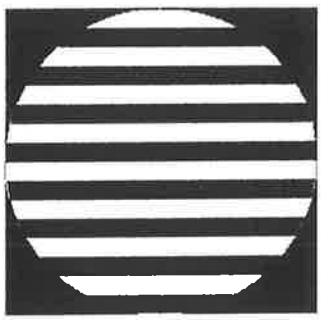

(b).

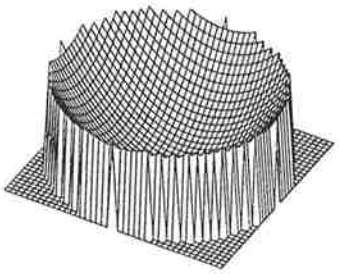

(c).

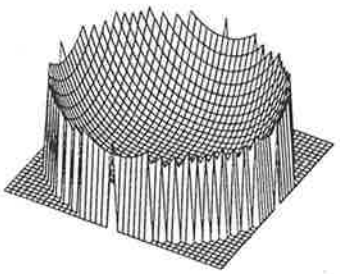

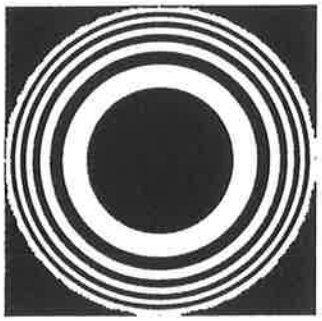

(d).

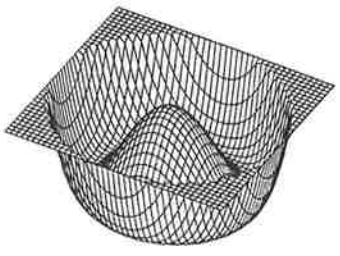

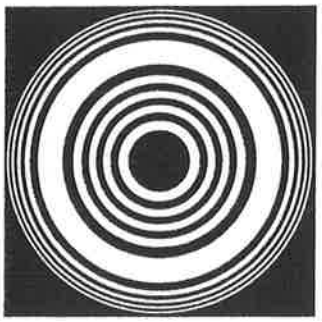

Figure 2.6: The wavefront maps and interference patterns of particular aberrations. (a). Tilt/Distortion: $\rho \cos\theta$ (b). Curvature of Field: ρ^2 (c). Spherical Aberration: ρ^4 and (d). Balanced Spherical Aberration: $\rho^4 - \rho^2$.

(a).

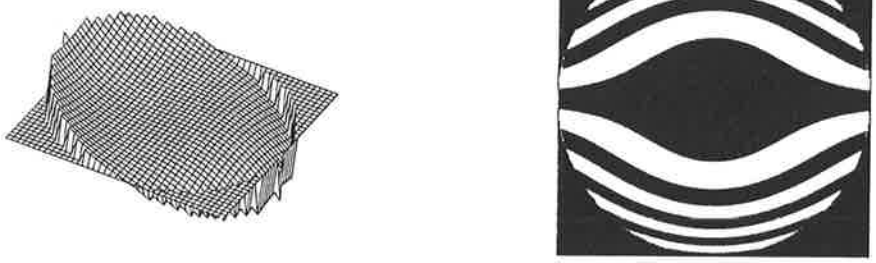

(b).

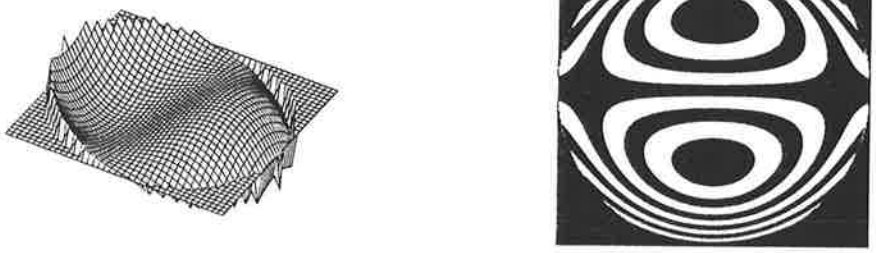

(c).

(d).

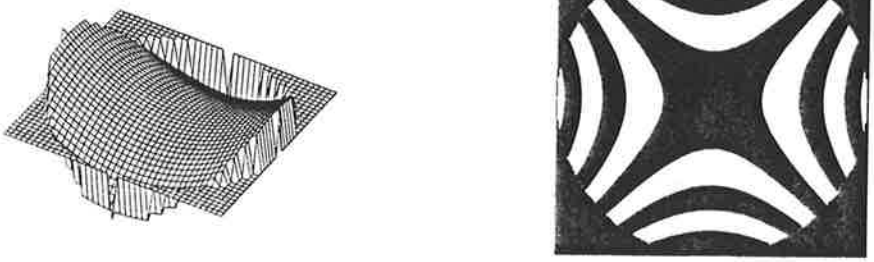

Figure 2.7: The wavefront maps and interference patterns. (a). Coma: $\rho^3 \cos\theta$ (b). Balanced Coma: $\rho^3 \cos\theta - \frac{2}{3}\rho\cos\theta$ (coma + tilt) (c). Astigmatism: $\rho^2 \cos^2\theta$ and (d). Balanced Astigmatism: $\rho^2 \cos^2\theta - \frac{1}{2}\rho^2$ (astigmatism + defocus).

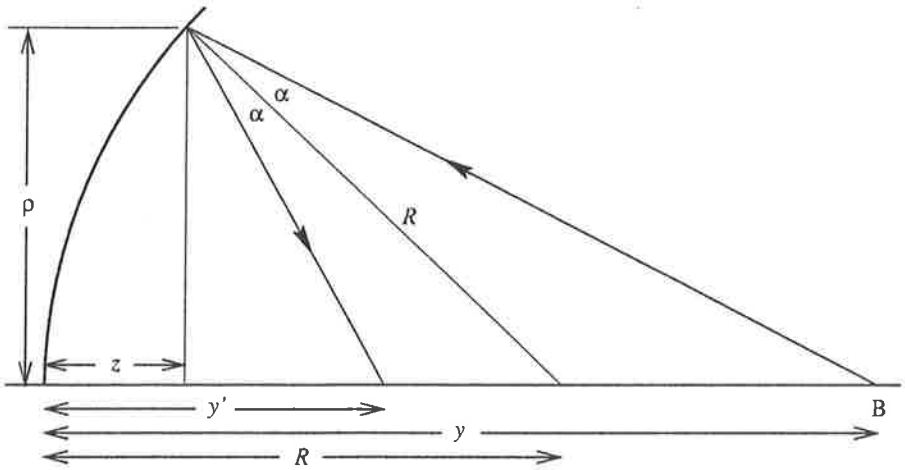

Figure 2.8: A ray from a distant beacon (B) strikes the spherical mirror at an arbitrary point on the mirror at a distance ρ from the axis and reflects off to a point on the optical axis at an image distance y'. The beacon distance, y, is always greater than or equal to the radius of curvature R of the mirror.

2.4 Spherical Aberration

2.4.1 Spherical Mirrors

On reconstruction, collimated light is focussed by the spherical mirror to a spherically aberrated focus. In most of the designs to follow, the hologram is recorded with a beacon located at a finite distance from the spherical mirror. This means that there will be less spherical aberration recorded (and in many cases none at all) than present on reconstruction. The difference will be passed on to the reconstructed reference beam. In this case, the higher order spherical aberration terms can be calculated directly, rather than resorting to the Zernike polynomials.

To begin with, consider a spherical mirror illuminated by a beacon at some finite distance y. For every ray striking the mirror from a distance y on-axis, there will be a corresponding image distance, y', on-axis. The magnitude of y' will vary according to the focal length of the mirror, the distance of the beacon and the radial extent, ρ, of the ray at the mirror. The situation is shown graphically in Figure 2.8. As always, for a sphere;

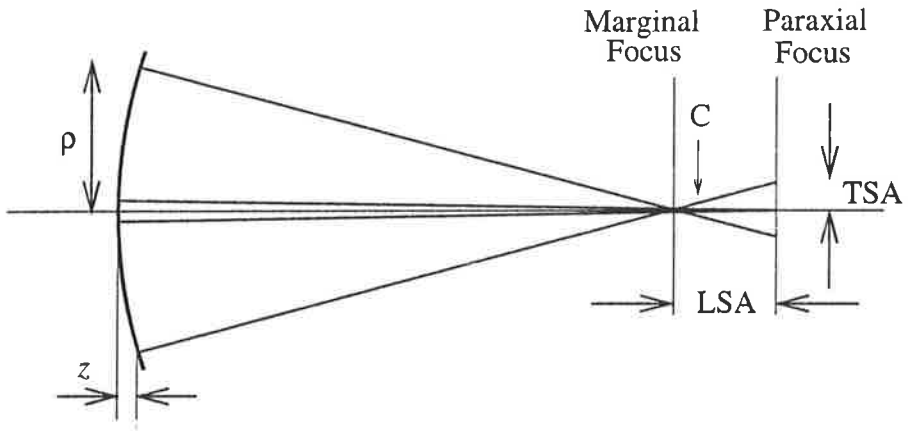

Figure 2.9: Longitudinal and transverse spherical aberration (*LSA* and *TSA* respectively) at the focal plane of a spherical mirror. The circle of least confusion (C) lies three quarters of the distance from the paraxial focus to the marginal focus.

$$z = R - \sqrt{R^2 - \rho^2} \tag{2.19}$$

From the diagram, the following relationships can be derived;

$$\frac{1}{y'} + \frac{1}{y} = \frac{2}{R} - 2z\left(\frac{1}{R^2} - \frac{1}{Ry'} - \frac{1}{Ry} + \frac{1}{y'y}\right) \tag{2.20}$$

$$\Rightarrow \qquad y' = \frac{2Rzy - R^2y - 2R^2z}{R^2 - 2Rz - 2Ry + 2yz} \tag{2.21}$$

Equation 2.20, is a more explicit form of the paraxial imaging equation ($1/y + 1/y' = 2/R$). The additional terms in the equation account for spherical aberration. Using Eq. 2.21 it is possible to derive expressions for the *exact* longitudinal and transverse spherical aberration (*LSA* and *TSA*) at the image point for any given object distance. These quantities are depicted in (Figure 2.9).

For the paraxial ray (y'_o);

$$y'_o = \frac{yR}{2y - R} \tag{2.22}$$

The expression for the marginal ray, y'_ρ, is that given in Eq. 2.21. The longitudinal

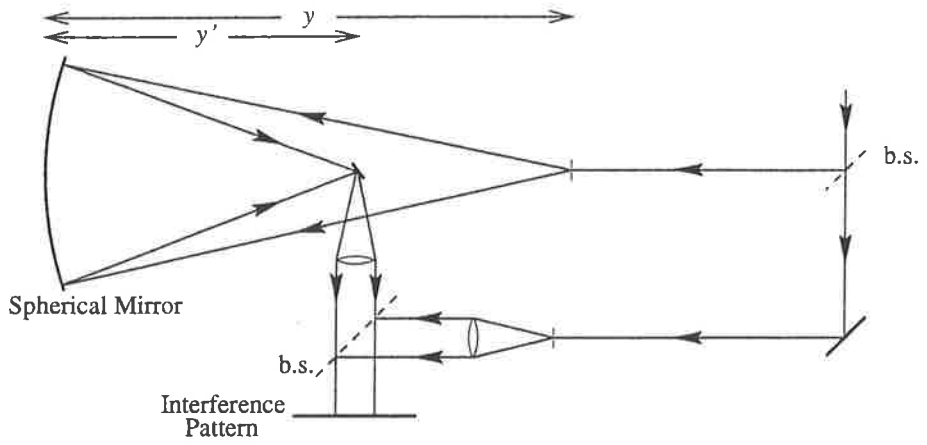

Figure 2.10: A beacon at a distance $y \geq R$ from a spherical mirror is imaged at a distance $y'(\rho)$. This wavefront is collimated and made to interfere with a plane wave. The resulting interference pattern will consist of curved fringes or concentric circles indicating the amount of spherical aberration present.

spherical aberration (LSA) is thus;

$$LSA = y'_o - y'_\rho = \frac{2Rz(y-R)^2}{(R-2y)(R^2-2Rz-2Ry+2yz)} \tag{2.23}$$

For the transverse spherical aberration (TSA);

$$TSA = \frac{\rho.LSA}{y'_\rho - z} = \frac{2\rho Rz(y-R)^2}{(2y-R)(R^2y-R^2z+2\rho^2R-2\rho^2y)} \tag{2.24}$$

The diameter of the circle of least confusion (the smallest spot size from the aberrated focus) is $|TSA|/2$.

These are ray aberrations from which we can calculate the wavefront aberration. It is the wavefront aberration which determines the appearance of the aberration in an interferometer such as the one shown in Figure 2.10. The wavefront aberration, W, is related to the transverse ray aberration, T, and the radius, r, of a reference sphere centered on the paraxial image point by [71];

$$\frac{\partial W}{\partial \rho} = \frac{T(\rho)}{W-r} \tag{2.25}$$

In this case, with the paraxial image point located at a distance $r = y'_o$ from the mirror, the spherical aberration wavefront error is;

$$\frac{\partial W}{\partial \rho} = \frac{TSA}{W - y'_o} \tag{2.26}$$

$$W = y'_o - \sqrt{y'^2_o - 2\int_0^\rho TSA \ \partial\rho} \tag{2.27}$$

We can now substitute Eq. 2.24 into this expression and express the result as a series expansion for simplicity. In most cases, an expansion up to the fifth order will suffice;

$$W_{3+5} = \frac{(R-y)^2\rho^4}{4R^3y^2} + \frac{(R-y)^2(3y-2R)\rho^6}{8R^5y^3} + ... \tag{2.28}$$

Figure 2.11(a) shows a plot of the ratio of the 5th order spherical aberration term to the 3rd order term (*i.e.* W_5/W_3), as well as 7th/5th. The ratio has been plotted for $y = \infty$ and $D = 1$m as a function of mirror speed. This graph gives a good indication of the region in which the fifth order term starts to become a large compared to the third order spherical aberration. As a further guide, the absolute 3rd and 5th order spherical aberration terms are shown in Figure 2.11(b). This plot shows that the 5th order spherical aberration term exceeds the diffraction limit (a quarter of a wave of spherical aberration) when $F < 4$.

2.4.2 Parabolic Mirrors

Spherical aberration can arise in parabolic mirrors when the illuminating point source of light is not at the focus or at infinity. Although the work in this thesis will concentrate on the correction of spherical mirrors, it may be necessary to consider using a parabolic mirror for spherical aberration correction. The method for incorporating such correction will be explained in more detail later. For now, I will simply present the relevant equations.

Unlike a spherical mirror where the reference ray is the radius of curvature R, the only quantity which does not vary with increasing aperture in a parabolic mirror is the focal length, f. As a result, the spherical aberration will be presented in terms of semi-aperture, ρ, and focal length, f.

(a).

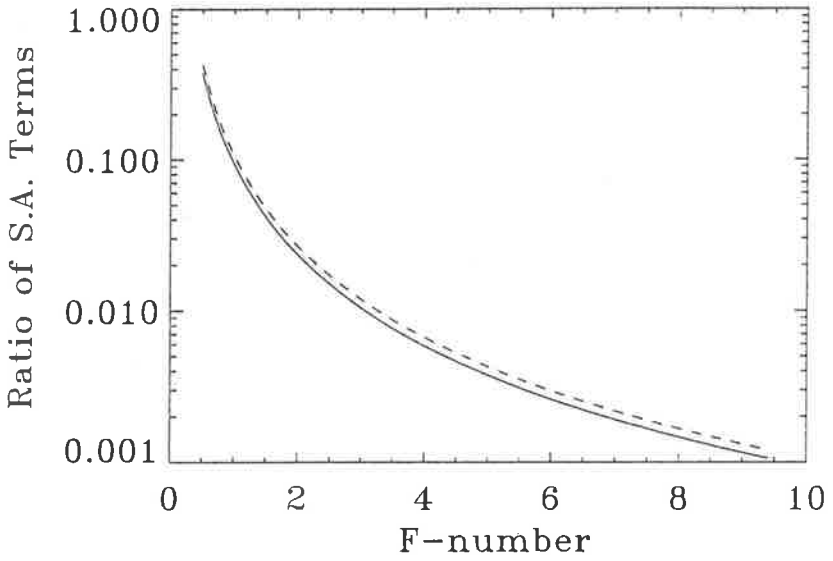

(b).

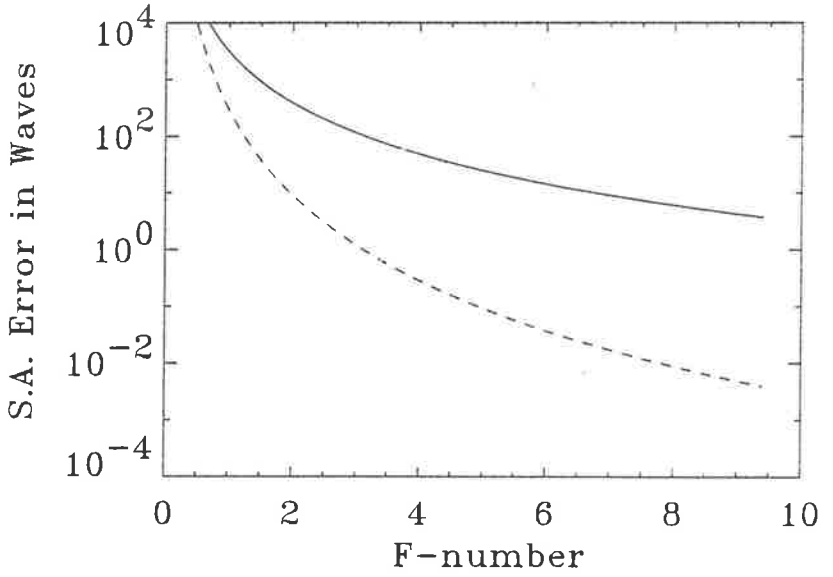

Figure 2.11: Spherical aberration for a 1m diameter spherical mirror and an object distance of $y = \infty$: (a). A plot of the ratio of the 5th order to 3rd order spherical aberration terms (solid line) and 7th to 5th order terms (dotted) as a function of mirror speed. (b). The absolute spherical aberration is evaluated under the same conditions (with $\lambda = 632.8$nm). 3rd order spherical aberration term is plotted as the solid line and 5th order term as the dotted line.

For a beacon at distance y from the mirror, the image point will lie at y', given by;

$$\frac{1}{y'} + \frac{1}{y} = \frac{1}{f} - \frac{\rho^2}{2fyy'}\left[1 + \frac{\rho^2}{8f^2yy'}\right] \tag{2.29}$$

$$\Rightarrow \quad y' = \frac{8f^2\rho^2 + \rho^4 + 16f^3y}{16f^2(y-f)} \tag{2.30}$$

These equations are equivalent to those shown previously for a spherical mirror (Eqs. 2.20 & 2.21). Once again, for the paraxial case, $\rho \to 0$, we have the normal image equation; $1/y' + 1/y = 1/f$. The longitudinal and transverse spherical aberration relations are

$$LSA = \frac{8f^2\rho^2 + \rho^4}{16f^2(y-f)} \tag{2.31}$$

$$TSA = \frac{8f^2\rho^3 + \rho^5}{16f^3y + 12f^2\rho^2 - 4fy\rho^2 + \rho^4} \tag{2.32}$$

From these, the corresponding wavefront aberration can be found using Eq. 2.27. The following is a series expansion to 5th order;

$$W_{3+5} = \frac{(y-f)\rho^4}{8f^2y^2} - \frac{(2f-y)(y-f)\rho^6}{32f^4y^3} + \ldots \tag{2.33}$$

Naturally, as $y \to \infty$ or $f \to 0$ then $W \to 0$.

2.5 Summary

In this chapter, equations for both the holographic correction and geometrical aberrations have been presented. In the first instance, the derivation of a "correction factor" has resulted in an expression which will be useful in analysing the correction achievable with a given recording beacon position and reconstructing wavefront. The general nature of this formula will allow most schemes to be analysed to predict the extent of the correction.

As well as the surface aberrations of the mirror, there are the ray aberrations

from the recording and replay geometries. In most cases the third order Seidel coefficients should suffice in determining the amount of introduced wavefront error, but with very fast mirrors and large off-axis angles, higher order terms should be considered. In such cases a commercial optical ray-tracing program will be used. For spherical aberration, however, an exact expression has been derived for the wavefront error introduced with a spherical or parabolic mirror illuminated from any arbitrary distance y.

Chapter 3

The Off-Axis Beacon

3.1 Introduction

There are many possible schemes for the recording and subsequent replay of the hologram. I decided that one design which had some potential would involve off-axis recording with on-axis replay. This chapter will present a discussion of the concept along with a theoretical analysis and experimental results.

3.2 The Design Concept

To holographically correct an aberrated mirror, it is necessary to illuminate the surface and interfere the reflected light with a reference beam. To do this, the beacon must be placed in front of the mirror with the reflected light forming the object wave to be recorded. On reconstruction, collimated light will be incident on the mirror on-axis, and thus the recording optics will be in the way. These optics must either be removed after recording or a scheme must be developed with the recording optics situated outside the useful aperture of the telescope. The off-axis design uses the second approach.

The basic concept for the recording and reconstructing of the hologram is shown in Figure 3.1. On recording, a spatial filter (beacon) is placed off-axis from the centre of curvature, at edge of the mirror aperture (Figure 3.1(a).). The beacon illuminates the mirror and the light is reflected to a conjugate point on the opposite side of the

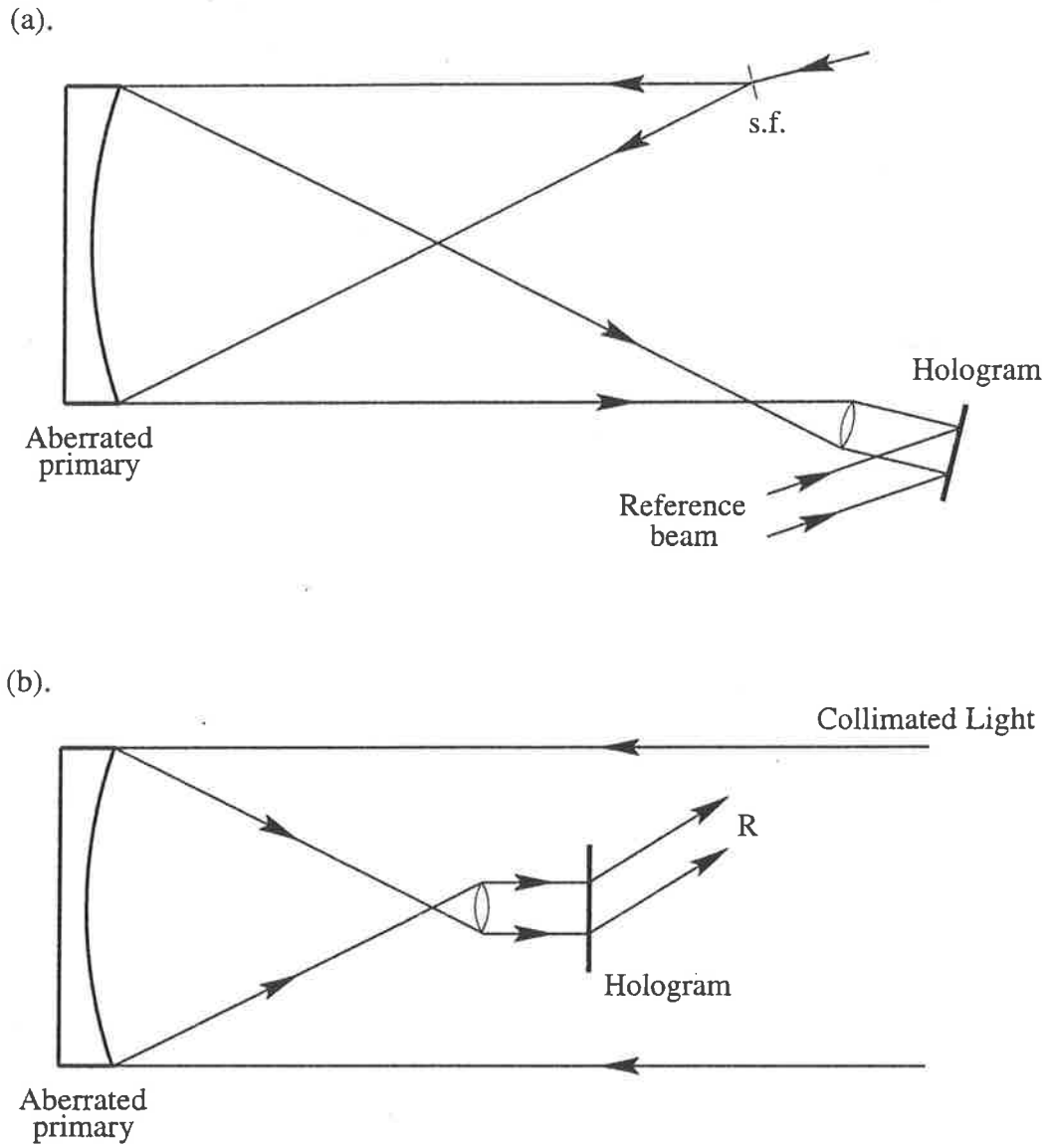

Figure 3.1: (a). Recording: A spatial filter (s.f.) is placed at the edge of the mirror aperture at the radius of curvature. The reflected light is collimated and used to form an image of the mirror at the plate. (b). Replay: Collimated light, focussed by the mirror, is re-collimated by an appropriate imaging lens to reconstruct the hologram, producing a diffracted beam (R).

aperture. The light is then collimated by a lens which images the mirror surface onto the plane of the hologram. The holographic plate is placed perpendicular to the incident object beam. A hologram is formed by recording the interference pattern between this beam and a diffraction limited, collimated reference beam.

For reconstruction (Figure 3.1(b).) the processed hologram is moved to a holder at the focal plane of the mirror. Incident collimated light will reflect off the mirror and pass through a lens which images the mirror onto the plate *with the same image size as in the recording stage.* On replay, this object wave will reconstruct the original reference beam. It is important to ensure that the size and orientation of the image, formed at the plate, stays constant so that the image of the aberrated mirror on reconstruction is congruent to recorded image.

The advantages to this concept are apparent when we look at the correction achieved over various parts of the mirror. As discussed in Chapter 2, the magnitude of the correction factor varies with the difference in angle that a ray from the recording beacon and a reconstructing ray make to the mirror normal. As with most telescopes, the viewing (or reconstruction) will be on-axis. In this scheme, rays from the beacon strike the outer edge of the mirror at the same angle as the rays from the reconstructing starlight (Figure 3.2(a).), thus the correction is a maximum here. At the centre, the rays from the recording beacon make some angle with the mirror but the starlight is incident along the optical axis (Figure 3.2(b).). The maximum angular difference between them implies a minimum correction in this region. The best correction occurs around the edge of the mirror which is the largest collecting area. Added to this is the fact that the inner portion of the mirror will be obscured by the secondary optics (either a flat pick-off mirror or the imaging optics and hologram themselves), so it makes sense to have the minimum correction here.

The disadvantage of this scheme is the introduction of a large amount of off-axis aberration on recording which is not present during the on-axis reconstruction. The main off-axis aberration is astigmatism. Third order coma is not a problem for a beacon at the centre of curvature and so even in this scheme the system is virtually aplanatic. It was initially thought that the astigmatism could be removed from the reconstructed beam with the use of tilted or cylindrical lenses or even computer

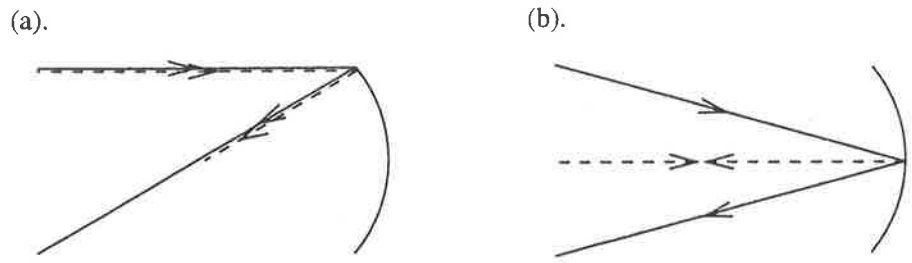

Figure 3.2: (a). A ray from an off-axis beacon (solid) makes the same angle to the mirror edge as the collimated light on reconstruction (dashed). (b). In the centre of the mirror these rays have their maximum angular difference.

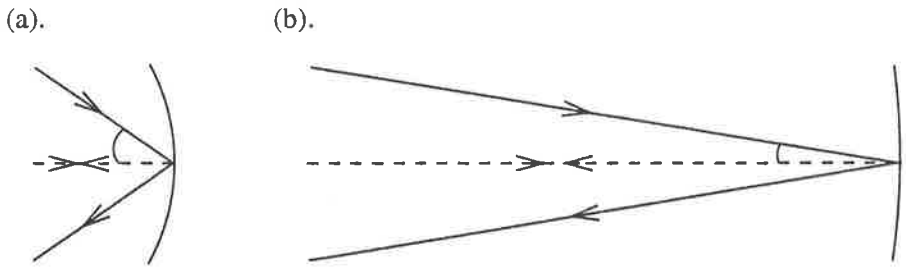

Figure 3.3: (a). A ray from an off-axis beacon (solid) makes a large angle to the centre of a fast mirror, compared to the on-axis light on reconstruction (dashed). (b). For a slower mirror, this maximum angular difference is reduced.

generated holograms.

If the speed of the mirror is decreased, the correction improves due to the decrease in the angular difference between the recording and reconstructing beams (Figure 3.3). Unfortunately, this increase in F-number, lengthens the telescope and the compactness of this design suffers. Optimisation of the acceptable length of the final instrument and the severity of the aberrations initially present will be necessary for individual requirements.

3.3 A Theoretical Analysis

In the previous chapter an expression was derived for the correction obtained with a given beacon position (Eq. 2.9). In this off-axis design, the beacon is placed at the edge of the mirror aperture ($x = \rho$) at a distance equal to the radius of curvature of the mirror ($y = R$) which simplifies Eq. 2.9 to;

$$\Delta = \frac{\lambda' \left(\rho u + R^2\right)}{\lambda \left((R - z)\cos\phi - [u\cos\delta + v\sin\delta]\sin\phi\right)\sqrt{\rho^2 + 2\rho u + R^2}} - 1 \qquad (3.1)$$

This equation allows for the full analysis of the many permutations of off-axis reconstruction angle and wavelength. For the case of on-axis reconstruction ($\delta = \phi = 0$) at the recording wavelength ($\lambda = \lambda'$):

$$\Delta = \frac{\rho u + R^2}{\sqrt{(R^2 - u^2 - v^2)(\rho^2 + 2\rho u + R^2)}} - 1 \qquad (3.2)$$

In terms of mirror speed ($F = R/4\rho$),

$$\Delta_F = \frac{\rho u + 16\rho^2 F^2}{\sqrt{(16\rho^2 F^2 - u^2 - v^2)(\rho^2 + 2\rho u + 16\rho^2 F^2)}} - 1 \qquad (3.3)$$

A plot of how the correction varies across the face of the mirror aperture is shown in Figure 3.4(a). In this case the mirror has a radius of curvature of 5.2m and diameter of 0.86m. Notice that the relative phase difference is at a maximum in the centre, ($\Delta = 0.0034$), and the correction factor is at a minimum ($\Delta^{-1} = 1/0.0034 = 294$). This means that even at the centre, the height of a bump will be reduced by a factor of 294. The second graph, Figure 3.4(b). shows how the correction factor changes with the speed of the mirror. The correction factor is calculated for the centre of the mirror ($u = 0, v = 0$) over a range of mirror F-numbers. As illustrated in Figure 3.3, the slower the mirror (the larger the F-number). the smaller the angular difference between the beams on recording and replay and thus the correction in the centre improves.

Not only are we concerned with the on-axis correction, but any practical scheme must give rise to a finite field of view. In Figure 3.5 we can see the effect of the

(a).

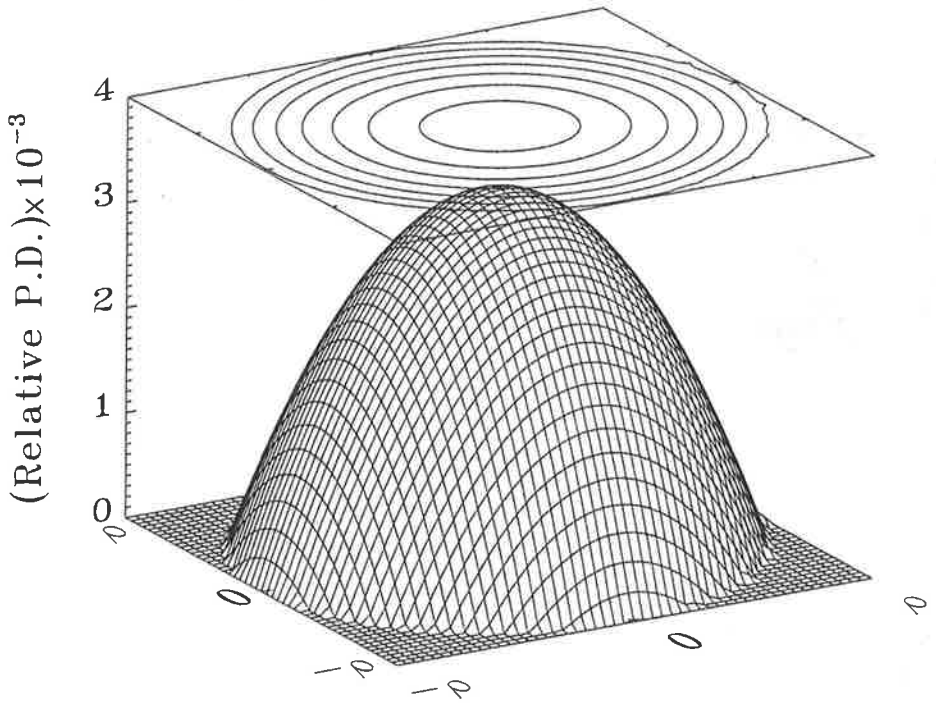

(b).

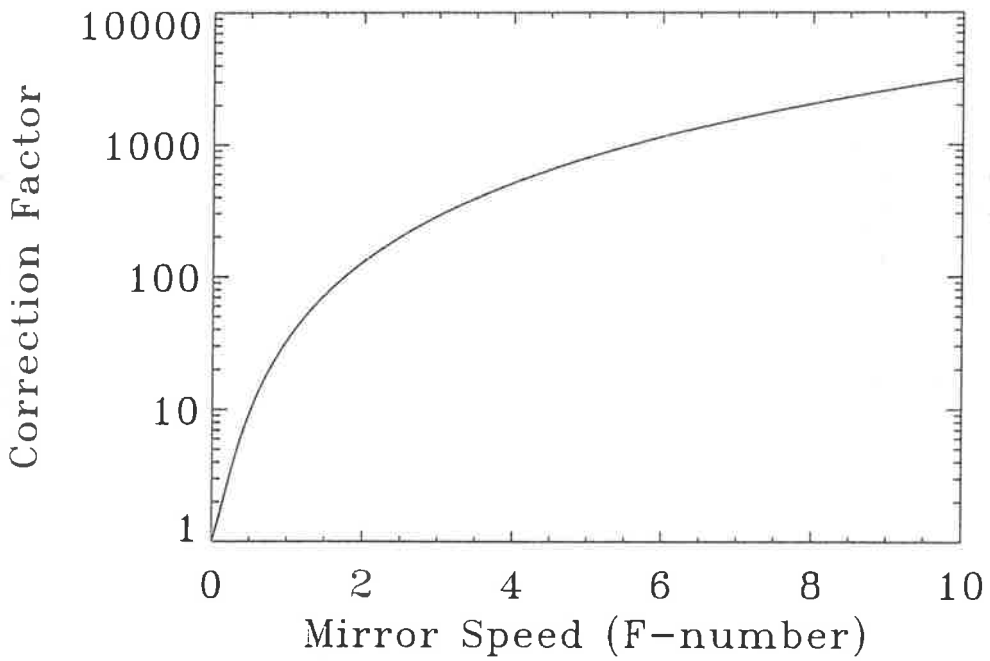

Figure 3.4: (a). The relative phase difference (Δ) shown as a function of mirror aperture for a mirror with $R = 5.2$m, $\rho = 430$mm, $x = \rho$ and $y = R$. (b). How the correction factor (Δ^{-1}) varies with mirror speed at the centre of a mirror with the same diameter and relative beacon position.

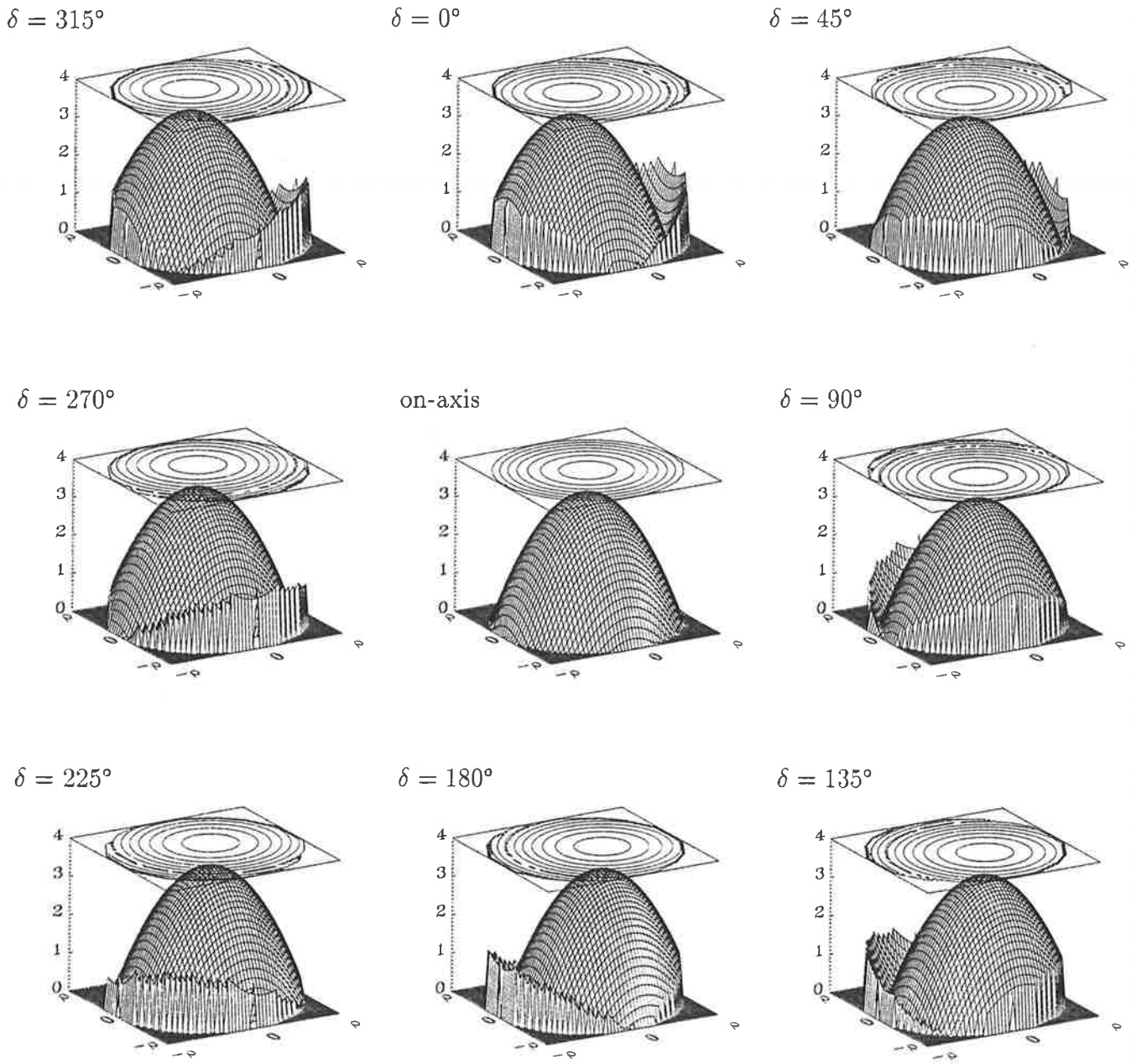

Figure 3.5: These plots show the effect of a finite field angle on the relative phase difference ($\times 10^{-3}$) over the mirror surface. The mirror has dimensions $R = 5.2$m and $\rho = 0.43$m and the off-axis beacon has a direction angle of $\delta = 270°$). The central graph shows the on-axis reconstruction ($\theta = 0°$ and the surrounding graphs have a constant field angle of $\theta = 1°$ with various direction angles.

off-axis angle on the relative phase difference over a field of $\phi = 1°$ and various values of δ. The correction factor seems to be largely unaffected, even with such a large field angle, so it would seem that a large field of view can be expected. It is important to note, however, that the correction factor means little without first knowing the extent of the aberrations present on the mirror. The final image formed by the telescope will depend, ultimately, on the surface error remaining after the holographic correction, as well as the off-axis geometrical aberrations which will appear as a natural consequence of the finite field angle.

3.4 Small Scale Experiment

To test the off-axis correction scheme, a small scale experiment was carried out with a near-diffraction limited spherical mirror ($f = 0.68$m, $\rho = 66.5$mm) with a 3mm thick piece of warped glass placed in front to provide the distortions. The recording scheme is shown in Figure 3.6(a). With the glass plate removed the image spot of the beacon showed a large amount of astigmatism. To correct for this astigmatism, a tilted, off-axis achromatic lens ($f = 0.3$m) was placed in the path of the reflected beam. The position and orientation of the lens was adjusted until the spot had a minimum aberration remaining, as observed using a microscope. The glass aberrator was then put in place against the mirror. It is important to note that the glass plate had to be fairly thin to avoid the problem of a "thick aberrator". Also, a plane glass slab will introduce astigmatism to a transmitted beam. The thinner the glass, the smaller the astigmatic wavefront error introduced. The reflected light was collimated by an achromatic doublet ($f = 0.2$m) which imaged the mirror's surface on the plane of the hologram. A hologram was recorded with a plane wave reference beam. The method used in recording the holograms in this experiment (as in all the experiments) is outlined in more detail in Appendix A. A photo of the mirror/aberrator combination is shown in Figure 3.7 along with an interferogram of the wavefront produced with an incident collimated plane wave.

On reconstruction, the set-up was as shown in Figure 3.6(b). A collimated plane wave was produced with a spatial filter at the focal point of a Jaegers achromatic

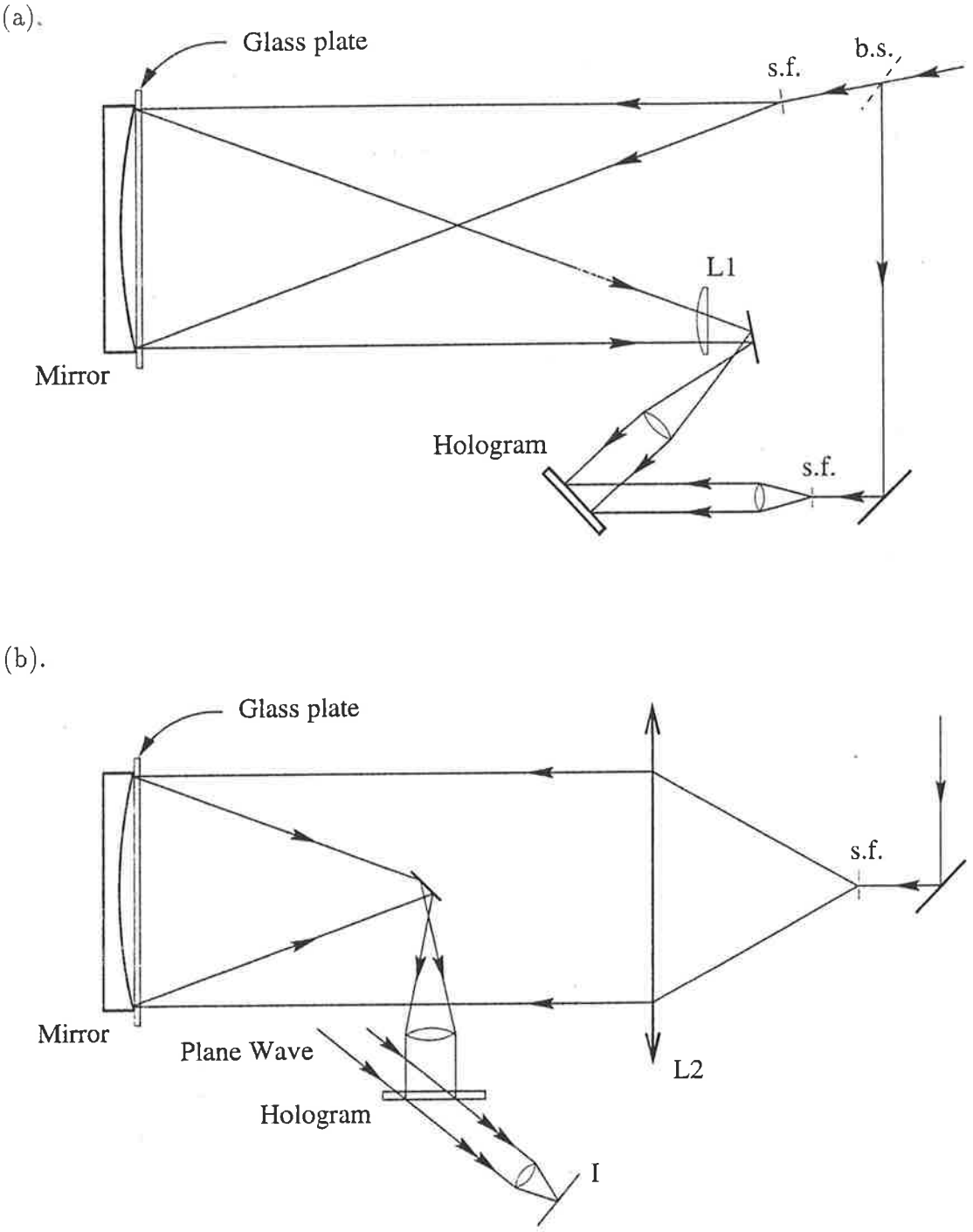

Figure 3.6: (a). Recording: A spatial filter (s.f.) illuminates the mirror with the glass plate attached. The tilted lens L1 corrects for the off-axis aberrations. A hologram is recorded with a path matched plane wave reference beam. (b). Reconstruction: A diffraction limited achromatic doublet lens (L2) is used to produce a plane wave incident on the mirror. The reconstructed reference beam is interferometrically tested against a known plane wave and the resulting pattern is focussed so that the mirror surface is imaged at I.

(a).

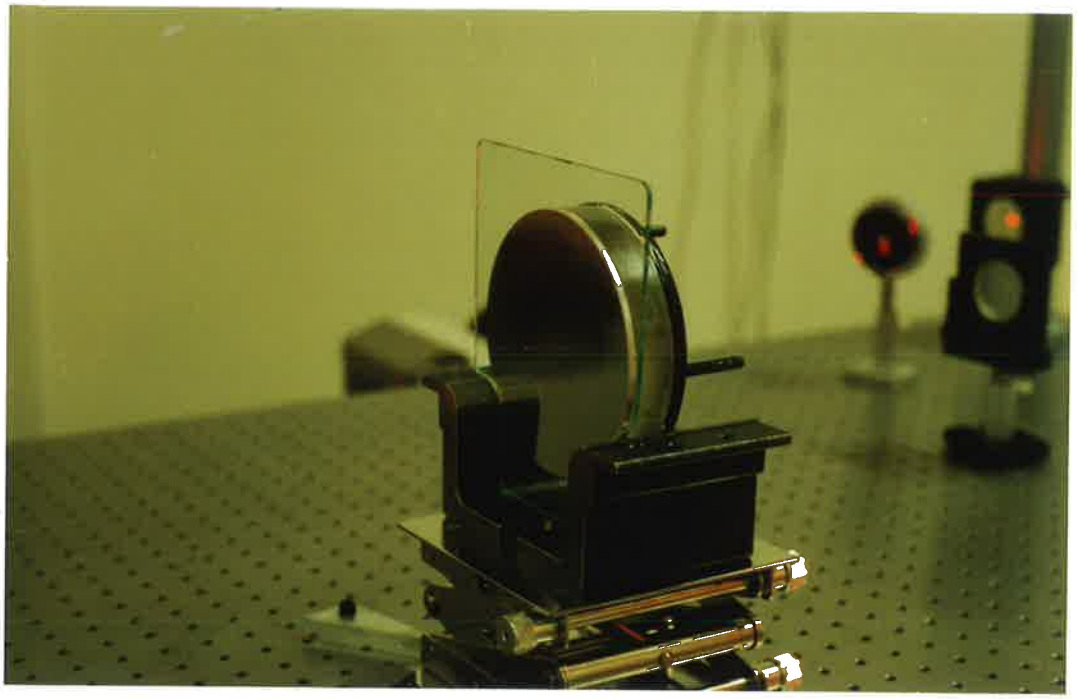

(b).

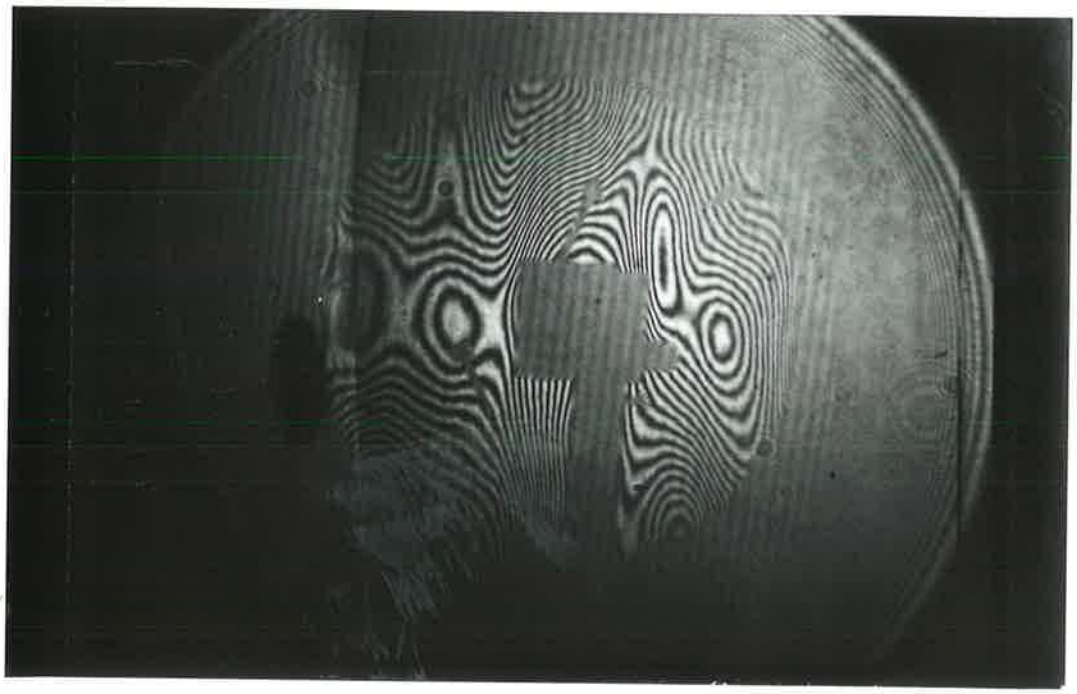

Figure 3.7: (a). A photo of the glass aberrator/mirror combination. (b). Before correction: The interference pattern shows the wavefront error on reflection from the aberrator/mirror combination.

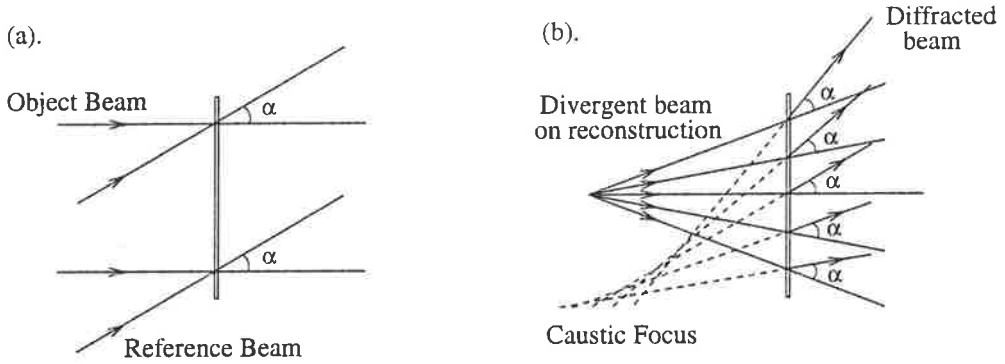

Figure 3.8: (a). On recording the two beams are collimated. (b). On replay the object beam has some divergence. Due to the diffraction condition at the plate the reconstructed wave diverges from a virtual caustic focus.

doublet (D = 125mm, f = 0.6mm). This lens was interferometrically null tested with another identical lens and showed no detectable spherical aberration. The collimated beam produced in this case is thus taken to be diffraction limited. The plane wave entered the telescope on-axis and reflected off the mirror/aberrator combination. Once again, the light has double passed the aberrator, but in this case it was on-axis. The hologram was moved from its off-axis recording position to an on-axis position at the focal plane of the mirror where the reconstruction took place. The eyepiece achromatic doublet was selected in such a way as to match the image magnification in the recording procedure.

The second restriction is that the object beam have the same divergence at the plate on reconstruction as on recording. The reason for this can be shown with the aid of Figure 3.8. Two beams interfere with a constant angle α between them to form a hologram. On reconstruction, any object beam rays reaching the hologram will be diffracted through a constant angle α. If a divergent object beam is used, these rays will not diverge from a common virtual point but some caustic surface. The result is an aberrated reconstructed reference beam. This wavefront aberration will be introduced whenever the reconstructing beam has a different divergence to the recording beam. In general, with the hologram recorded at twice the focal distance from the mirror, and the reconstruction at the focal plane, the speed of the imaging

system is doubled. If the image magnifications are to match in both cases, then the angular divergence of the object beam on reconstruction will be double that on recording. The only way they can be made equal is if the divergence in both cases is zero, *i.e.* they are collimated. Thus in all the tests to be described in this thesis, the object beam will be collimated by the imaging optics before reaching the plate.

The image of the mirror was formed using an achromatic doublet ($f = 0.1$m). The alignment of the hologram with the image of the mirror at this new position was made possible by the addition of fiducials (shapes cut out of tape) applied to the surface of the glass plate. Once aligned, the object beam incident on the hologram produced a diffracted beam which should have been a diffraction limited plane wave. This beam is diffracted at an angle from a hologram which is circular in cross-section and as a result, the beam will have an elliptical profile. This aspect ratio is corrected by passing the beam through a prism.

The reconstructed wavefront was tested interferometrically against a plane wave and as the holographic plate was expected to introduce some wavefront distortions of its own, these were cancelled out by passing the reference beam through the plate, collinear with the diffracted beam. The results are shown in Figure 3.9. The wavefront error has been reduced to $W_{p-v} = 0.36\lambda$ or $W_{rms} = 0.086\lambda$, with the reconstructed wavefront as shown in Figure 3.9(b) (see Appendix C for more details on how this wavefront is generated from the interferometric data).

Total correction had not been achieved. The expected minimum correction factor (using Eq. 3.2) is 840, which should be large enough to reduce the maximum wavefront error to better than $\lambda/50$. In this case, however, the correction factor does not tell the whole story. The use of Eq. 3.2 assumes that the aberrations form part of the mirror surface. In this set-up, however, the flat aberrator is distinct from the mirror surface, resulting in a separation between the glass and the mirror which increases towards the centre. During the off-axis recording the light incident near the center of the mirror double-passed slightly different sections of the aberrator to that on reconstruction. Nearer to the edge, this is less of a problem as the angle of the light on recording matches that on reconstruction. This difference in recording and replay aberrations cannot be accounted for in the previous calculations. Since

(a).

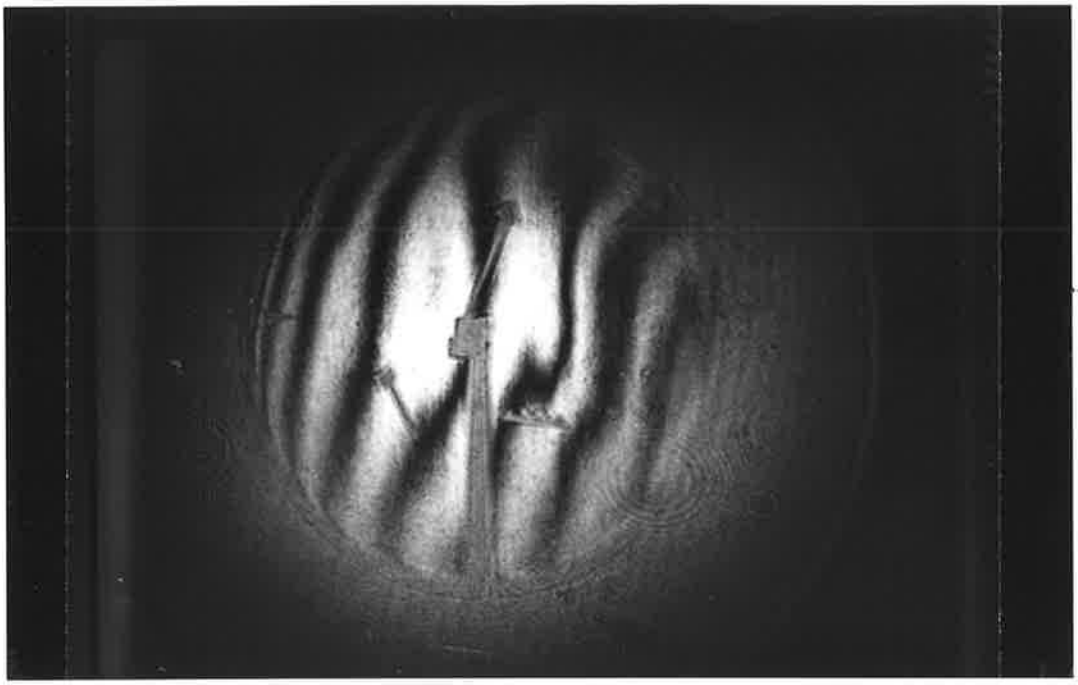

(b).

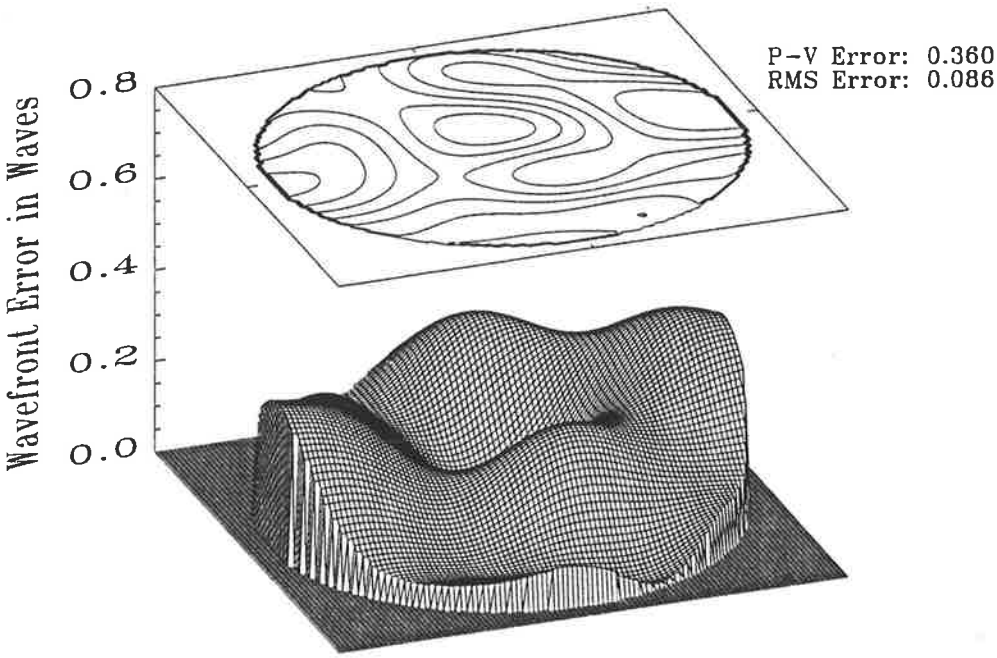

Figure 3.9: (a). An interferogram of the corrected wavefront (*c.f.* the uncorrected pattern shown in Figure 3.7(b).) (b). A reconstruction of the wavefront calculated using the interferogram shown in (a).

the "after" photo shows that the correction does fail towards the centre it seems to suggest that this is indeed the problem. Given the qualified success of this experiment, a more realistic test was performed using a larger diameter. aberrated mirror.

3.5 Large-Scale Experiments

3.5.1 The Large Mirror

In order to test the correction on a larger scale, a large imperfect mirror was required. The BIGRAT telescope, run by the Cosmic Ray Group of this university. is a multi-mirror telescope which uses slumped-glass mirrors as light collectors [16]. Using their equipment it was possible to slump and coat large diameter, low-quality mirrors. The process involves placing a circular piece of 12mm thick float glass over a concave, cast iron mould which has the rough shape of the desired mirror. The whole arrangement is heated in an oven until the glass sags into the mould and is then allowed to cool. When the glass is removed from the mould, the concave, inner surface is coated with aluminium in a vacuum chamber. Using this technique I made several spherical mirrors up to 0.86m in diameter with a focal length of $\sim$2.6m.

Figure 3.10 shows two photos which give an indication of the quality of the central 0.45m diameter section of the large mirror. The first is a through-the-focus contact print of the one-to-one imaging of a 10μm diameter pinhole (a spatial filter beacon illuminating the mirror from the radius of curvature). The astigmatic error is very evident from the change in the tilt of the elongated spot. The second photo is an enlargement of the focussed spot of an incident diffraction limited collimated beam (0.45m diameter). The magnification factor is about 15 (*c.f.* the diffraction limited central Airy image, at the same magnification, would be only 150μm in diameter).

As a further test, the focussed light was collimated and made to interfere with a diffraction limited plane wave. The interferogram produced, imaged to the mirror surface, is shown in Figure 3.11.

Several features are immediately apparent. The first is that the mirror seems to have several concentric "rings". These are mostly likely a result of the top surface

(a).

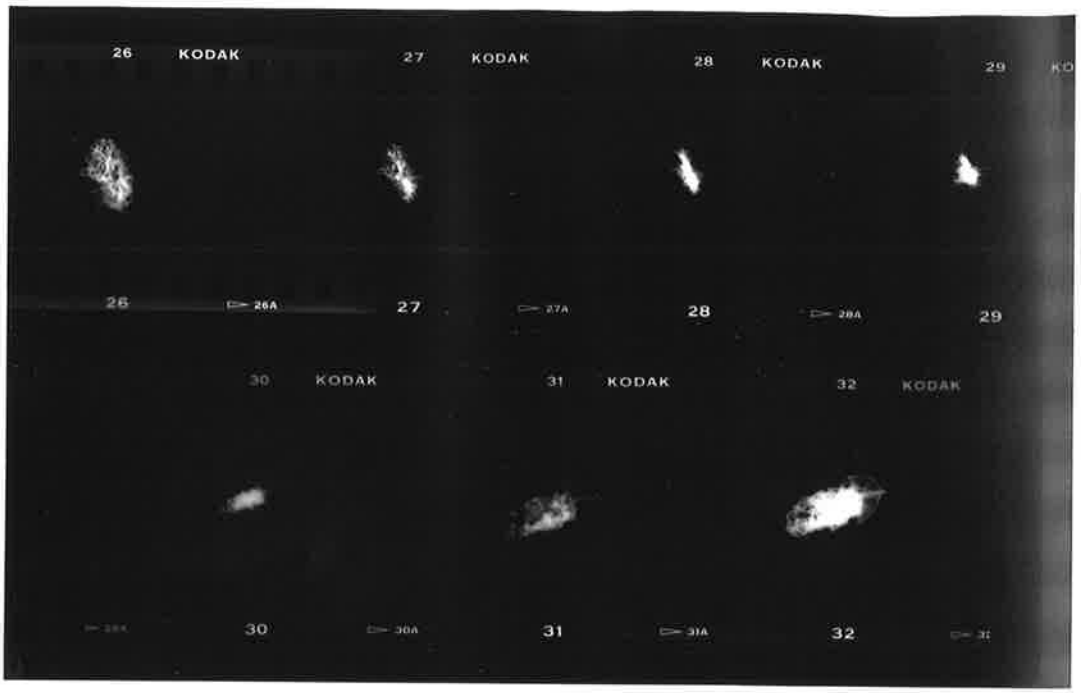

(b).

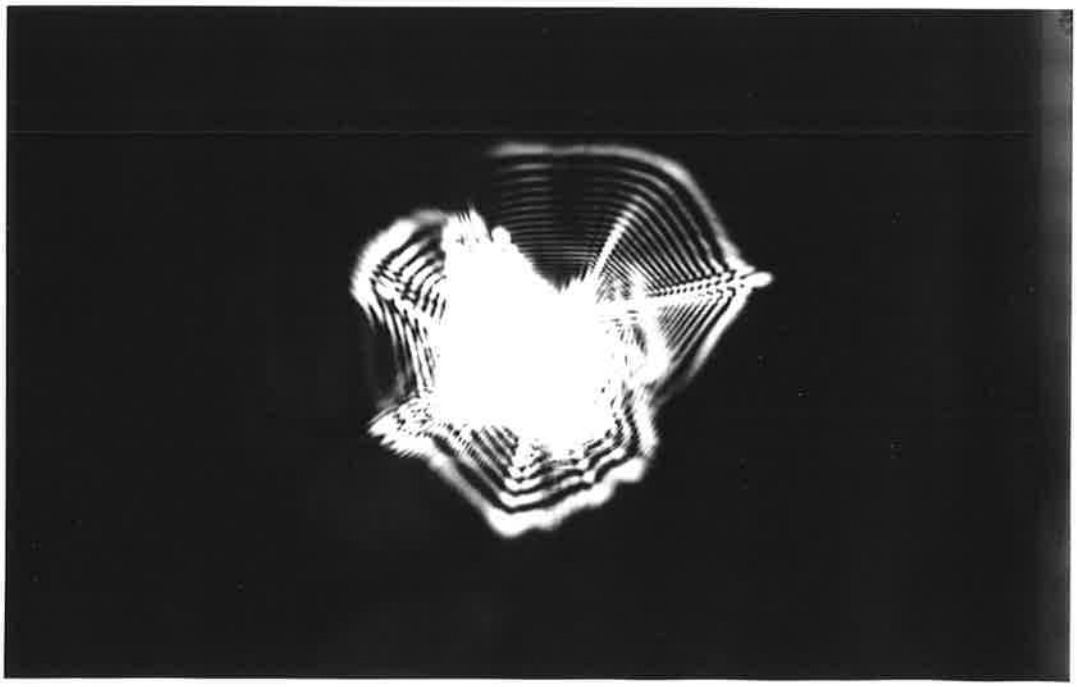

Figure 3.10: The central 0.45m diameter section of the large mirror: (a). Through-the-focus, one-to-one imaging of a 10μm pinhole (true size). Notice the astigmatic focus which is elongated in one direction and then in the perpendicular direction. (b). A photo of the focal spot magnified 15 times.

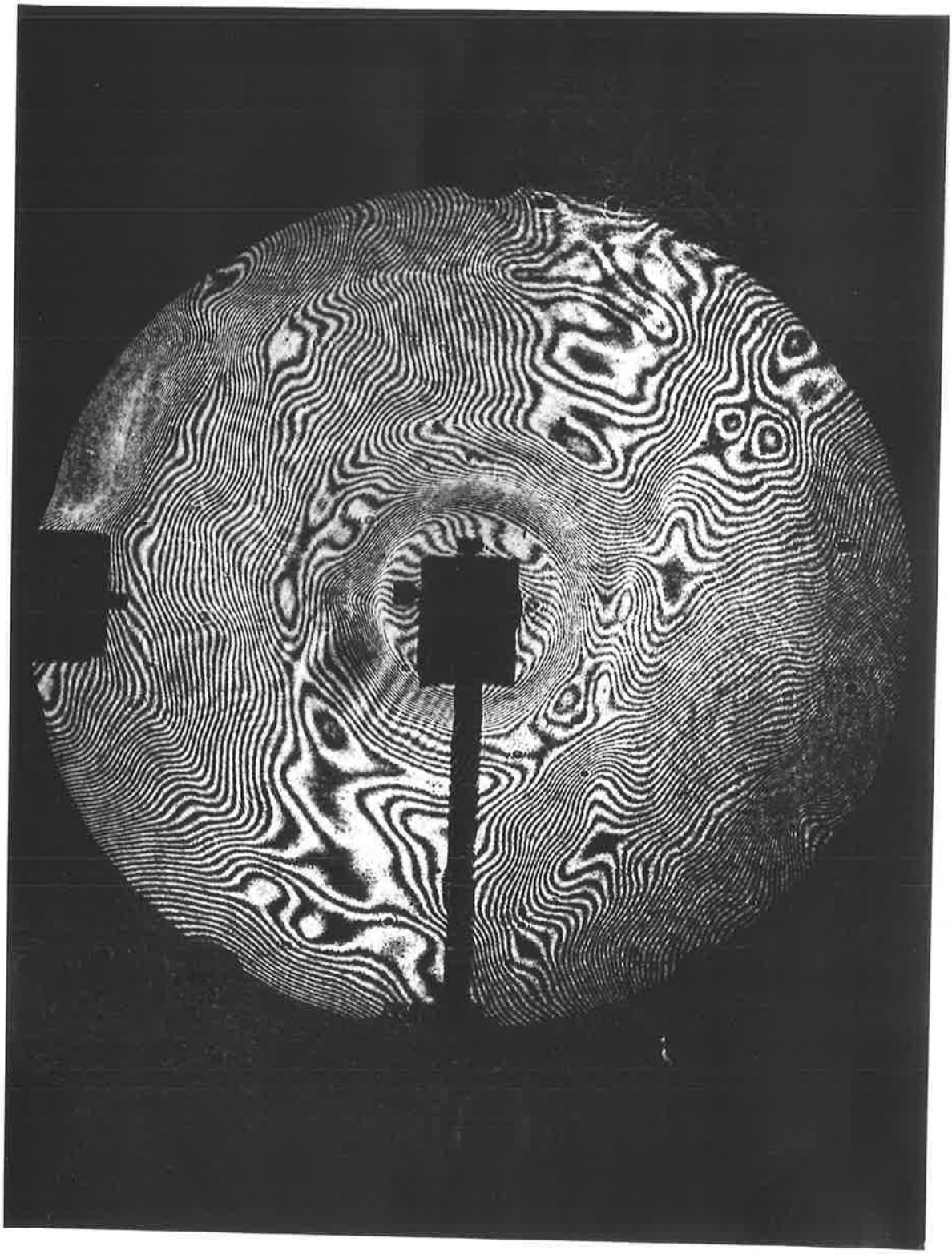

Figure 3.11: An interferogram of the central 450mm section of the mirror surface, taken at the focal plane.

of the glass folding and buckling as it slumps into the mould. The other feature evident in the interferogram is the excess of fringes in one direction (about 45° to the vertical) compared to that in the perpendicular direction. This indicates that the mirror has a slight cylindrical error along the axis of minimum fringe. Further evidence comes from the image spot (Figure 3.10(b)) which shows an elliptical shape in one direction changing to an elliptical shape in the perpendicular direction with increasing distance from the mirror. This is typical of an astigmatic focus as would be expected for such a surface error. With holographic aberration correction, this error is just as correctable as any random aberration, so long as the phase error can be correctly recorded and reproduced on reconstruction. As a result, thin mirrors (which would normally sag under gravity) can be used in a holographically corrected telescope, since any original overall figure errors as well as subsequent changes in shape due to gravitational sag of the primary, can be recorded and corrected.

The radius of curvature of the mirror is $\sim$ 5.2m, and the length of the optical bench is 3.6m, so an extension to the table had to be made which would allow for holographic recording of the mirror. The final design had the large mirror sitting on the end of a cantilever (see Appendix A for more details). To provide common-mode rejection of the cantilever vibrations, the reference beam, in all of the large scale tests, was subjected to the same vibrations. To do this, the 5mm diameter laser beam was reflected off the mirror and then directed through a spatial filter, which removed any small wavefront aberrations which may have been introduced by both the off-axis angle, as well as the mirror deformations. The light was then collimated to form an aberration-free reference beam.

3.5.2 Recording and Reconstruction

The recording set-up for the holographic correction of the large mirror is shown in Figure 3.12(a) and is basically the same as that used for the small-scale test but without the tilted lens. The correction of the astigmatism with a lens was not incorporated in the recording because it is now not possible to separate the mirror aberrations from the off-axis aberrations. As such, it would be impossible to know if the correct position and orientation of the lens had been found. Also, the off-axis

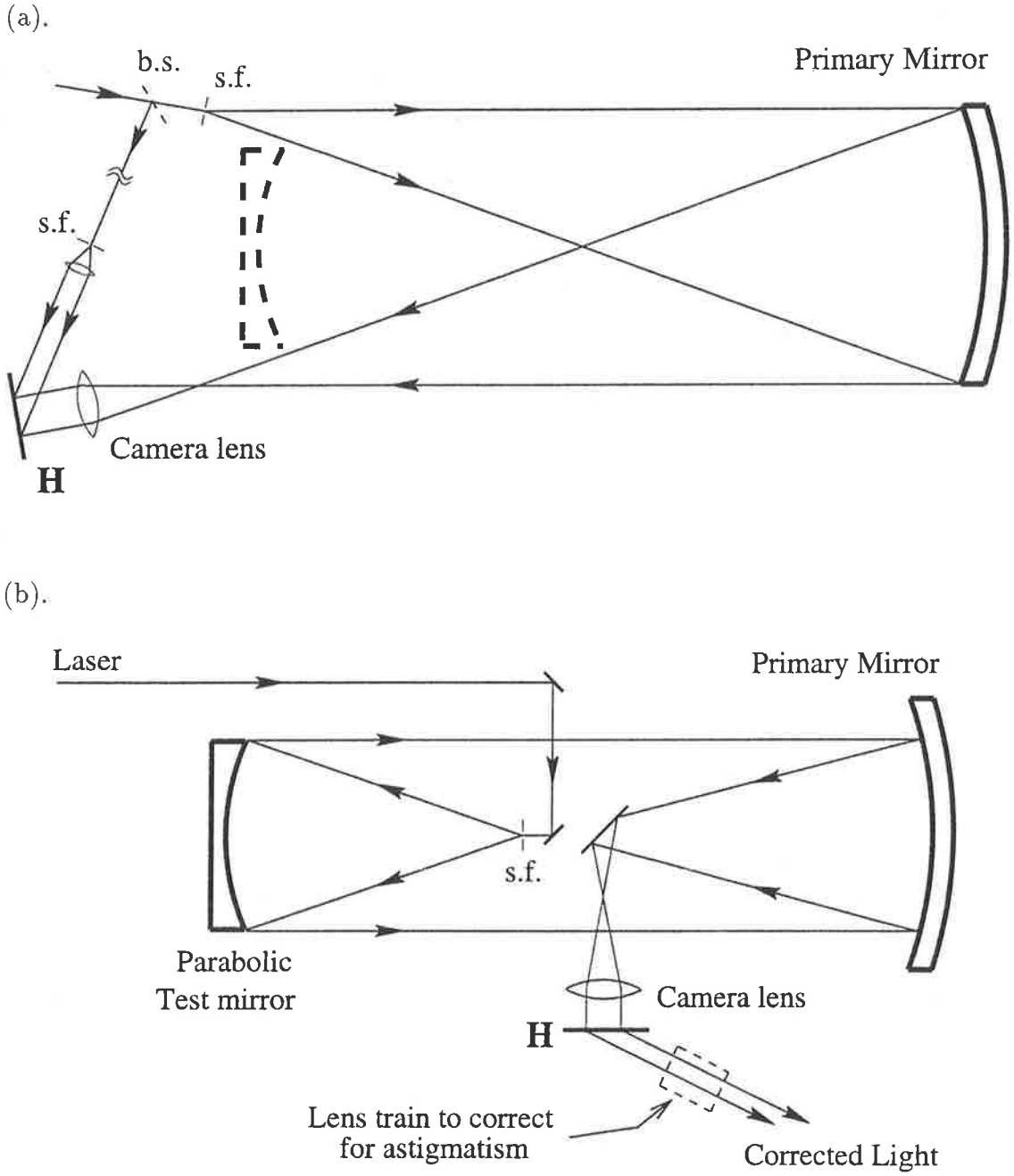

Figure 3.12: (a). Recording: The beacon (s.f.) illuminates the mirror from off-axis. The reference beam is reflected off the primary mirror to reduce the effects of vibrations (not shown). The position of the collimator is shown (dashed). (b). Replay: A collimated beam from the parabolic mirror is reflected off the primary mirror to reconstruct the hologram, producing the diffracted beam. This beam was corrected for astigmatism using a train of lenses.

aberration in this case is much larger than in the small scale experiment and cannot be removed with a single lens.

Once again, the phase holograms were made according to the recipe outlined in Appendix A. The imaging (or eyepiece) lens had a focal length of 100mm for recording and 50mm for replay. In the final set-up, camera lenses were used since they give a reduction in distortion and a flat image field which makes it possible image the entire mirror aperture on the flat holographic plate film. The distortion and curvature of field affect the quality of the recorded image, so it is essential that the amount present in the recorded image is matched in the reconstructed image. A single lens will introduce a large amount of both aberrations, but camera lenses are made to reduce or even eliminate them.

Due to the extremely short depth of focus of camera lenses, the plate had to be placed perpendicular to the object beam to ensure correct matching of the image planes on recording and reconstruction. Obviously, it is important to make sure that the camera lenses are of a high quality over the aperture used to ensure they do not introduce uncommon aberrations into the system. In all the tests performed, the lenses used were interferometrically tested and found to have less than $\lambda/4$ error.

The set-up for reconstructing the hologram is shown in Figure 3.12(b). The collimator in this case was a parabolic mirror ($D = 0.45$m, $f = 2$m). This meant that only the central 450mm diameter section of the corrected mirror could be tested, even though the hologram recorded a larger aperture. Given this restriction, there seemed little point in actually recording a hologram of the entire mirror, so the off-axis recording angle was reduced. The parabolic mirror had to be aligned with the large mirror before recording the hologram, and remained in place during the recording of the hologram. The recording beacon distance of $x = 350$mm was chosen as it was the smallest off-axis distance that would allow unobscured illumination of the large mirror.

3.5.3 The Collimator

The alignment of the collimator is critical. If the spatial filter is not located at the focus of the mirror with sufficient accuracy, spherical aberration or off-axis aber-

rations will be introduced into the system. In the case of the parabolic mirror, a positioning error along the optical axis (Δz) will result in spherical aberration, and a perpendicular ($\Delta x - y$) shift will give rise to a large amount of coma and a smaller amount of astigmatism. Figure 3.13 shows the effect of such shifts, for the parabolic mirror used in these experiments.

The surface quality of the parabolic mirror was documented by the manufacturer (Galaxy Optics), and the results of the interferometric test that they performed are shown in Figure 3.14.

3.5.4 Results

As has been mentioned previously, if the correction is perfect, then the reconstructed reference beam should be a plane wave. The hologram is formed over the circular image of the mirror on the plate. When the reconstructed reference beam diffracts from this region at the original recording angle, the beam will have an elliptical cross-section. The wavefront itself (and any aberrations present) will be subjected to this same change in aspect ratio.

Unlike the small scale experiment, the surface aberrations of the mirror could not be separated from the geometrical aberrations. As such, with no attempt to allow for the recorded off-axis aberrations and spherical aberration on replay, the reconstructed reference beam will have both of these aberrations present.

The primary aberration is astigmatism ($\sim$ 100 waves) with some spherical aberration (7.2 waves) also present. In order to reduce the astigmatism, the reconstructed beam was directed through a series of tilted and decentered spherical lenses as well as cylindrical lenses (Figure 3.15). The optimum position, orientation and focal lengths of the lenses used were found by observing the focussed spot size (at A in the figure) with a microscope and adjusting the conditions until the focal spot was as small as possible. The result was a bright central spot with a minimum diameter $\sim$ 14μm surrounded by a diffuse halo $\sim$ 0.8mm in diameter. This is a dramatic improvement over the original spot size of 8mm as shown previously in Figure 3.10(b). As expected the spot was elliptical and maintained its aspect ratio through the focus. The corrected beam was then collimated and made to interfere

(a).

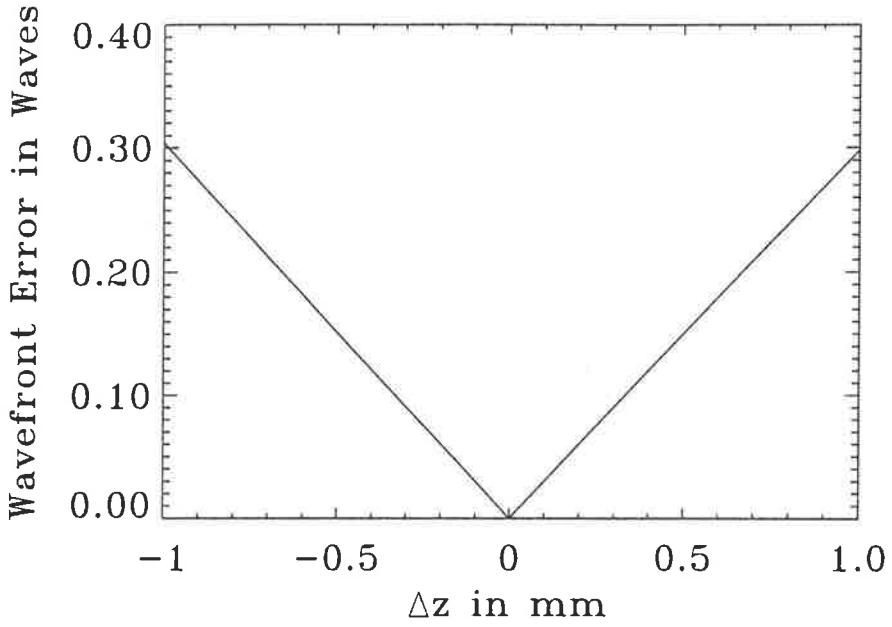

(b).

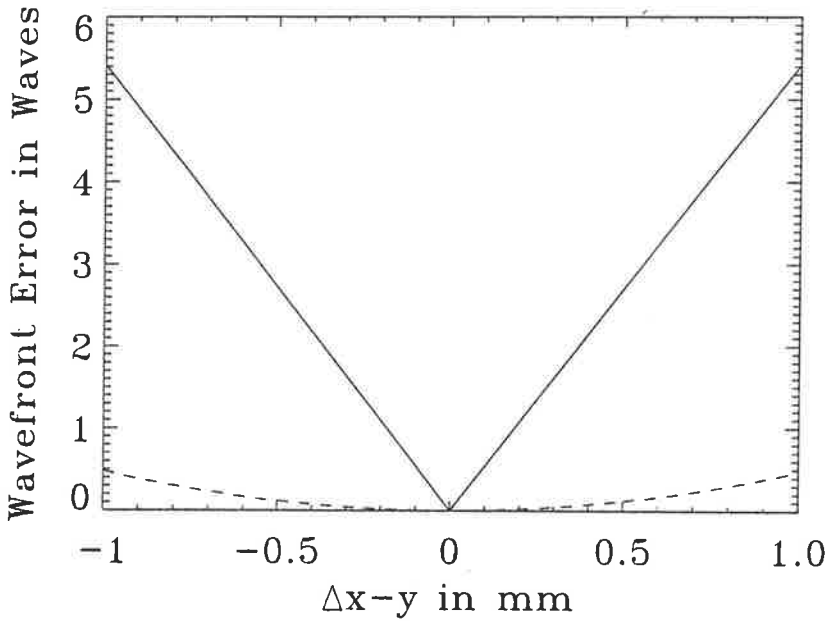

Figure 3.13: (a). The 3rd order spherical aberration wavefront error (@ 632.8nm) resulting from a positioning error (Δz) in the spatial filter along the optical axis. (b). The absolute 3rd order comatic (solid) and astigmatic (dotted) wavefront error from a lateral positioning error ($\delta x - y$). Both cases are for a parabolic mirror, $D = 0.45$m, $f = 2$m and with distances given relative to the true focal position.

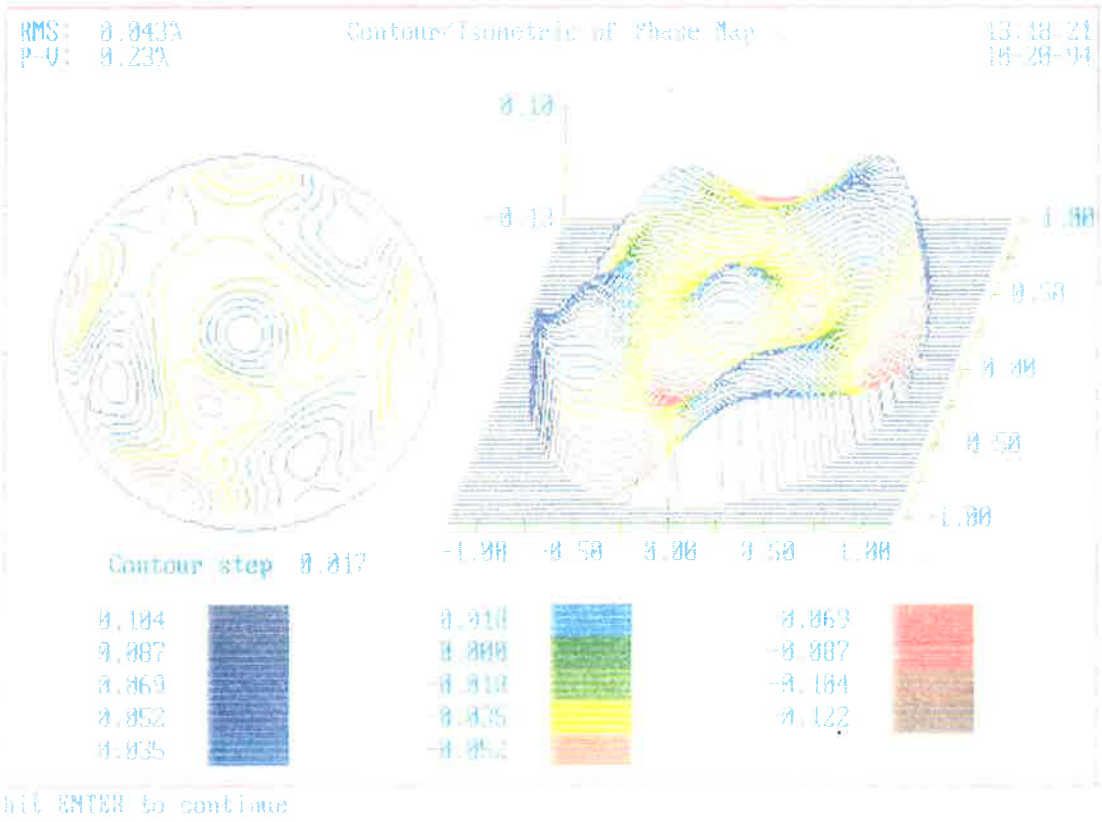

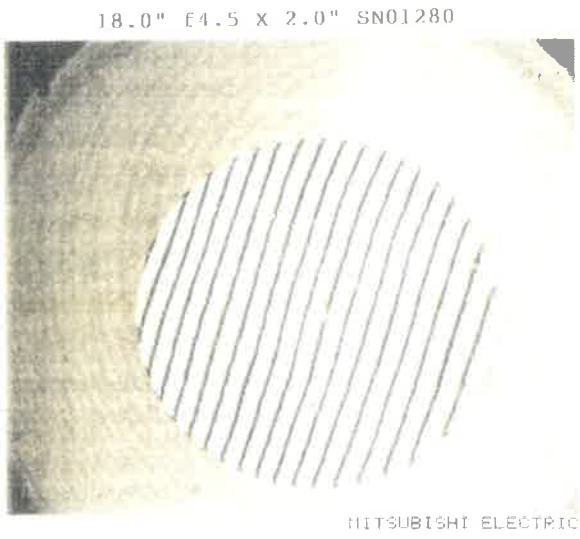

Figure 3.14: Interferometric analysis data from the makers of the parabolic mirror.

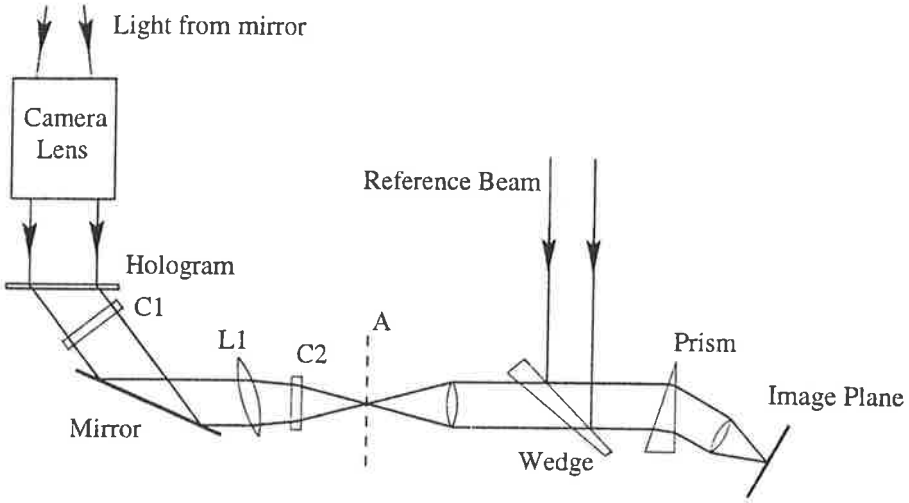

Figure 3.15: The lens train required to produce the minimum spot size (viewed at plane A) is shown. Cylindrical lenses are indicated by rectangular boxes (C1=400mm, C2=250mm). The tilted, decentered lens L1 is a 10cm achromatic doublet. The interferogram is recorded at the image plane of the mirror.

with the original reference beam (Figure 3.16). The interferogram of the uncorrected mirror was shown in Figure 3.11.

The aspect ratio of the interference pattern has been corrected so that it is circular. This was achieved by passing the combined beams through a prism (Figure 3.15). The effect is purely cosmetic since the beams have already been combined and thus they are equally affected by such a change. The combined beams are then passed through a lens which is used to image the plane of the mirror (which is also the plane of the holographic plate) onto the photographic film plane for recording.

The final wavefront error is 7-8 waves, as was expected since no attempt was made to correct for spherical aberration. The amount of spherical aberration calculated for a perfect spherical mirror with the same dimensions as the aberrated mirror is 7.2 waves. The pattern produced should be a series of concentric rings. Since third order spherical aberration has a ρ^4 dependence, we should see an increase in the ring concentration towards the edge. The regular separation of the fringes in Figure 3.16 is caused by the addition of a slight amount of defocus in the object beam. Further evidence that the remaining error is spherical aberration is the appearance of the

Figure 3.16: An interferogram of the corrected aperture imaged to the plane of the mirror surface (*c.f.* uncorrected image in Figure 3.11). This is the diffracted beam, after the lens train.

focussed spot. The beam had a classic spherical aberration profile, with a bright marginal focus surrounded by the diffuse halo of unfocussed marginal rays.

From the regularity of the concentric fringes in the final interferogram, it would seem that the hologram has successfully removed most of the mirror surface aberrations. The remaining fringes deviate by less than half a wave from the regular circular pattern, which would suggest that once spherical aberration has been removed, the remaining error should be just this $\lambda/2$. The correction of the spherical aberration can be achieved in either the recording or reconstruction process.

3.6 Spherical Aberration Correction

3.6.1 Spherical Aberration Removal on Reconstruction

The simplest method of removing the spherical aberration would be to add the required amount of negative spherical aberration to the reconstructed wavefront. This could be done by reflecting the diffracted beam off a spherical convex mirror, passing it through a simple negative lens or by using a specially designed phase retarding screen. The latter method could involve a programmable liquid crystal display. Such an LCD can retard the phase of a transmitted beam through a pixel element by changing the voltage applied to that particular pixel. This idea is being investigated as part of a different research project but it has the problem that it has a limited resolution determined by the finite pixel size. It is also difficult to get a full 2π phase change with these devices. In my experiments I have concentrated on using available, conventional optics for the whole of the aberration correction scheme. This was seen as essential in maintaining the simplicity and immediate scalability of any successful design.

The reconstructed beam is elliptical and most common optics have a circular cross-section which will result in the correct amount of spherical aberration being added in one direction only. In order to see if any reduction in wavefront aberration could be achieved using this approach, I passed the elliptical beam through a simple negative lens at such a beam diameter and divergence as would balance the expected spherical aberration. The result is shown in Figure 3.17 and represents the minimum

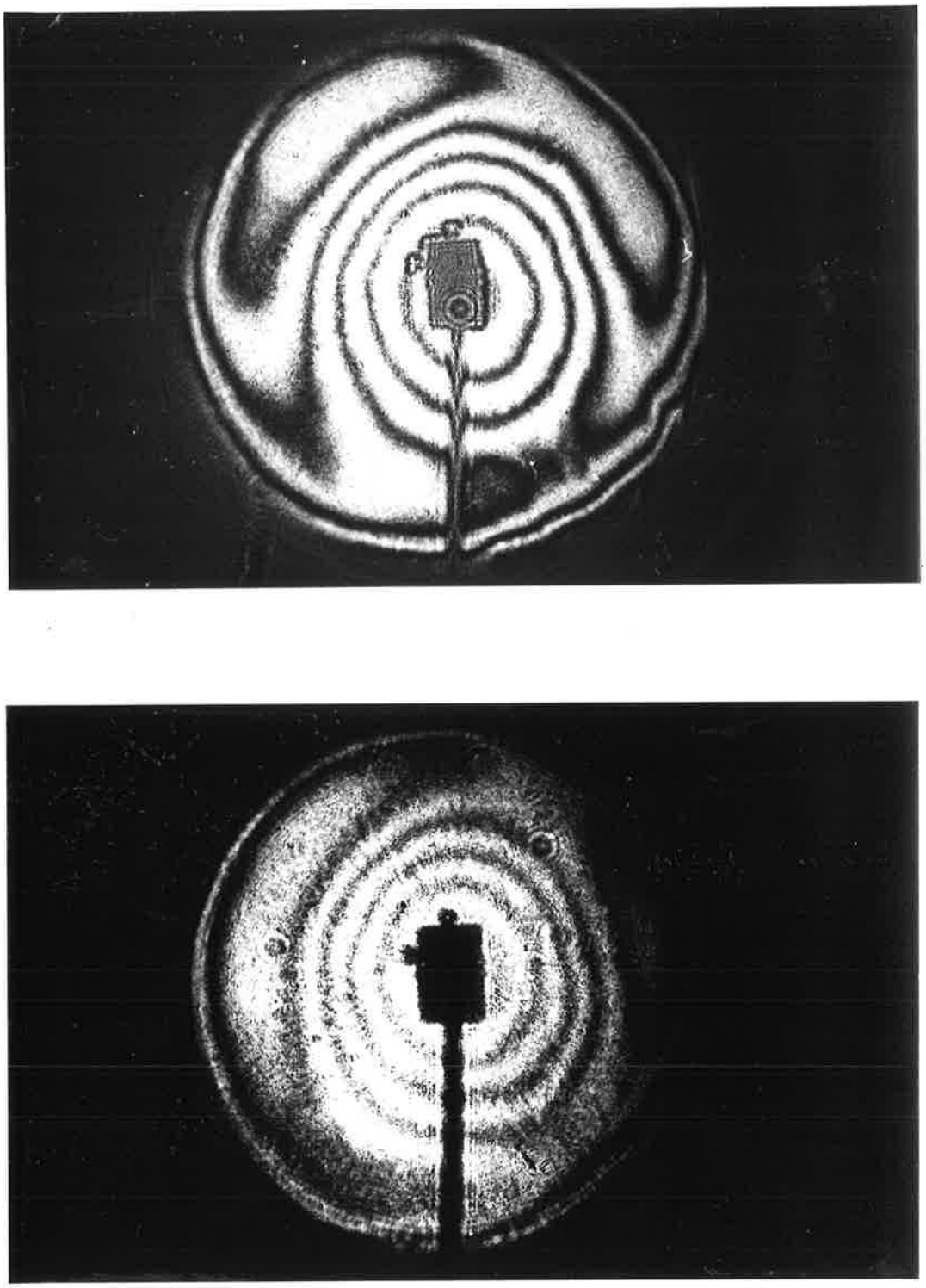

Figure 3.17: The reconstructed beam with partial spherical aberration correction added in the corrective lens train. The two images are of the same wavefront, but with some tilt introduced in the top image.

aberration which was achieved in the off-axis scheme. While this method of spherical aberration correction is fairly successful it is not perfect. A better method would involve adding the correct amount of spherical aberration during recording so that the diffracted beam is free of this aberration. This can be done by putting positive spherical aberration into the object beam or negative spherical aberration into the reference beam.

3.6.2 Spherical Aberration Removal on Recording

The appropriate amount of spherical aberration can be added to the object beam either before it reaches the mirror or after the light reflects off it. One possibility would be to spherically aberrate the beacon which illuminates the mirror, by using a suitable simple positive lens in a configuration like the ones shown in Figure 3.18. These arrangements, however, will only provide a partial spherical aberration correction because the circularly symmetric cross-section of the aberration will not precisely match the elliptical shape of the mirror as seen from the off-axis position of the beacon. This problem will worsen as the mirror speed increases beyond the F/6 system tested.

An alternative would be to spherically aberrate the lens which images the mirror onto the holographic plate. This is similar to the usual method of correcting spherical aberration in telescopes using a secondary conic mirror. In this case, however, because the rays reflect of the large mirror in a random fashion, they will not strike the correct place on the lens surface to produce the required phase shift. The only place where required spherical aberration could be correctly added, after the beacaon light reflects off the aberrated mirror, is at the image plane of the mirror. Several schemes could be used, and these are shown in Figure 3.19. The only constraint is that the image plane of the mirror has to coincide with the holographic plate position without the introduction of any further aberrations such as curvature of field and distortion.

Another method of recording the spherical aberration is to add the correct amount of negative spherical aberration into the reference beam. This could be done using a simple negative lens illuminated at the required aperture size and

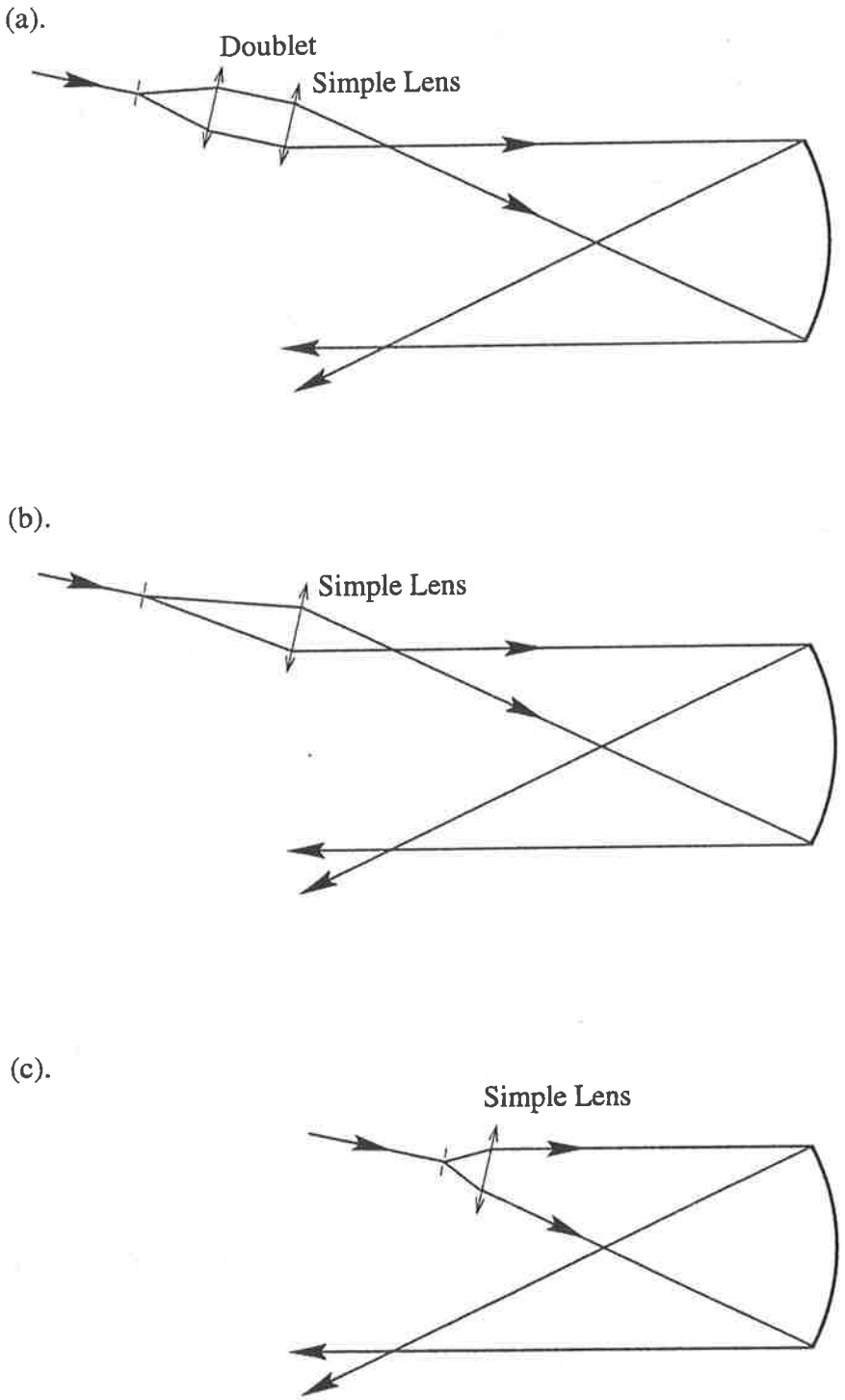

Figure 3.18: Several possible schemes for adding positive spherical aberration to the object beam beacon on recording. The simple lens is chosen to introduce the required spherical aberration in the given configuration.

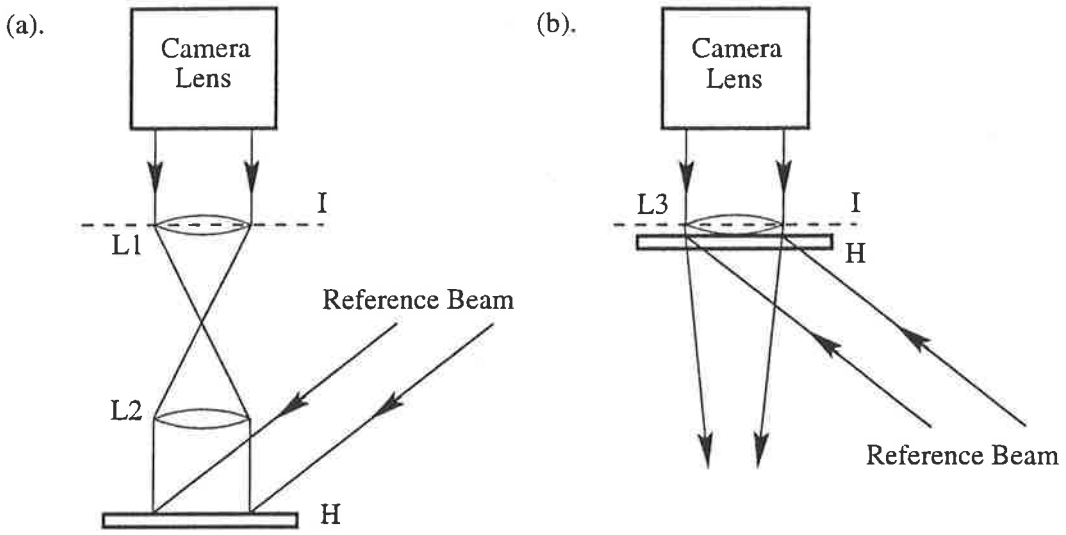

Figure 3.19: (a). L1 is a simple lens introducing spherical aberration into the object beam at the image plane of the mirror (I). L2 is a good quality lens which will restore a flat-field image at the plane of the hologram. (b). The simple lens L3 is placed against the hologram (close to the image plane) and a reflection hologram is formed.

beam divergence. In the current schemes with the object beam normal to plate, the image of the mirror is circular. Since the reference beam (with a circular cross-section) intersects the plate at an angle, the shape of the beam on the plate will be an ellipse. The reference beam will only form a hologram where it intersects the circular object beam, so the full amount of spherical aberration will be recorded in the vertical direction only. To overcome this problem, the aspect ratio of the reference beam must be adjusted so that the precise amount of spherical aberration is added to the whole of the image of the mirror. One way to do this would be to pass the reference beam through a prism, prior to the hologram, to alter the aspect ratio in such a way that the beam lays perfectly over the circular image at the plate (Figure 3.20(a)). This introduces astigmatism, as shown in Figure 3.20(b), which is difficult to remove on reconstruction given the added complication of the astigmatism from the off-axis beacon arrangement itself. This idea will be investigated in more detail in the on-axis beacon in the next chapter, however, where there is no astigmatism from the recording arrangement.

(a).

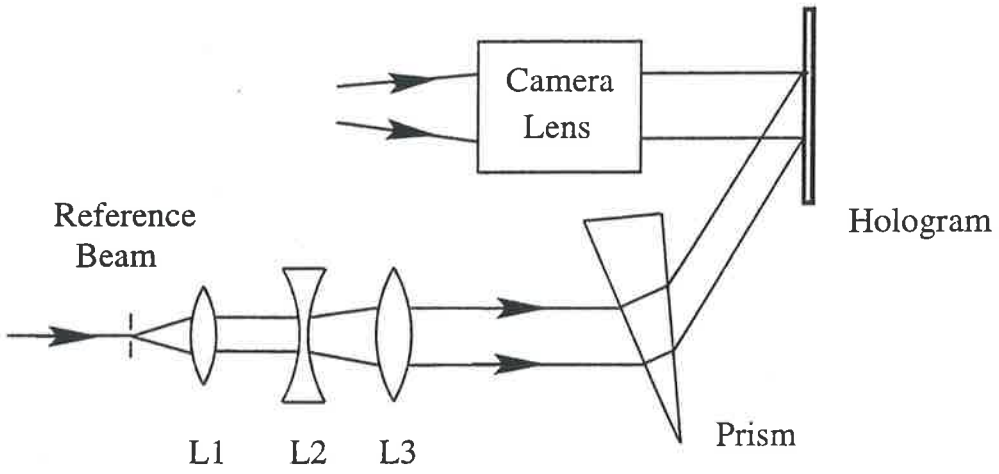

(b).

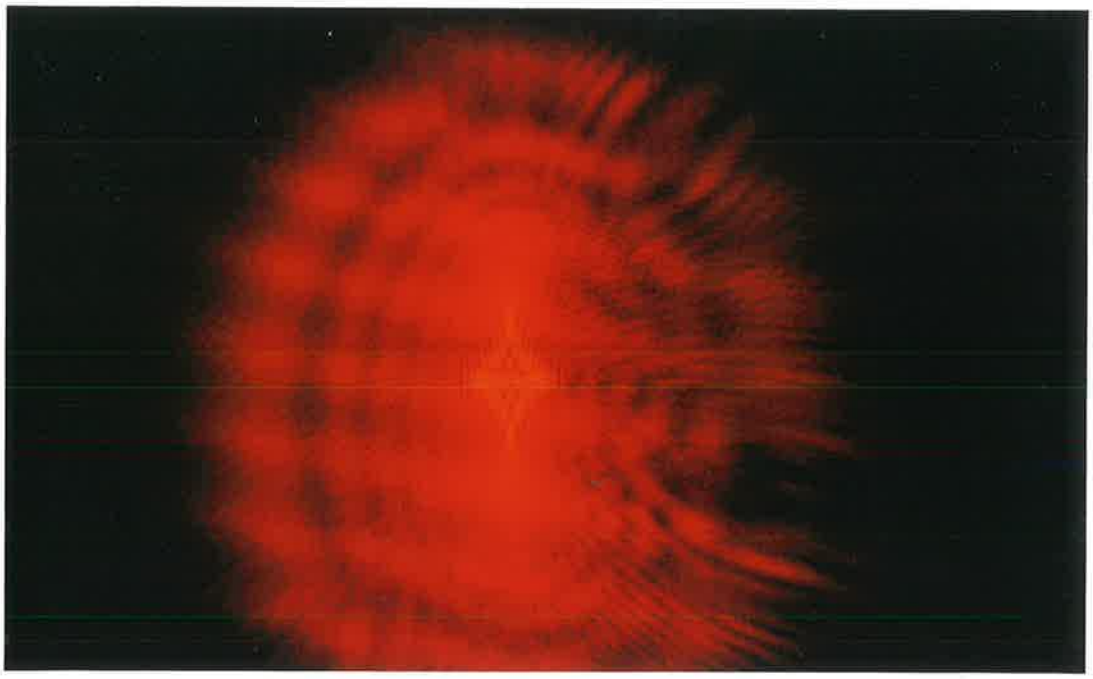

Figure 3.20: (a). The layout for putting negative spherical aberration into the reference beam on recording. Lenses L1 & L2 are achromatic doublets and L2 is the simple lens which introduces the negative spherical aberration. The prism corrects for the aspect ratio of the beam onto the hologram. (b). The effect of the prism on the reference beam is to introduce astigmatism as shown by the appearance of the cross-like structure in the far-field. Notice the blurred "fuzz" around the edges which is indicative of the presence of spherical aberration.

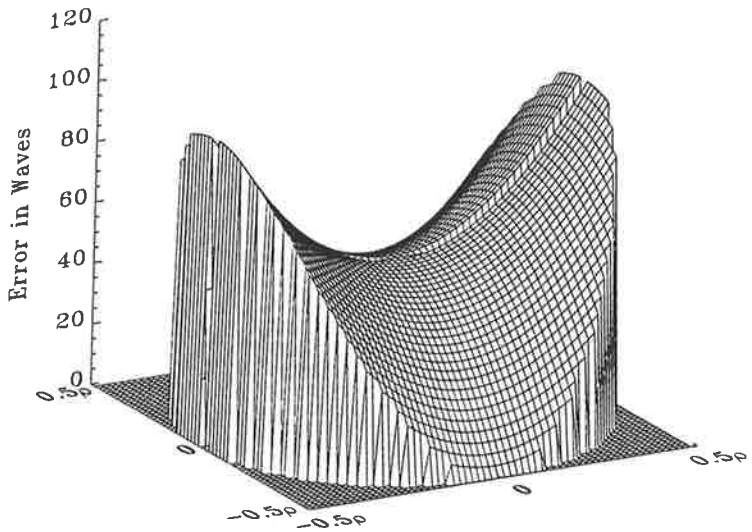

Figure 3.21: The wavefront error (in waves) introduced by a beacon at $x = 0.35$m, $y = R = 5.2$m and reconstructed on-axis. The aperture over which the wavefront is sampled is just the 450mm diameter which was tested.

3.7 Off-axis Aberrations

The off-axis scheme introduces a large amount of off-axis aberrations, mostly third order astigmatism. A plot of the expected wavefront error, (using the first 24 Zernike polynomials) is shown in Figure 3.21. The dominance of the astigmatism is quite evident (*c.f.* Figure 2.7(c)). In order to correct for astigmatism, the reconstructed beam was directed through a train of cylindrical lenses. This method of correction is attractive as it allows for precise visual feedback on the effectiveness of any given arrangement. As mentioned earlier, however, with broadband operation, different wavelengths of light will be diffracted at different angles from the hologram, so they will not pass through this lens train as we would want. It would be much better to correct for the astigmatism on recording rather than on replay.

The simplest solution would follow along much the same lines as for spherical aberration correction. The cylindrical lenses could be just moved to the recording phase and placed in either the reference or object beams. Common cylindrical lenses

are simple lenses, and even in ideal configurations, the introduction of some spherical aberration cannot be avoided. In order to reduce this aberration multi-element cylindrical lenses are required. Even with the astigmatism removed, however, there is still be the problem of the higher order off-axis aberrations.

A better solution would involve reflecting either of the recording beams off a conic mirror with the correct dimensions and orientation to give the desired amount of off-axis aberrations. One obvious solution would involve a perfect mirror with the same dimensions as the large mirror. If the beacon illuminates this mirror at the same angle but out of the plane of the previous recording scheme, most of the major aberrations are eliminated. This would probably be an acceptable solution as a way of correcting several large aberrated mirrors with the fabrication of just one large perfect mirror.

A small, high quality, null corrector with a complex conic shape could be used instead of a large mirror. This secondary could be either a dynamic or static mirror. Dynamic secondaries use a membrane mirror with individually controlable actuators which can adjust the shape of the surface [62]. This type of mirror would have the benefit of being adaptable to different large mirrors and off-axis beacon positions. A static mirror would be cheaper to manufacture but would be limited to correction of the off-axis aberrations in a specific mirror and beacon position. Using the optical design program, I found a configuration which gave a residual error of $W_{p-v} = 0.77$ waves as shown in Figure 3.22. This approach would only be feasible in a final design, with a large primary, as the cost of fabrication of such a null-corrector is significant.

3.8 Summary

It is clear from both the small and large scale tests of this scheme, that correction of a large amount of mirror aberration is possible, but that the introduced off-axis aberrations are sufficiently large to make perfect imaging difficult. The large scale test resulted in 4-5 waves of error over a 450mm diameter which is seeing limited for a telescope at most sites. While the telescope may not be useful for astronomy, where

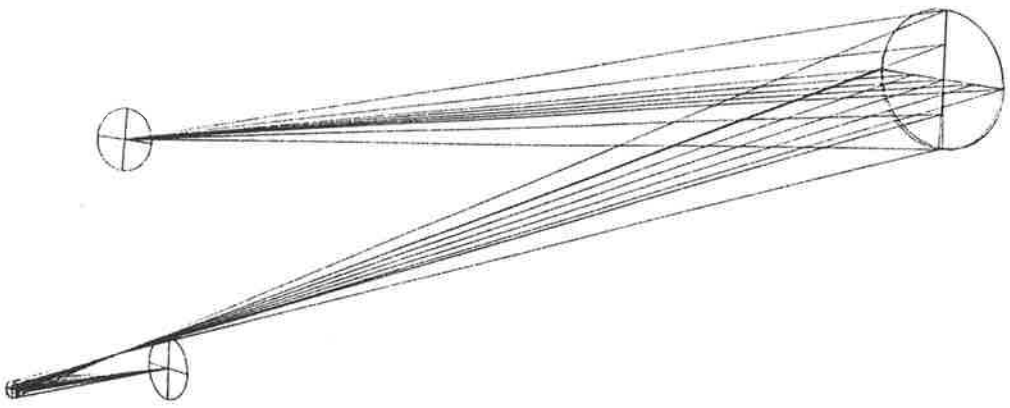

Figure 3.22: The set-up for the off-axis null-correction of the object beam is as shown. The point source beacon beam (bottom) is reflected off the small conic mirror (left) and the refocussed beam is then directed onto the large aberrated mirror (right). This reflected light will be collimated and used to form the image hologram of the mirror as before. The secondary mirror has a conic constant, $K = 1.3884$, off-axis illumination angle of $\theta = -11.11°$, $R = 0.623$m and $\rho = 28$mm.

at ideal sites seeing can exceed $r_o = 100$mm, the surface quality is still acceptable for lidar, since the size of the central maximum of focal spot has been reduced from 8mm in diameter to 14μm which gives a dramatic improvement on signal to noise.

Chapter 4

The On-Axis Beacon

4.1 Introduction

In the previous chapter I discussed an off-axis recording scheme. Although the holographic correction proved capable of removing a large amount of surface aberration, the necessary introduction of a sizable amount of off-axis aberrations, which had to be removed separately, made the scheme less attractive. An on-axis recording scheme with a recording beacon located at the centre of curvature of the spherical mirror avoids this problem. Such a design will result in a telescope limited only by spherical aberration. In this chapter I will present two on-axis designs which incorporate the addition of spherical aberration in the recording process, along with experimental results which demonstrate the complete correction of a heavily aberrated spherical primary.

4.2 The Design Concept

The on-axis recording and replay set-ups are shown in Figure 4.1. To record the hologram, the beacon and the imaging lens are placed as close as possible to each other and the optical axis of the mirror to minimise the off-axis aberrations. The replay procedure is the same as for the off-axis design, though it will be necessary to remove the recording optics before using the corrected telescope.

To calculate the correction achievable with this set-up, we once again return to

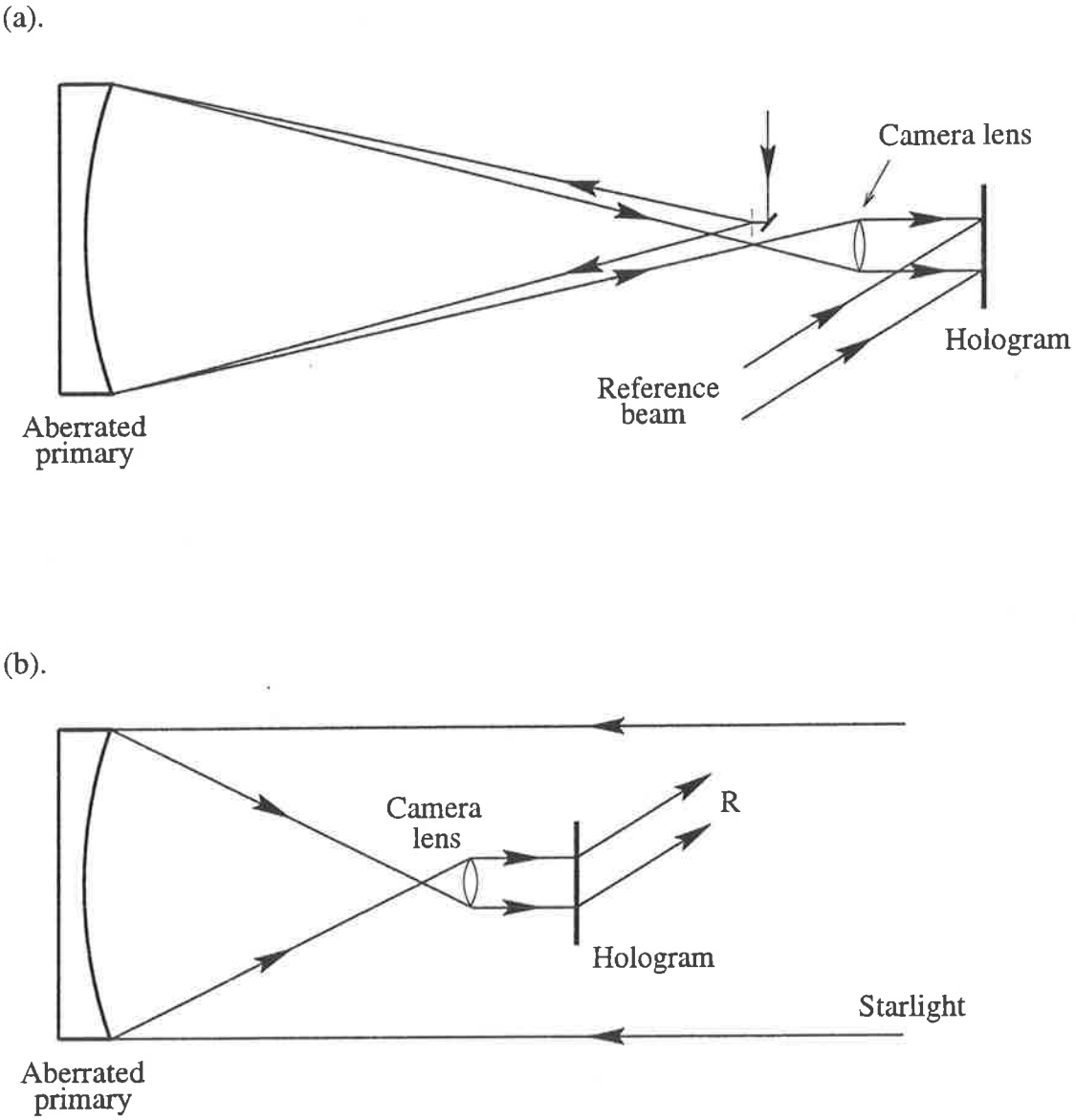

Figure 4.1: (a). Recording: The beacon illuminates the mirror from the centre of curvature. The reflected light is collimated and the mirror is imaged by a camera lens onto the plate were a hologram is made. (b). Reconstruction: Collimated starlight is focussed by the mirror and collimated by the imaging camera lens to reconstruct the reference beam.

Eq. 2.9. In this case the off-axis distance is zero ($x = 0$)[1] and the beacon is at the centre of curvature ($y = R$) so we can simplify the equation to;

$$\Delta = \frac{R\lambda'}{\lambda((R-z)\cos\phi - [u\cos\delta + v\sin\delta]\sin\phi)} - 1 \tag{4.1}$$

With on-axis reconstruction, this simplifies to;

$$\Delta = \frac{R\lambda'}{\lambda\sqrt{R^2 - u^2 - v^2}} - 1 \tag{4.2}$$

In the on-axis design, the maximum correction will be at the centre of the mirror and the minimum correction at the edges. On reconstruction, however, the area of the mirror with the best correction will be obscured by the secondary optics. This may not pose a serious problem, however, as it was demonstrated with the off-axis design that the correction factor in an F/6 system was not the limiting factor, even with a heavily aberrated primary. Of course, as the speed of the primary increases, the decreasing correction factor will become more critical, which may set a limit on the initial surface quality.

4.3 Spherically Aberrated Reference Beam

4.3.1 Small Scale Experiment

In the previous chapter, it was suggested that one method of incorporating spherical aberration correction could involve adding the correct amount of negative spherical aberration into the reference beam using a simple negative lens. The aspect ratio of this beam is then corrected before it intersects the object beam by passing it through a prism. As has been mentioned previously, this will introduce aberrations such as astigmatism, but it was envisioned that these could be removed by using a mirror image of the set-up on the reconstructed beam, as shown in Figure 4.2

This scheme was tested on a small, spherical mirror ($D = 85$mm, $f = 140$mm). The mirror had a fair surface quality ($\sim 3\lambda$), with wavefront error dominated by

[1]The actual off-axis distance is non-zero but the angle is so small that, except for very fast mirrors, this approximation is valid. Of course, an exact value for x can be used if necessary.

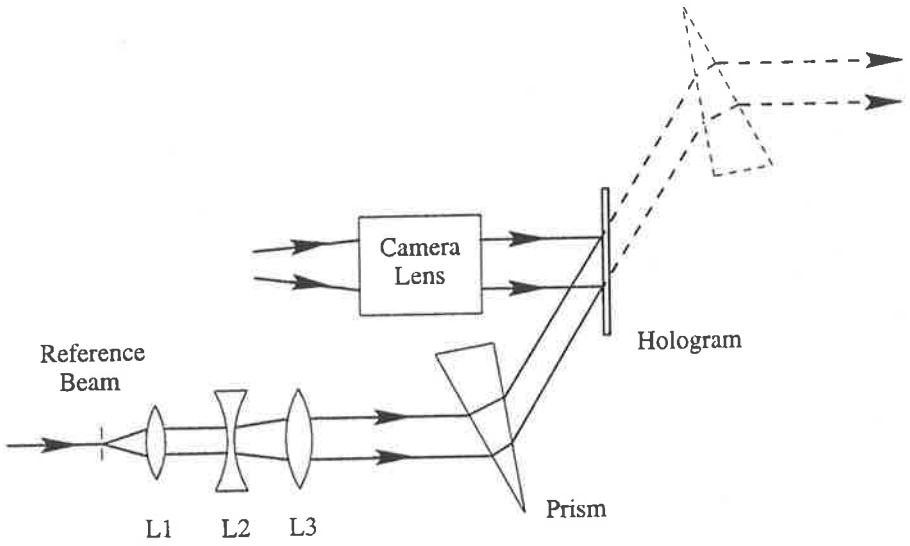

Figure 4.2: Recording (solid lines): Spatially filtered light is collimated by a doublet (L1) to give a diffraction limited beam with then passes through a simple negative lens (L2) before being recollimated by a doublet (L3). This beam is then directed through a prism before reaching the plate. Reconstruction: The diffracted beam (dashed) will pass through the prism in the mirror-image of the recording set-up.

spherical aberration. The aperture was reduced to $\rho = 27.5$mm to give a similar amount of spherical aberration to that of the mirror used in the large scale tests.

The third order longitudinal spherical aberration of a double-concave negative lens (L2) with focal length $-f$, refractive index n, illuminated by a collimated beam of semi-diameter h is [68, 56];

$$LSA = \frac{fh^2(4n^3 - 4n^2 - n + 2)}{8f^2n(n-1)^2 + h^2(4n^3 - 4n^2 - n + 2)} \tag{4.3}$$

The third order wave aberration associated with this ray aberration can be found in [57];

$$W = \frac{LSA.\rho^2}{4f^2} = \frac{h^4(4n^3 - 4n^2 - n + 2)}{32f^3n(n-1) + 4fh^2(4n^3 - 4n^2 - n + 2)} \tag{4.4}$$

Equating this to the third order spherical aberration for the mirror ($W = \rho^4/4R^3$) will provide a solution for a given lens type. Using the mirror parameters $R =$ 280mm and $\rho = 27.5$mm, 10.3 waves of spherical aberration are introduced ($\lambda =$ 632.8nm) and choosing a BK7 ($n = 1.51508$) lens of $f = -50$mm, the semi-aperture

size required was $h = 6.74$mm. The recollimating lens (L3) was an 80mm focal length doublet and the object beam was imaged onto the hologram using a camera lens ($f = 100$mm).

For reconstruction, the set-up was as shown in Figure 4.1(b), with the collimated beam produced by the 5-inch diameter doublet used in the small off-axis experiment. In this case, however, the diffracted beam was directed through the prism as shown in Figure 4.2. The position and orientation of the prism was determined by minimising the focussed spot size of the output beam. This beam was then recollimated and made to interfere with the *original* plane wave reference beam.

The results are shown in Figure 4.3. Initially, the uncorrected image shows the expected 10-11 waves of spherical aberration. After correction, the wavefront error is $W_{p-v} = 0.6\lambda$ and $W_{rms} = 0.146\lambda$. The remaining error is thought to be due to the fact that the mirror image technique can only work if the beams are exactly the same in both cases. The reference beam on recording, however, has a spherically aberrated wavefront, while the diffracted beam on reconstruction does not have this aberration, so the effect of the prism on each wavefront will be slightly different. This difference was partially corrected by orientating the prism for "best result" on reconstruction, rather than the exact mirror-image of the recording set-up. It should be noted that although a prism was used to alter the aspect ratio in both recording and reconstruction, a diffraction grating could also be used. Experiments carried out using a reflective grating gave similar results.

By replacing the spatial filter at the focal plane of the Jaegers lens with a USAF resolution test chart, the resolution of the corrected mirror can be determined. The chart consists of groups of 3 white bars on a black background (aluminium deposited on an optically flat glass slide). The bars start with a spatial frequency of 1 cycle/mm (Group 0, Element 0) and decrease in size with each element by the sixth root of two. Corresponding elements in successive groups differ in size by a factor of 2.

The resolution chart results are shown in Figure 4.4. The uncorrected image shows the characteristic blurring of the bars, indicative of spherical aberration with the "haze" due to the unfocussed marginal rays. In the corrected image, Column 6 Row 6 is resolved at a spatial frequency of 114 cycles/mm which is in good agreement

(a).

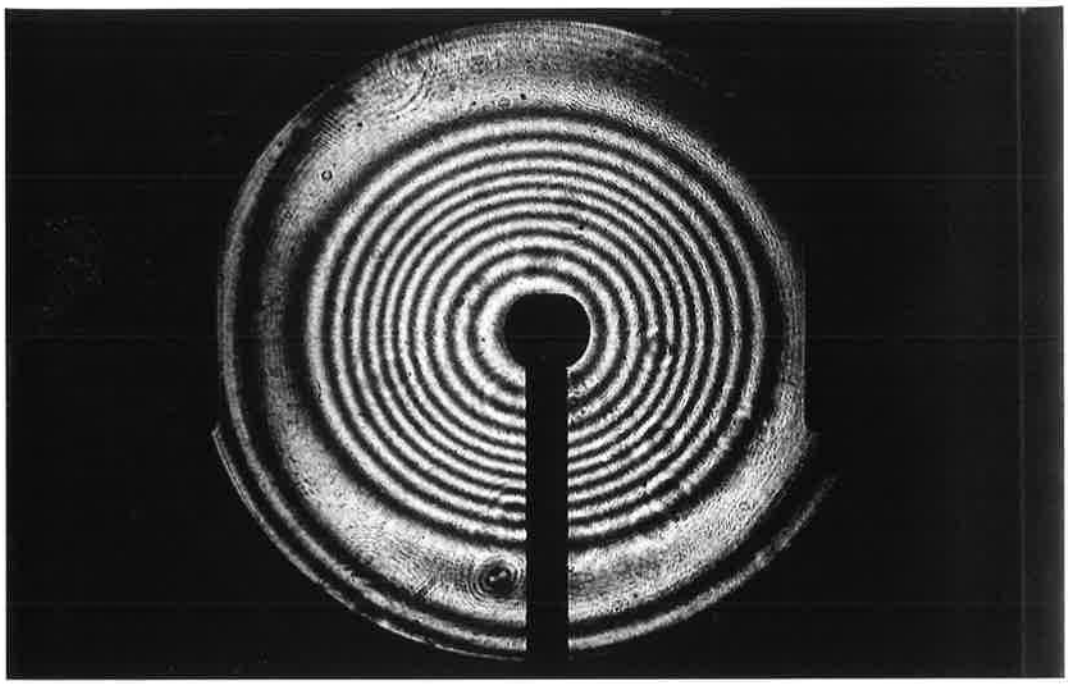

(b).

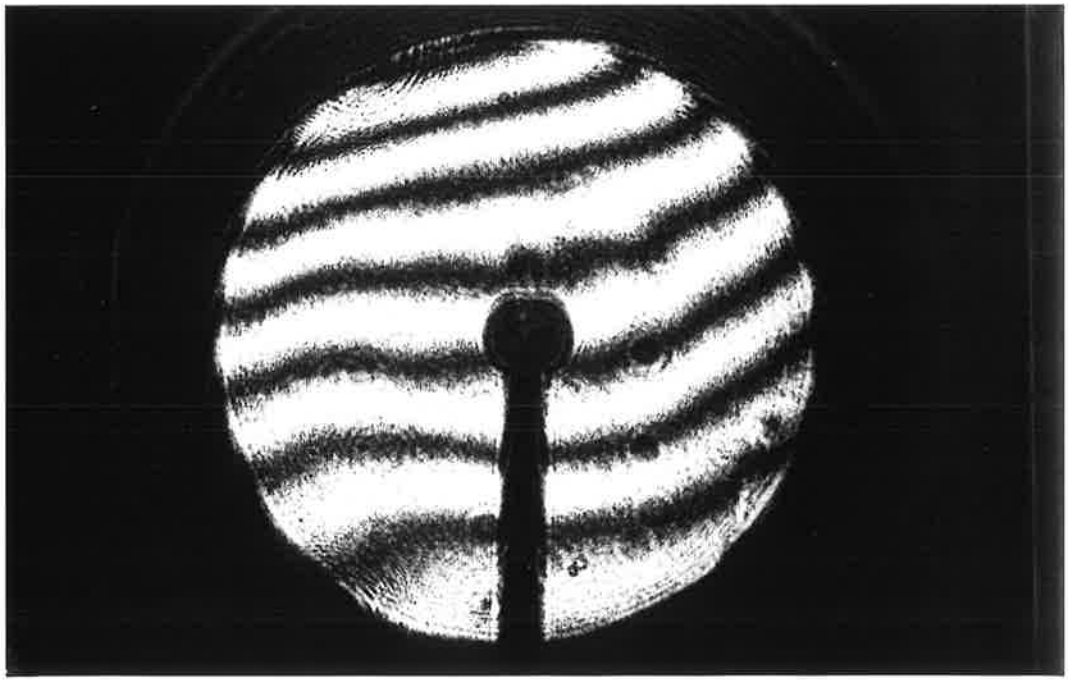

Figure 4.3: (a). Before correction. The interference pattern shows the recorded wavefront error over the 55mm aperture. (b). After correction.

(a).

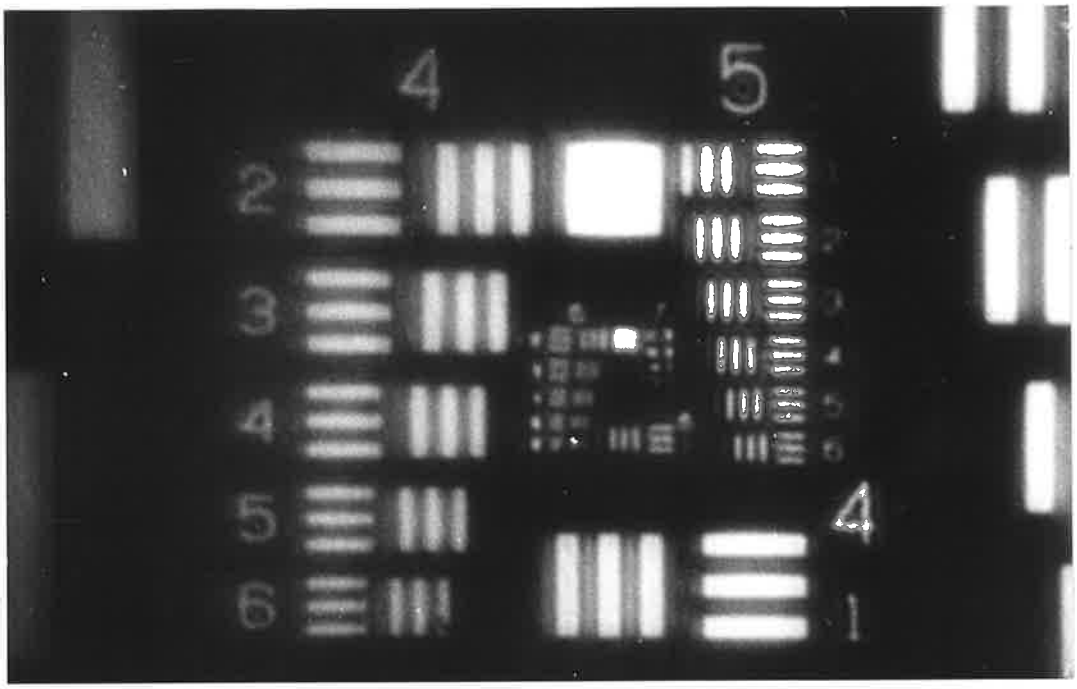

(b).

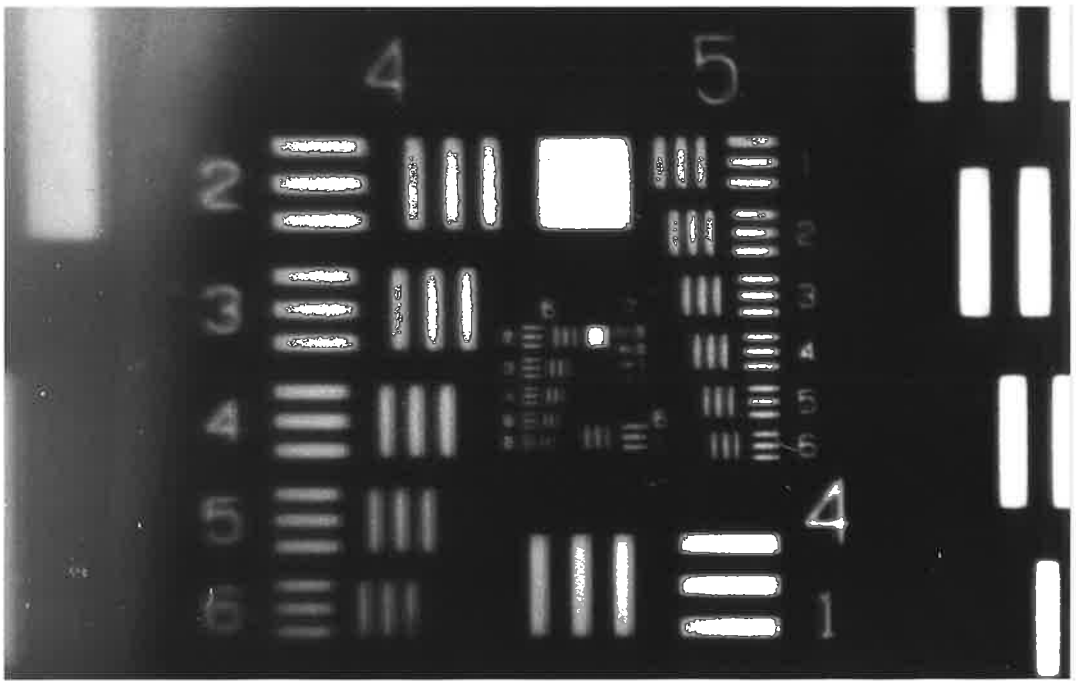

Figure 4.4: (a). Before correction: The resolution chart shows blurring of the bars indicative of spherical aberration. (b). After correction. The faint secondary image is due to a double reflection in the glass of the resolution chart. Note that both images are printed with the same degree of contrast.

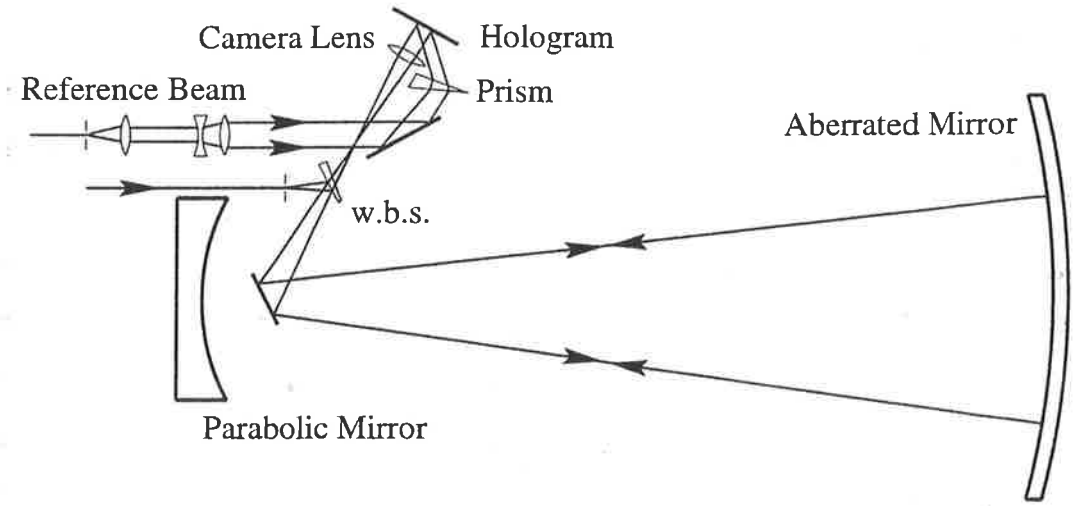

Figure 4.5: The recording arrangement for the large scale on-axis correction. The object beam is folded along its path and the return beam passes through the wedge beamsplitter (w.b.s.) to be collimated and imaged onto the plate. Spherical aberration correction is applied by the same method used in the small scale test.

with the theoretical diffraction limited resolution of 118.7 lines/mm (8.43μm).

4.3.2 Large Scale Experiment

The small scale experiment used an almost perfect spherical mirror with only spherical aberration correction required. For this experiment, I returned to the 0.86m diameter slumped glass mirror used in the large off-axis experiments in order to demonstrate the simultaneous holographic correction of both the surface aberrations and the spherical aberration. Due to space limitations, the recording beams were folded according to the arrangement in Figure 4.5, with the imaging camera lens having a focal length of 0.2m. The negative lens used to add the spherical aberration had a focal length of -50mm and was used at an aperture of 12.3mm. On reconstruction the diffracted beam was directed through a prism which was adjusted in position and orientation, as before, to give the minimum focussed spot size. In addition, the beam had to be passed through a slightly tilted lens in order to remove some remaining off-axis aberrations left uncorrected by the mirror-image arrangement of the prism. This resulted in a small distortion of the beam aspect

ratio, which should not be a problem, as it can be corrected (if necessary) by simple digital image processing. The results are shown in Figure 4.6.

The corrected interferograms show a residual wavefront error of $W_{p-v} \sim \lambda$. The two images were taken under the same conditions, but (a) has some tilt applied to the beamsplitter, while (b) shows the "zero fringe". Total correction has not been achieved but, once again, the error is fairly regular with a large spatial frequency, indicating that the random surface error is still not a limiting factor. The introduction, and subsequent removal, of the off-axis aberrations using the prism is obviously a problem which restricts the correction which can be achieved with this scheme. A more attractive solution would not require the introduction of any such aberrations.

4.4 Spherically Aberrated Object Beam

4.4.1 Recording Scheme

The second method for removing the spherical aberration is to add positive spherical aberration into the object beam on recording. This can be done by placing a positive singlet in front of the spatial filter in order to "spherically aberrate" the beacon. The simplest configuration is to have a plano-convex lens refocussing the divergent light from a spatial filter to form a spherically aberrated beacon at the centre of curvature of the large spherical mirror, as shown in Figure 4.7. The light is focussed to back to the centre of curvature (slightly off-axis) where a pick-off mirror directs it through to the imaging optics and the hologram. The reference beam is a diffraction limited plane wave. The wedge beam-splitter used in the previous experiment was replaced by a reflective arrangement as it was thought that it may be introduce a small amount of astigmatism on the transmitted return beam.

A small lateral separation is required between the spherically aberrated beacon and the reflected, focussed spot. Since the return spot was about 8mm in diameter, a 4mm separation at 5.2m was required. Computer modelling of this arrangement showed that less than $\lambda/100$ wavefront error is introduced by this off-axis angle.

Using the Zemax diffractive optics program, the on-axis Zernike polynomials (0, 3, 8, 15 & 24) were evaluated at the focal plane of a 0.45m diameter mirror with

(a).

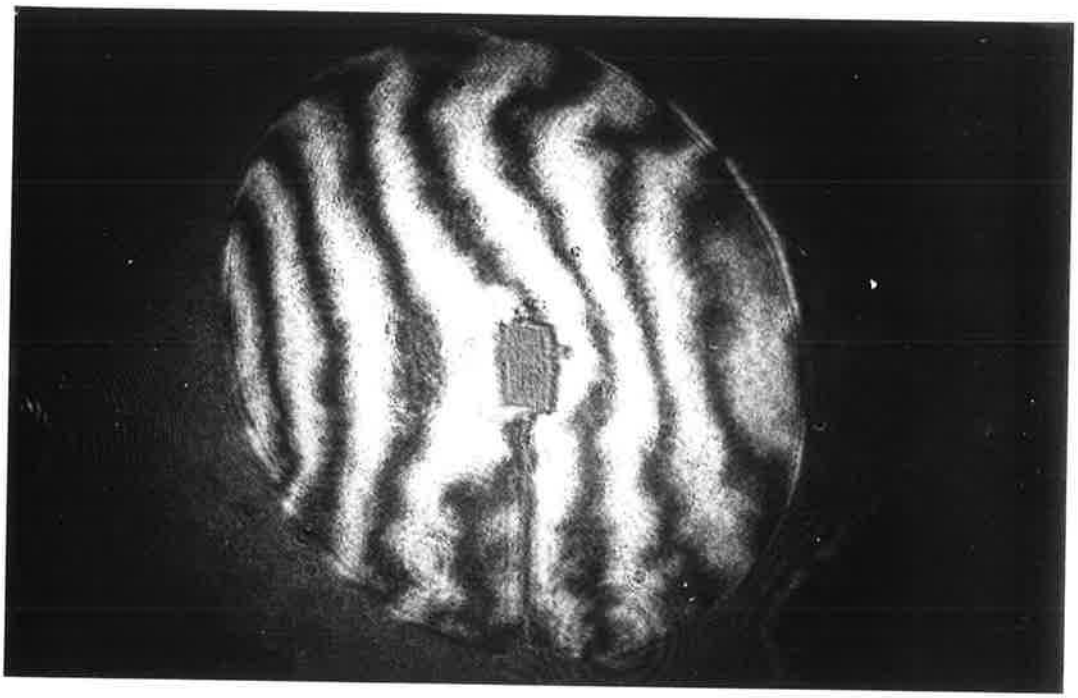

(b).

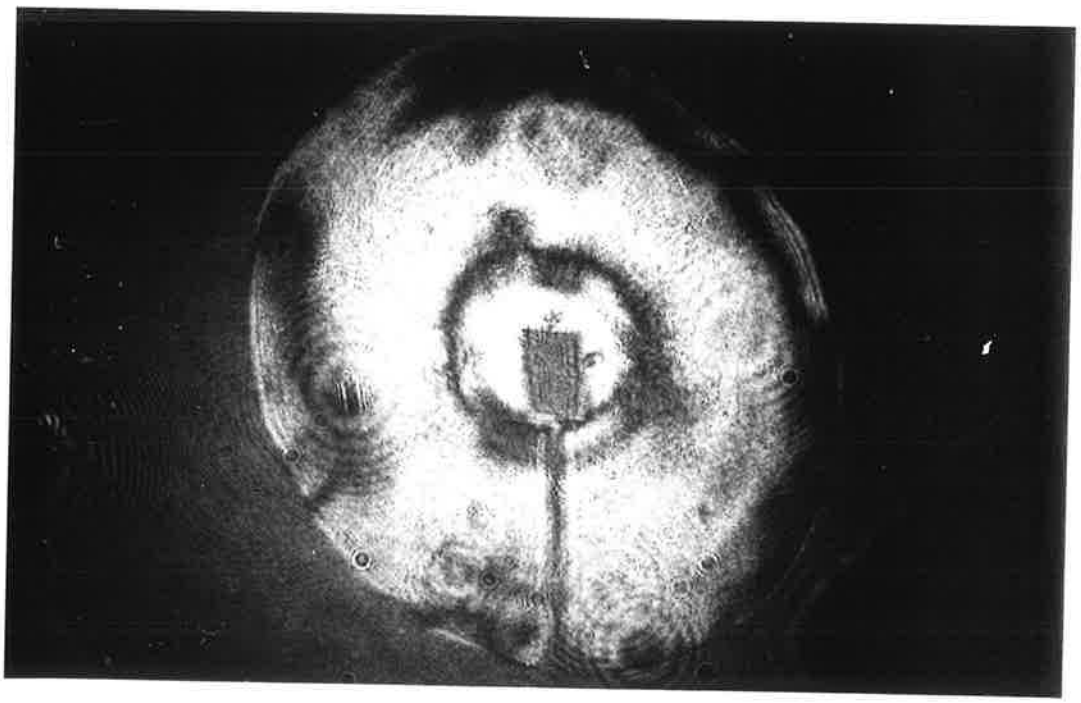

Figure 4.6: (a). The corrected wavefront showing the minimum wavefront error achieved. *c.f.* the uncorrected wavefront Figure 3.11. (b). The same wavefront but at "zero fringe".

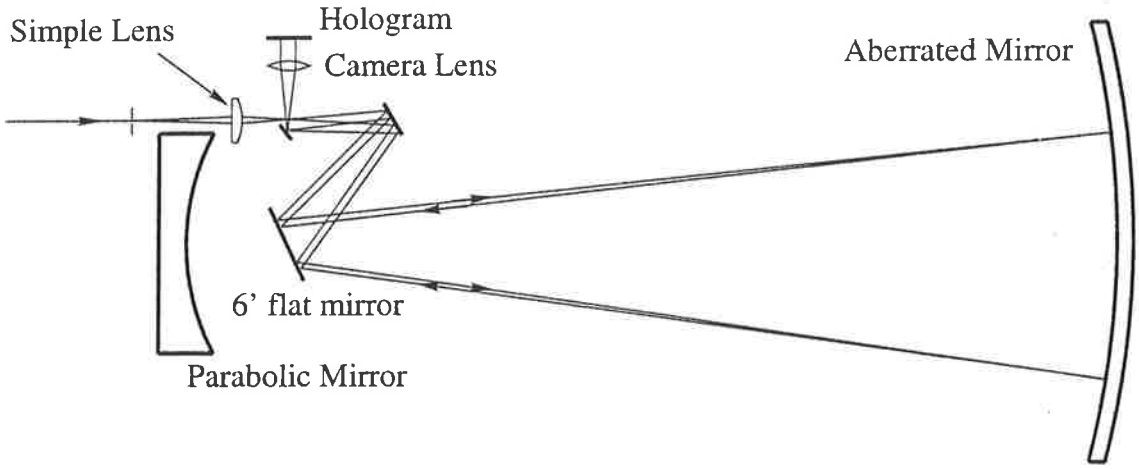

Figure 4.7: Recording Set-up. The spatially filtered light is focussed by a plano-convex singlet to a spherically aberrated focus at the centre of curvature of the aberrated mirror. The reflected light is collimated by a camera lens which images the mirror onto the holographic plate.

incident collimated light. The recording arrangement was then modelled with an available simple lens and optimisation of the spatial filter - lens distance was found to a best fit to all of these polynomials. For an available plano-concave BK7 lens, (f = 100mm, D = 30mm) the optimum distance is 179.88mm. The calculated remaining wavefront error, for this arrangement, is $W_{p-v} = \lambda/10$ ($W_{rms} = 0.03\lambda$).

As an indication of the sensitivity to the distance between the spatial filter and the lens, the remaining absolute peak-to-valley error for various distances is shown in the table to the right. The calculations show that a wavefront error of just $\lambda/10$ is introduced for a positional error of $\pm$1mm.

Distance	P-V Error
173.4mm	1.40λ
178.9mm	0.22λ
179.9mm	0.10λ
180.9mm	0.17λ
184.9mm	0.73λ

The total wavefront error can be calculated using the computer models for each of the recording and optimised reconstruction arrangements. In each case, the Zernike polynomial expansion of the wavefront can be found, and the difference between the two, plotted as a function of position over the mirror, gives the expected residual wavefront error. These plots are shown in Figure 4.8.

(a).

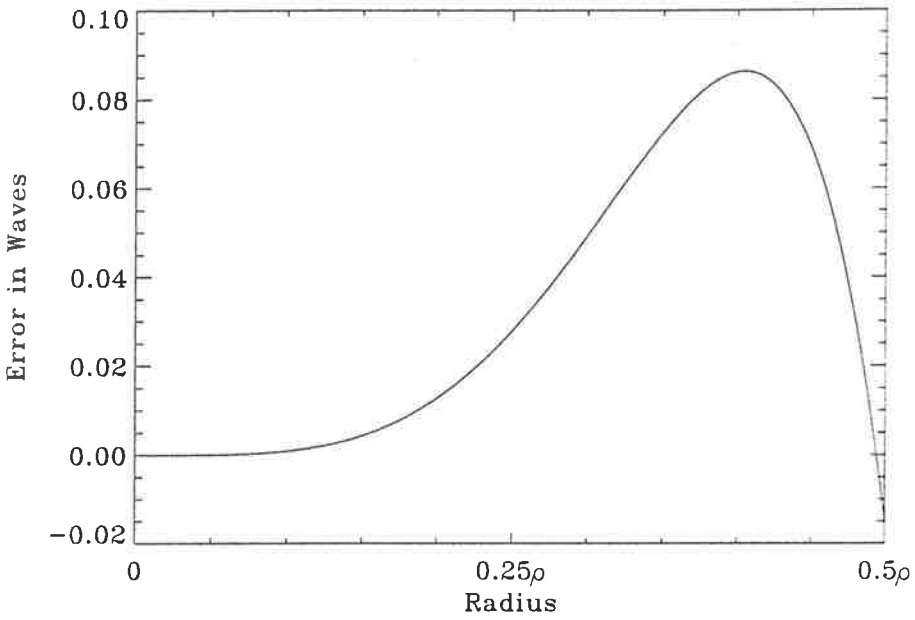

(b).

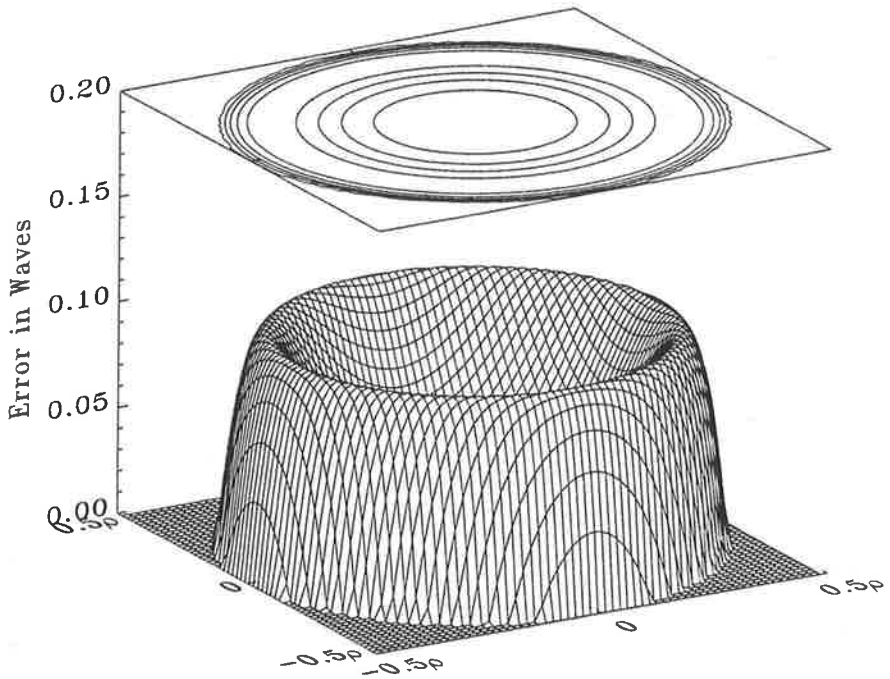

Figure 4.8: (a). A radial slice of the reconstructed wavefront calculated from the Zernike polynomial coefficients. (b). A 3-D surface map of the absolute error over the whole aperture.

4.4.2 Experimental Results

The large scale experiments once again used a 450mm diameter aperture. A 100mm Zuiko camera lens was used for imaging during recording and a 35-70mm zoom lens (Nikon F/2.8 "D") was used during reconstruction. The zoom was adjusted to give the correct image size while producing a collimated beam. Interferometric results from the experiment are shown in Figures 4.9 & 4.10.

The final wavefront has an error of $W_{pv} = 0.5\lambda$ ($W_{rms} = 0.11\lambda$). Figure 4.11 shows a wavefront surface generated from the aspect-ratio corrected image in Figure 4.10. The remaining wavefront is not diffraction limited due to two factors; non-common recording and reconstruction optics, including the parabolic mirror and the holographic substrate, and incomplete correction of both the mirror surface aberrations and spherical aberration. In this set-up there is a total of 7 non-common mirrors (including the parabolic collimator) and 3 lenses which are used over their full aperture and 4 mirrors and 2 lenses used to a smaller portion of their aperture. Given a performance of $W_{pv} = \lambda/10$ for each element, it is expected that the total wavefront error introduced by these surfaces should contribute to at least part of the remaining wavefront error observed.

The surface error of the parabolic mirror was shown in Figure 3.14. It is interesting to note that the corrected surface error in Figure 4.11(b) has the same overall form as that of the parabolic mirror. Since it is certain that this wavefront error will be present on the corrected wavefront. this must be taken into account. A direct subtraction of the two wavefront errors is impossible but the similarity of the wavefronts is still a measure of success of the correction.

The holographic substrate was tested in transmission in a Mach Zender interferometer which was good to $\lambda/10$ without the plate present. The interferometer set-up is shown in Figure 4.12, along with the interference pattern produced (imaged to the plane of the substrate). Part of this error is due to the substrate, while some may be introduced by changes in the emulsion during processing. In a final telescope design, of course, the substrate would be a piece of high surface quality optical glass.

Two further contributions to the wavefront error in Figure 4.10 come from the

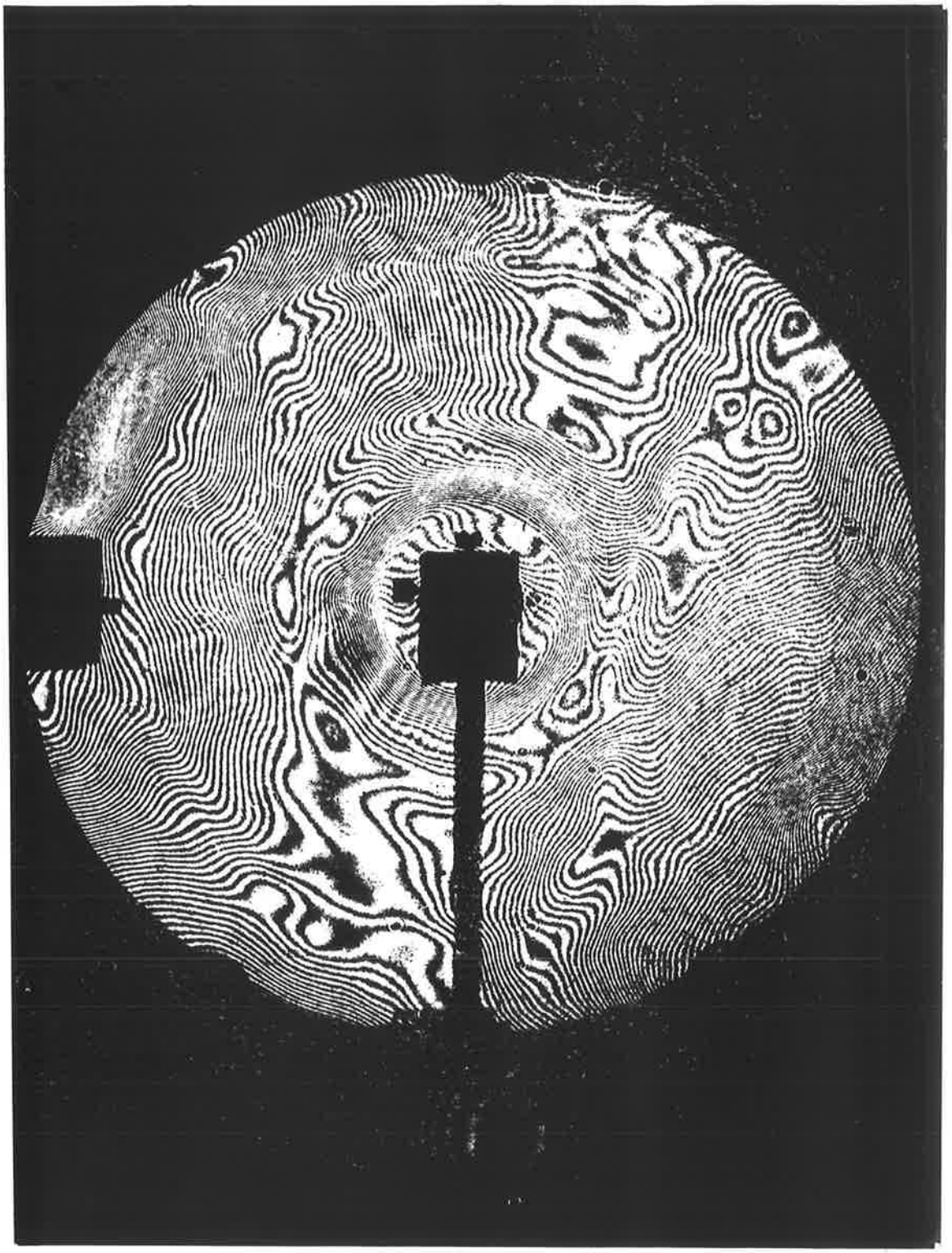

Figure 4.9: Before correction. An interferogram of the surface of the central 450mm portion of the aberrated spherical mirror.

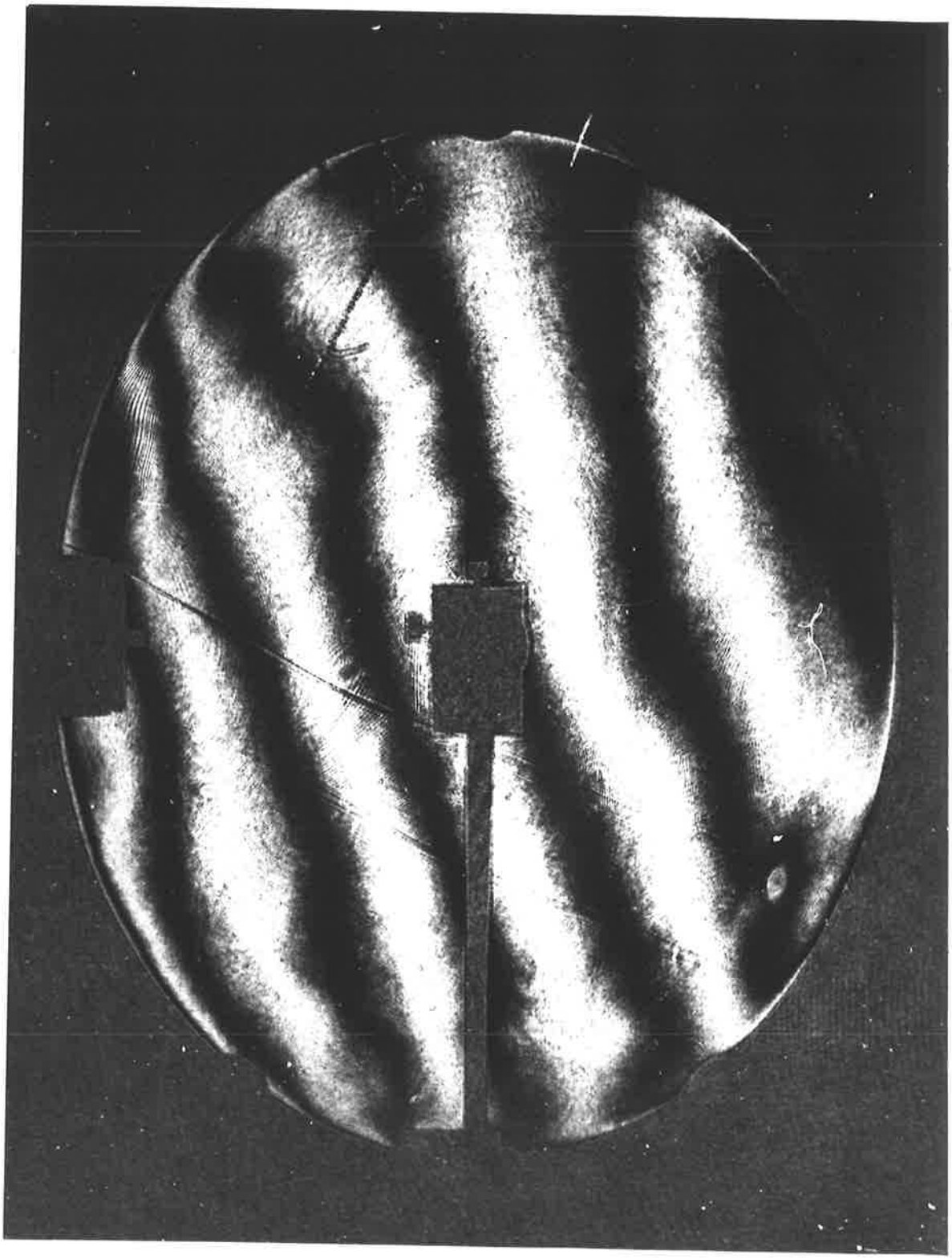

Figure 4.10: After correction. An interferogram of the reconstructed wavefront, imaged at the surface of the mirror. This aspect ratio has been left unaltered.

(a).

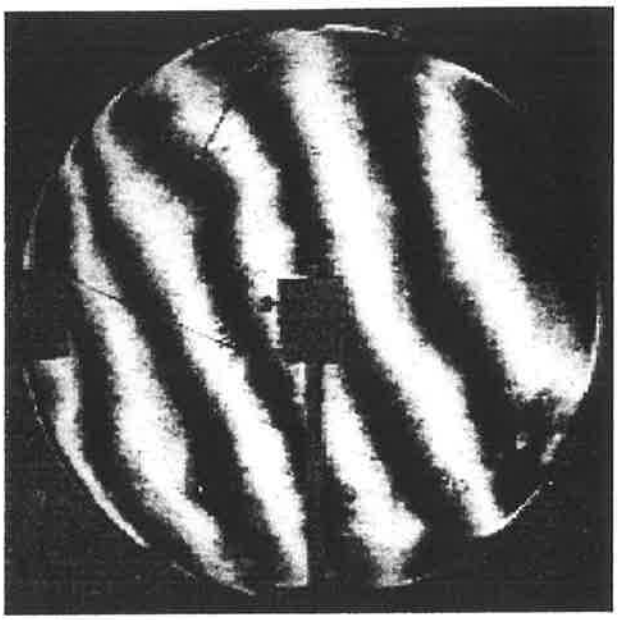

(b).

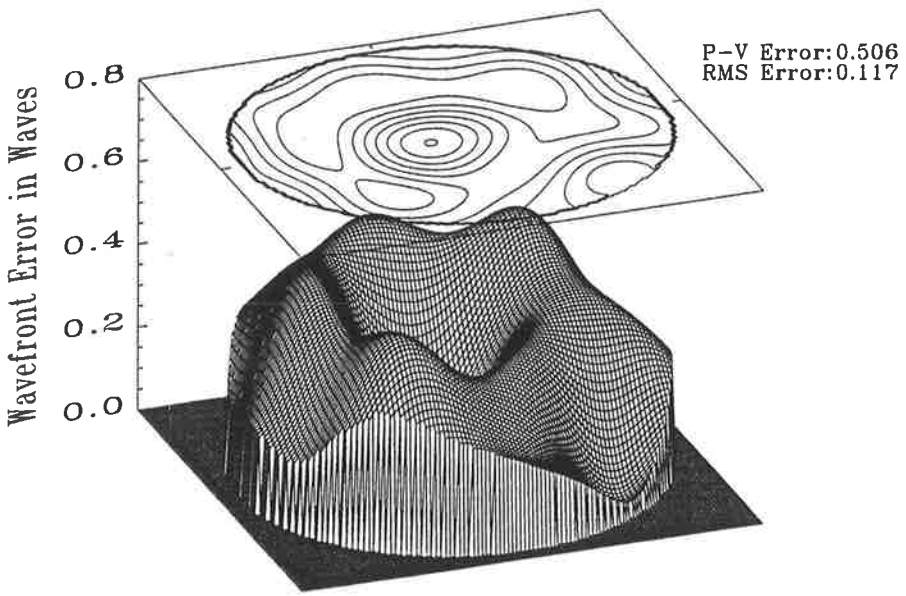

Figure 4.11: (a). The scanned image of the interferogram shown in Figure 4.10, with the aspect ratio digitally altered to make it circular. (b). The calculated wavefront generated from the digitised image in (a).

(a).

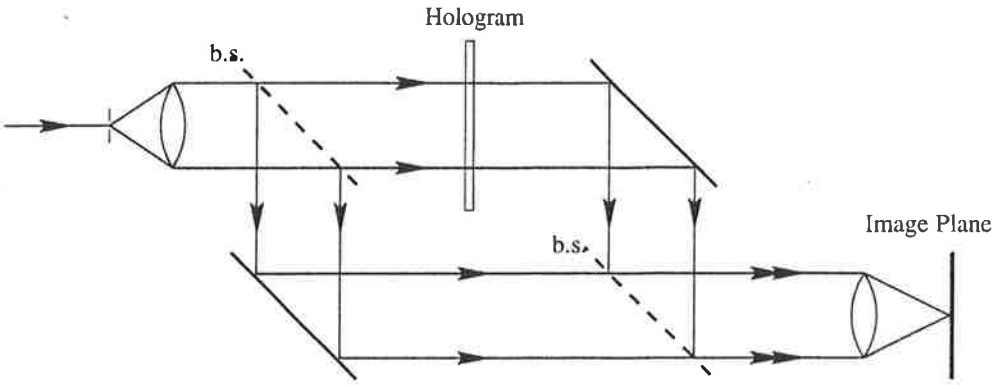

(b).

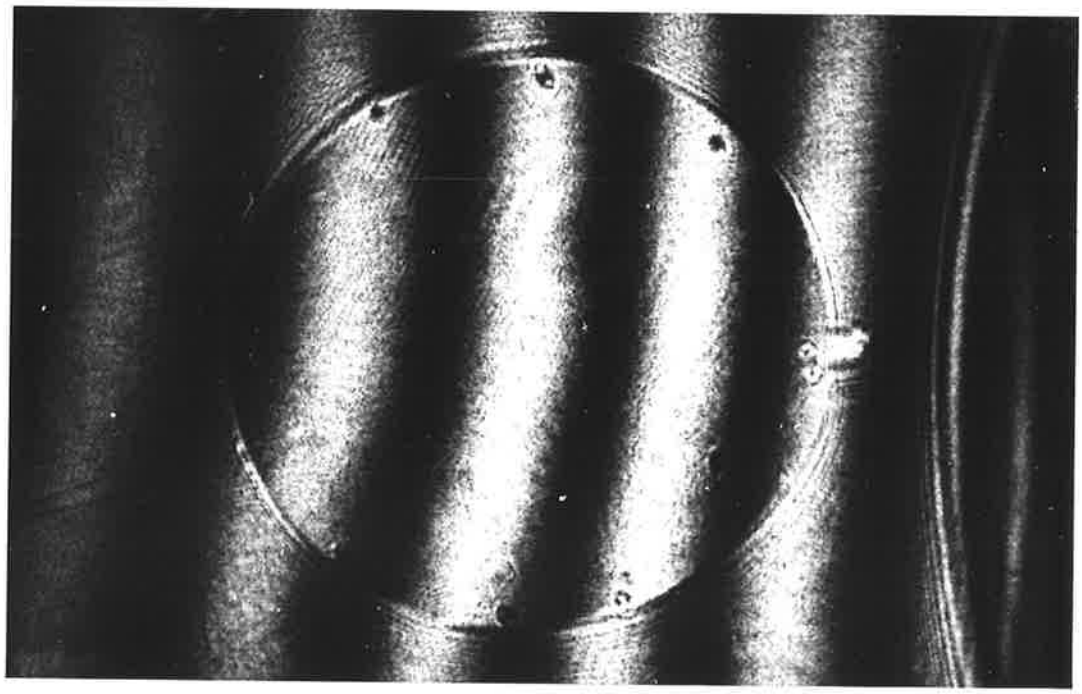

Figure 4.12: (a). The interferometer used to measure the wavefront error introduced by the hologram on transmission. (b). An interferogram of the hologram. The mirror aperture tested lies in the circle just inside the small circular fiducials. The hologram size is 9mm in diameter.

uncorrected surface error and the residual spherical aberration. The predicted minimum correction factor for this set-up is 1067 at the edge. The actual surface error of the aberrated mirror is largest at the edges, with about 100 waves deviation from the centre. It is thus expected that the holographically corrected wavefront will have a maximum error of $\sim \lambda/10$ decreasing towards the centre.

The residual spherical aberration was calculated to be $W_{p-v} = \lambda/10$ ($W_{rms} = \lambda/33$). The wavefront reconstruction of the calculated residual error over the aperture was shown in Figure 4.8. Once again, the overall surface shape is similar to that calculated from the interference pattern of the corrected beam (Figure 4.11(b)).

As a result of a combination of all of these errors, most of which could be corrected with better optical components, it is reasonable to say that diffraction limited correction of the mirror has been achieved.

To examine the increase in resolution of the corrected mirror, a test chart was placed at the focus of the parabolic mirror. The uncorrected and corrected images are shown in Figure 4.13 & 4.14. The uncorrected image shows Columns 2 & 3 (though not very clearly!) and the corrected image has been magnified to show the detail in Columns 6 & 7. The corrected chart is resolved to Column 7 Line 3 which corresponds to the diffraction limited resolution in this set-up.

The bars are quite sharp over the whole pattern which would seem to suggest that the field of view of the corrected telescope is quite large. This is a dangerous assumption to make, however, as the sharpness of Column 2, say, does not indicate how good the resolution is in this region, just that it does not degrade appreciably. A lateral translation in the resolution chart does not allow the field resolution to be tested since the parabolic collimator has its own field of view and will aberrate any images beyond a certain distance: as discussed previously, a lateral translation of just 1mm at the focus of the collimator will introduce 5 waves of coma (Figure 3.13(b)). The only way to truly test the field of view of a telescope is to observe a number of point objects at infinity over a large field - *e.g.* a star field[2].

[2]As a further note, the high resolution demonstrated with this instrument suggests an alternative use for holographically corrected optics - that of microscopes. This is discussed in more detail in Appendix E.

Figure 4.13: The uncorrected resolution test chart. The portion shown is that of Columns 2 and 3. The image contrast was adjusted to bring out as much detail as possible.

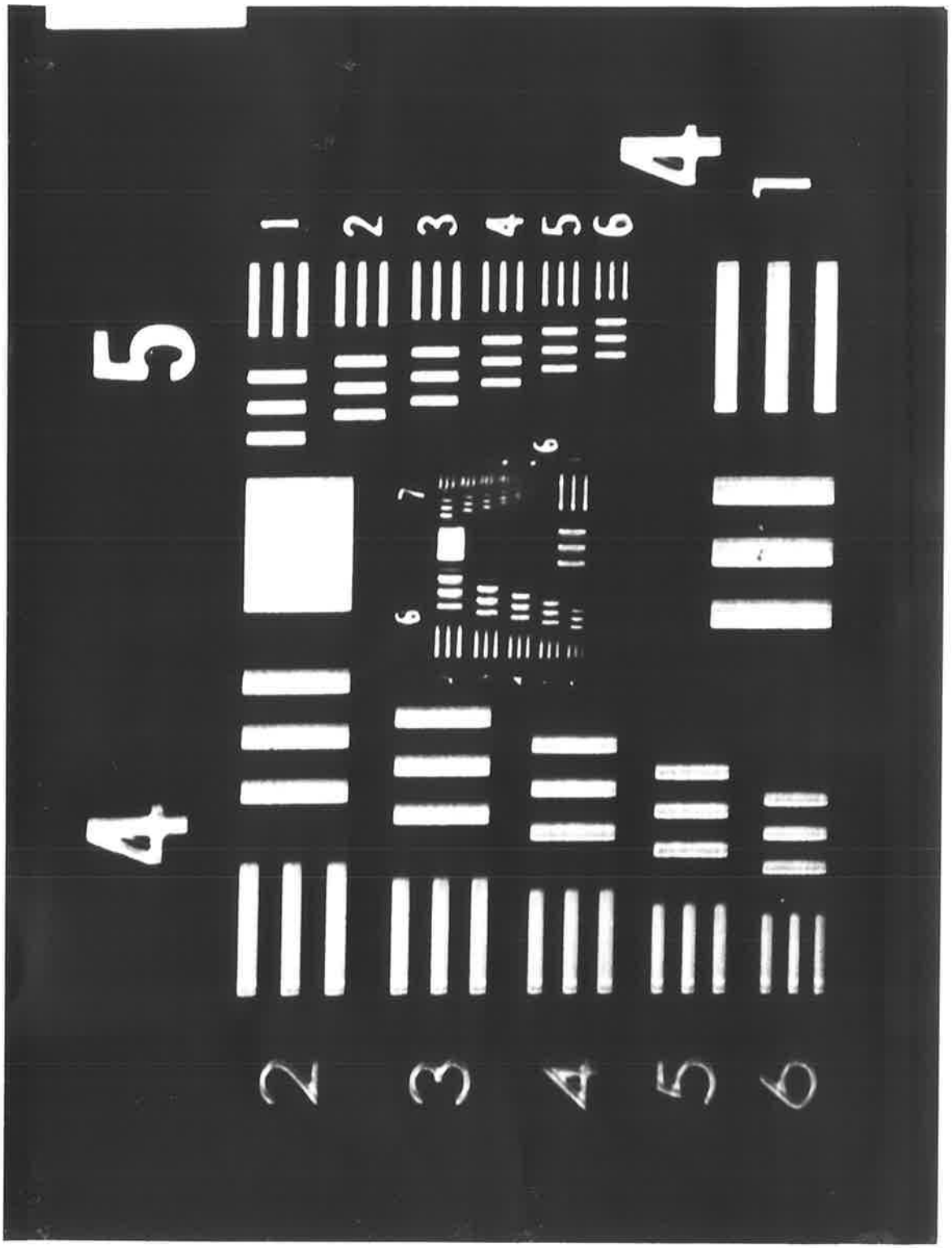

Figure 4.14: The corrected image of the resolution test chart - magnified 4 times compared to Figure 4.13 to show Column 7.

4.4.3 Wavelength Dependence

To determine the correction at another wavelength, a CW frequency-doubled, Nd:YAG laser ($\lambda' = 532$nm) was directed along the path of the HeNe laser to recreate the reference beam while at the same time reconstructing the hologram. The interferogram of the corrected wavefront is shown in Figure 4.15, along with the image of the resolution test chart. Note that the green light is diffracted through a smaller angle than the red light used to write the hologram due to the dispersion of the holographic grating. To produce these images, the optics used for the production of the earlier interference pattern and resolution test chart images had to be moved and re-aligned to the green diffracted wavefront.

The correction factor, from Eq. 4.1, varies as shown in Figure 4.16. The correction factor is ~ 6.3, so for every 6.3 fringes in the red interferogram (Figure 4.9), there should be 1 fringe in the interference pattern at $\lambda' = 532$nm. This is confirmed by the interferogram in Figure 4.15(a). Note that the overall cylindrical figure error is still evident, with an excess of fringes in one direction compared to that at right angles to it. This means that the corrected wavefront at this wavelength is still slightly astigmatic. This is confirmed by the resolution chart test which shows a definite astigmatism. The resolution is 14.3 lines/mm (Column 3, Row 6) in the vertical direction and 20.1 lines/mm (Column 4, Row 3) in the horizontal direction.

It should be noted that while the remaining error is quite large and may seem to indicate that the correction is severely bandwidth limited, the mirror did have an unusually large surface error to begin with. This was done in order to have a more dramatic test of the holographic correction. In any real telescope, the initial mirror surface quality could be made far superior to this with minimal effort. In such a case, the bandwidth will increase, as less correction (and hence a smaller correction factor) is required for diffraction limited operation [63, 64].

4.5 Future Directions

As the speed of the primary mirror increases, so do the problems associated with increased spherical aberration and reduced correction factor. In this section I will

(a).

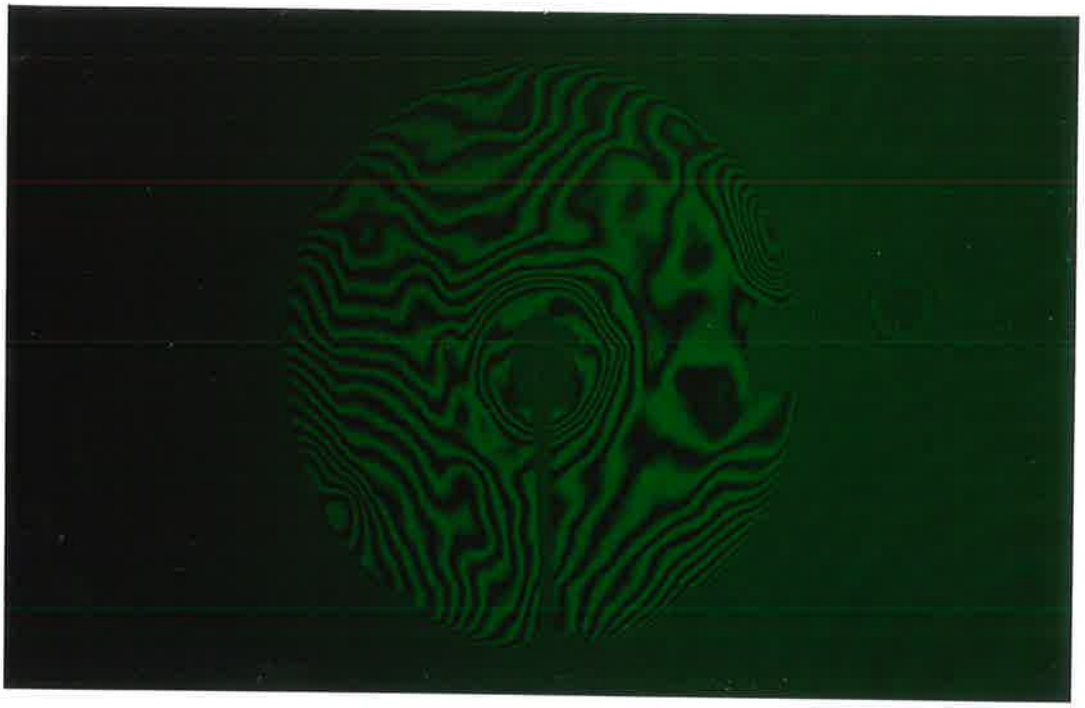

(b).

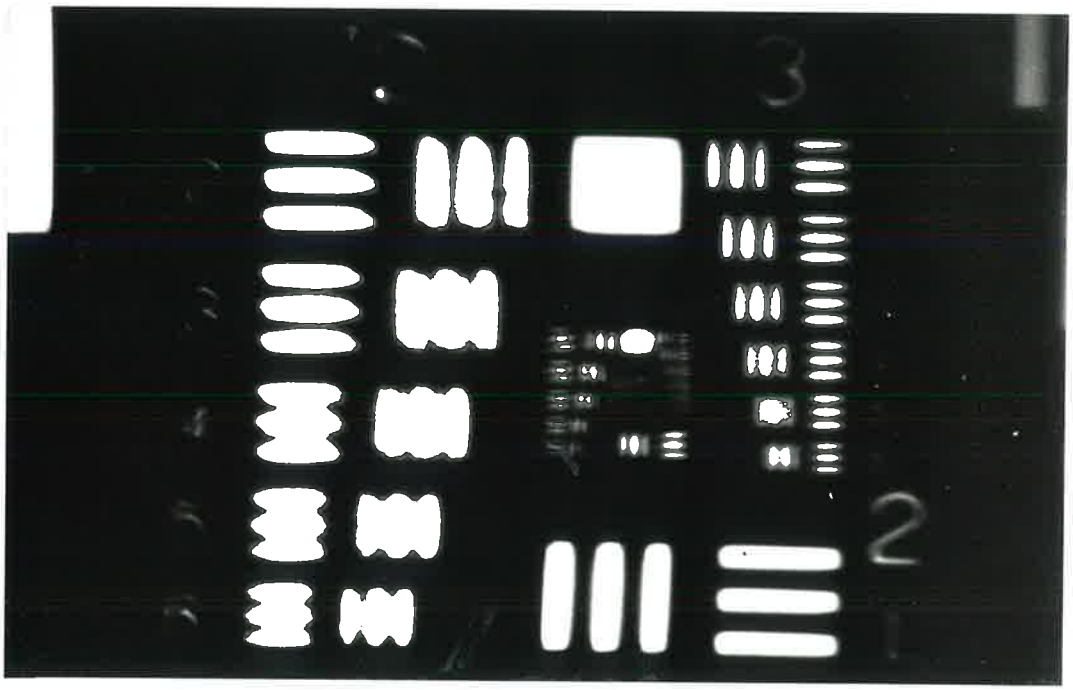

Figure 4.15: (a). The interference pattern of the reconstructed wavefront. (b). The corrected resolution chart.

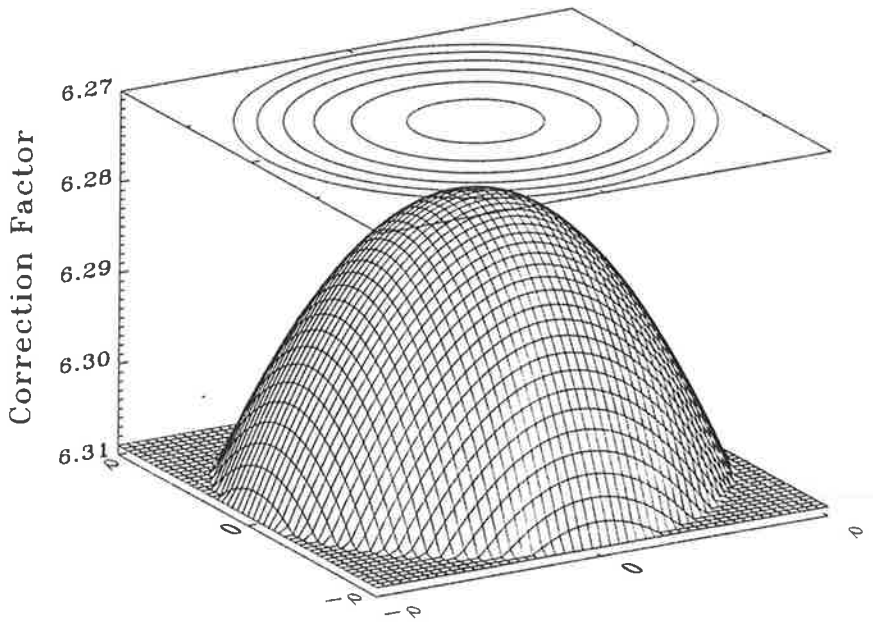

Figure 4.16: The correction factor (Δ^{-1}) for the on-axis recording and reconstruction is plotted as a function of position over the mirror ($R = 5.2$m, $\rho = 0.225$m). The recording wavelength is $\lambda = 632.8$nm and the reconstruction wavelength is $\lambda' = 532$nm.

briefly describe some possible solutions to these problems.

4.5.1 Spherical Aberration Correction

While the previous experiment demonstrated that complete correction of a heavily aberrated spherical telescope mirror was possible using a local beacon, its aperture and speed meant that only 7.2 waves of spherical aberration had to be removed. If the mirror is used to its full diameter of 0.86m there will be 96 waves, in which case a simple lens alone will not suffice for the removal of this aberration since the form of the wave aberration functions for a lens and a mirror are quite different (*c.f.* Eqs. 2.28 & 4.4). In such a case, a reflective null can be used for the introduction of spherical aberration on recording and one possibility is to use a small, high quality parabolic mirror. The beacon is placed at the radius of curvature of the parabolic secondary, and the conjugate point forms the spherically aberrated beacon which illuminates the spherical mirror from the centre of curvature as before.

The amount of spherical aberration wavefront error (to third order) at the focus of a spherical mirror can be found by using Eq. 2.28;

$$W_s = \frac{\rho_s^4}{4R^3} \tag{4.5}$$

Using Eq. 2.33, the spherical aberration wavefront error from a parabolic mirror illuminated from the centre of curvature (*i.e.* $y = 2f$) is

$$W_p = \frac{\rho_p^4}{32f^3} \tag{4.6}$$

If $f = R/2$, and the two mirrors are the same size, then the third order spherical aberration will cancel out. If we take a smaller secondary, however, with $\rho_p = \rho_s/10$, then the focal distance required (with $R = 5.2$m) is 0.3m which is more suitable for such a scheme. This method of introducing spherical aberration would completely remove third order spherical aberration over the entire surface as the two equations have the same ρ^4 dependence. It should be pointed out once again though, that the secondary mirror in this case would have to be diffraction limited, since the hologram will only be able to correct for the aberrations of the spherical mirror.

4.5.2 Other Factors

At the moment, even with a heavily aberrated mirror, the correction factor resulting from the geometry of the proximal beacon position does not seem to be a limitation. As the speed increases, however, the correction factor will become more important. For example, the minimum correction factor for a 1m diameter, F/2 mirror with the on-axis scheme is 127. Obviously, with such a mirror, the surface quality will have to fairly good to begin with. Given that the mirror was made from a crude process, it should be simple enough to improve on the original figure.

A further problem is that the imaging optics have to be faster than the primary in order to gather all of the light. In the previous experiments, the extent of the aberrations meant that the camera lenses had to be twice as fast as the large mirror in order to avoid vignetting of the extreme rays. Though fast camera lenses are available, this factor may prove to be a fundamental factor which limits the speed of the primary.

Lastly, the hologram itself will not only have to be written on better substrates, but increased diffraction efficiency will be essential for applications for lidar and astronomy. Dichromated gelatine holograms can be produced on high-quality substrates, giving low noise, near-100% diffraction efficiencies with operation into the near-UV. The only drawback is the high energy requirements for optimum exposure which can mean increased exposure times. This in turn, would translate into restrictions on the recording environment - most notably with the allowable air turbulence.

4.6 Summary

In this chapter I have discussed the correction of an aberrated telescope mirror using an on-axis recording beacon located at the centre of curvature of a spherical primary. The reconstruction of the hologram takes place near the focal plane, and as such, spherical aberration will be present. In order to correct for this, spherical aberration was added to the hologram during recording. This was achieved two ways; by adding negative spherical aberration into the reference beam or positive spherical aberration in the object beam.

The first method proved to be inferior due to the appearance of astigmatism in the reference beam which was a result of the required alteration in aspect ratio using a prism. Although a small scale test demonstrated the feasibility of this technique the aberrations introduced were too large to be completely removed in a large scale test.

The second method involved spherically aberrating the beacon which illuminated the mirror, making it possible to record the required amount of spherical aberration without the introduction of any off-axis aberrations. In this case, the large scale experiment resulted in near-diffraction limited correction at the recording wavelength, with the remaining error consistent with errors introduced by the non-common optics and a mis-match in the spherical aberration coefficients for the lens and mirror.

The correction of the telescope at a wavelength other than the recording wavelength was tested with the use of a CW frequency-doubled Nd:YAG laser, with the final wavefront error consistent with theoretical calculations.

Chapter 5

Conclusion

Large aperture imaging devices, with their high angular resolution and light gathering capabilities will always be necessary for lidar, surveillance and astronomical applications. New technologies are reducing the cost of very large diameter telescopes, but cheaper, simpler techniques are still desirable. One possibility is the use of inexpensive, low-quality, spherical primary mirrors which are holographically corrected to give diffraction limited performance over a narrow bandwidth. In the course of my research I have demonstrated a method for producing a simple, compact holographically corrected telescope using conventional optics.

The basic concept involves illuminating the mirror with a proximal laser beacon and using the reflected light to form an image hologram of the mirror surface. The hologram is then used as an optical element to correct for the aberrations of the mirror in the focussed light from an object at infinity.

5.1 Theoretical Model

The modelling of the holographic correction of a general surface defect has led to the derivation of an equation which can be used in calculating the correction factor - the factor by which such a defect is reduced. The general nature of this formula makes it suitable for the application to just about any scheme.

5.2 The Off-Axis Design

The off-axis design has a recording beacon located at the radius of curvature at the edge of the primary aperture. This beacon position will maximise the correction around the edge of the mirror with the minimum correction at the centre. The benefits of this scheme are that the best correction is applied to the largest area, while the telescope maintains a clear aperture. This scheme also allows the recording optics to remain in place for reconstruction of the hologram. The major drawback is the necessary introduction of a large amount of off-axis aberrations which are present on the reconstructed wavefront. These aberrations have to be removed from the final wavefront or holographically recorded in the first place.

Experimental results proved that the correction of the mirror surface aberrations and off-axis aberrations was fairly straightforward. The result was, in effect, the production of a perfect spherical mirror which, when used to focus collimated light, produced a spherically aberrated wavefront. The various schemes proposed for removing the spherical aberration could not be easily incorporated into the off-axis scheme and the best result, with a 450mm diameter F/6 mirror, was a reduction in wavefront error from > 100 waves to ~ 5 waves of spherical aberration. Though this is far from diffraction limited, this telescope would be suitable for ground-based astronomy and lidar as it is better than seeing limited.

The correct amount of spherical aberration and astigmatism could have been added using a secondary reflective optic on recording, which would cancel out that which appears on reconstruction with both fixed and adaptive mirrors - a technique which is used in many telescopes. Though these optics are not inexpensive, it should be cost effective to produce large aperture telescopes by this method.

5.3 The On-Axis Design

The on-axis correction scheme involved placing the recording beacon at the centre of curvature of the primary mirror. The correction in this case is largest at the centre which is now obscured on reconstruction and is a minimum at the edge. The off-axis experimental results, however, showed that corrected wavefront was limited by the

geometrical aberrations and not the mirror surface aberrations, so this approach is still practical. With the on-axis scheme there were no off-axis aberrations and spherical aberration information could be including during recording.

Two spherical aberration correction schemes were evaluated; one with the negative aberration added into the reference beam and the other with the positive aberration added in the object beam. The former met with limited success due to the necessary introduction of slight off-axis aberrations which had to be removed from the reconstructed beam. The latter idea, however, proved more successful. Results showed that the heavily aberrated mirror (> 100 waves surface error) could be holographically corrected to near-diffraction limited performance, with the remaining errors consistent with the limited quality of the non-common optics. The broadband performance is consistent with theoretical predictions.

The final on-axis scheme (with spherical aberration correction) is not only a simple and compact method of holographically correcting an aberrated spherical primary, but makes use of readily available optical components and is well suited to an increase in scale for larger diameter mirrors. Future work may concentrate on a reflective secondary for the addition of spherical aberration on recording.

5.4 Applications for Holographically Corrected Telescopes

The main advantage of holographically corrected telescopes is in the reduction in mass and fabrication costs of a perfect primary, and in the ability to correct for large changes in shape that may occur over a period of time. The major tradeoff is the reduction in useful bandwidth.

In the case of lidar, the production of a holographically corrected primary is relatively easy. Even with a fast, heavily aberrated mirror it is quite simple to produce a seeing-limited primary. An added feature is the narrow band correction and the angular dispersion of the corrected beam from the hologram which gives increased signal-to-noise benefits.

For ground-based astronomy, the effect of atmospheric turbulence in distorting

the beacon wavefront will make it impossible to produce a telescope that operates at better than seeing-limited even with the more successful on-axis scheme. However, this may not be seen as too much of a limitation given the large increase in light-gathering power that becomes available with this technology. Holographically corrected telescopes are particularly well-suited to all-sky survey astronomy as many receivers can be built, cheaply, which can be used to look at individual segments of sky.

Space-based telescopes are an important area in which holographically corrected telescopes could definitely make an impact. At the moment, the maximum diameter for a telescope with a monolithic primary is limited by the size of the space shuttle cargo hold, as in the case of the Hubble Space Telescope. To achieve further gains in primary mirror area, it is necessary to either assemble the telescope from many perfect segments or use an alternative technology. Holographic correction could be applied to inexpensive inflatable or segmented primaries which would reduce the need for exacting construction and transportation. While a space based telescope is a long way off, holographic correction could definitely produce useful gains in this field.

Lastly, it should not be overlooked that while holographic correction can be used to produce larger telescopes, the same technology could be used in the construction of a new generation of optical microscopes. Several schemes are available which could increase the resolution as well as the working distance in microscopes.

5.5 Summary

The design analysis and experimental results presented in this thesis show that a simple, compact holographically corrected telescope constructed from a heavily aberrated spherical primary mirror is a realistic concept. While research continues, it is clear that this technology offers an important alternative to many present telescope designs.

Appendix A

The Making of a Hologram

In this appendix, I will outline the equipment used in most of the experiments and the procedure involved in exposing and processing a typical hologram.

A.1 The Table and Laser

The hologram itself is a recording of the pattern produced when two or more coherent, waves interfere. There are several requirements for a successful hologram, the first of which is a stable environment. The fringes on the plate can not be allowed to move during the exposure as this will at least reduce the fringe visibility or destroy the interference pattern completely. The two beams used in writing the hologram, as well as all the optics involved, must be kept free from external vibration. To do so, the holograms were made on a vibration damped optical table, which itself was placed on vibration isolating air-legs. The table alone was too short for the large mirror experiments, so an extension was constructed from steel I-beams. The design is shown in Figure A.1. After construction the vibrations due to the cantilever were found to be causing too much vibration so they were stiffened by adding planks of ply-wood down the extended length of the beams. The vibration problem was further reduced by forcing both beams of the hologram to follow similar paths over the table. This meant that not only did the object beam reflect off the large mirror at the end of the table, but the reference beam also reflected off this same mirror before spatial filtering. With this arrangement, exposures of up to about 15 seconds

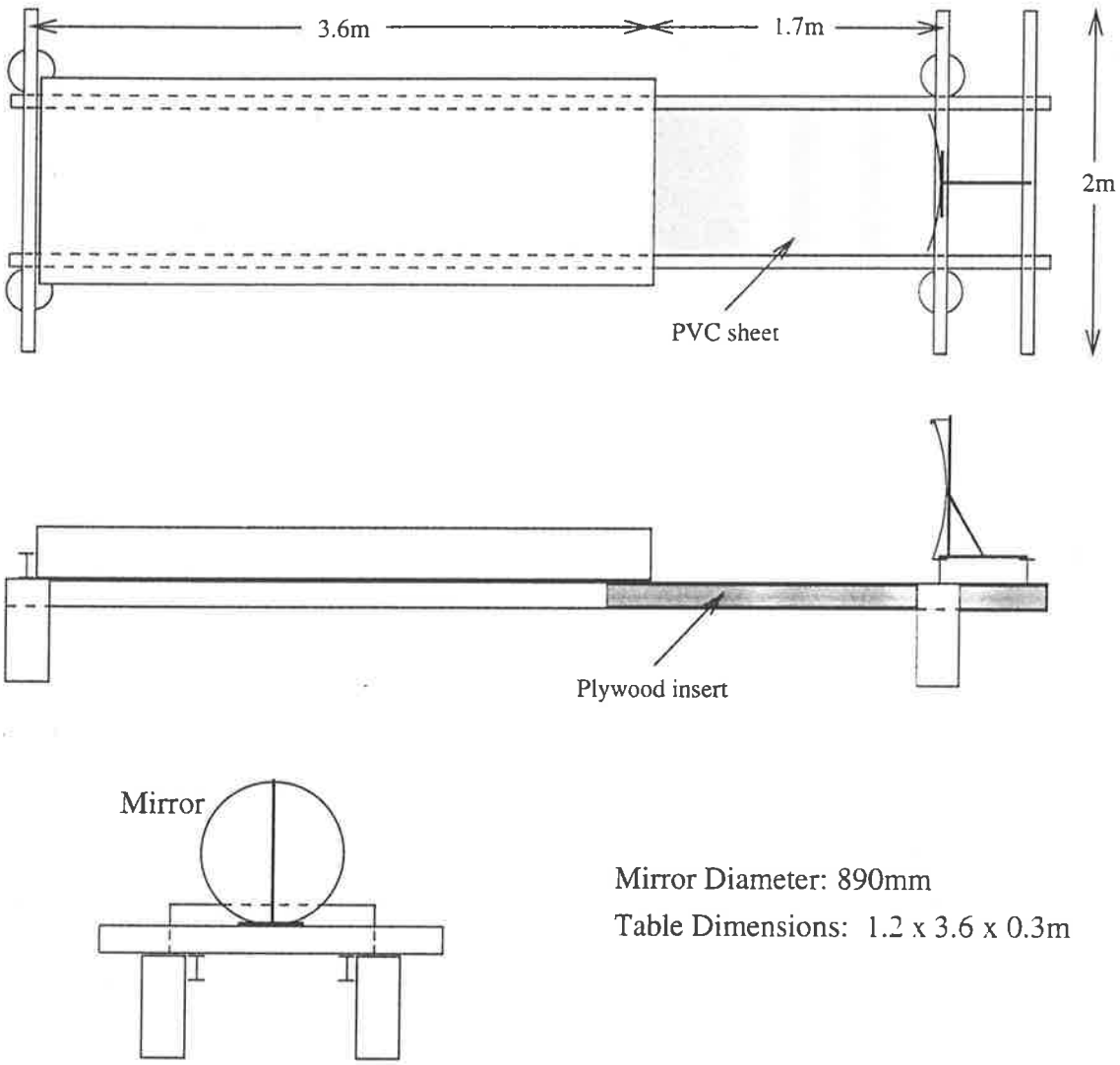

Figure A.1: A schematic of the table construction and mirror mount. The laser (not shown) hangs beneath the centre of the optical table.

could be tolerated.

The laser used in writing the holograms was a Russian-made HeNe laser ($\lambda = 632.8$nm) capable of delivering $90-100$mW of multi-mode power. With the inclusion of the intra-cavity etalon, the single-mode power is $40-65$mW. The multi-mode operation gave a coherence length of $100-150$mm and single mode operation increased this to ~ 6m. Although such a large coherence length was available, path-matching to within 50mm or less was still necessary since the laser tended to lose alignment in a short period of time, due to thermal expansion of the aluminium laser mirror mounts, which reduced the coherence length. The loss of single-mode operation and general beam movement was less of a problem after the laser was allowed to thermally stabilise over a period of about 3 hours.

Air currents were also a problem with such a large volume of air being traversed on both recording and reconstruction. Since the laser was mounted beneath the table, this caused hot air to rise around the edges. To reduce the effect of this turbulence, a sheet of PVC was placed over the gap between the large mirror and the table. Also, on recording, plastic sheeting was attached to the side of the table which was raised to form a "wing" which reduced the turbulence near the edge. These additions had a dramatic effect, both on the efficiency of the holograms recorded, and the stability of the reconstructed image/interference pattern.

Two photographs of the laboratory and optical bench are shown in Figure A.2.

A.2 The Plate Holder

The holographic plates were held in kinematic holders for writing and reconstruction. The design of these holders is shown in Figure A.3. These holders allowed the hologram to be placed in a given position for recording, removed for processing and placed back in the same position for reconstruction. Most experiments had one holder for recording at the centre of curvature of the mirror and another at the focal plane. The images of the mirror formed at each plane had to be identical in position and orientation. The position of the plate could be changed by simply adjusting the translation stages to which it was mounted. For slight differences in rotational

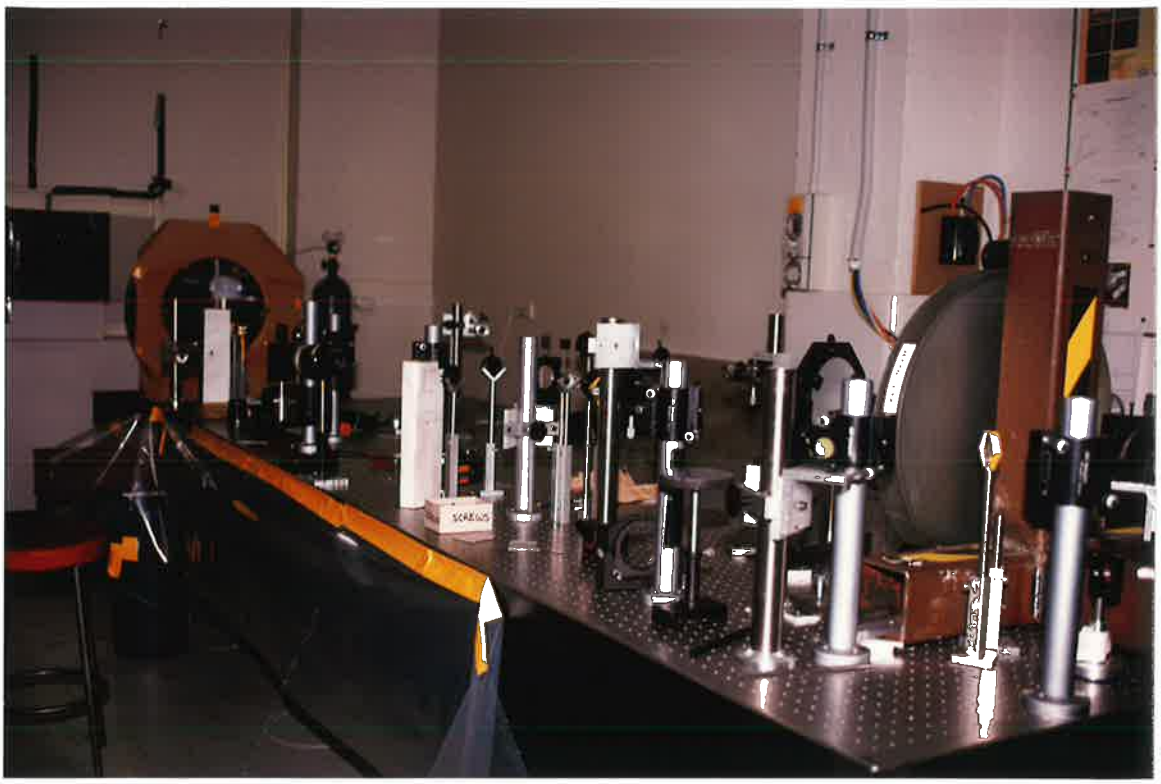

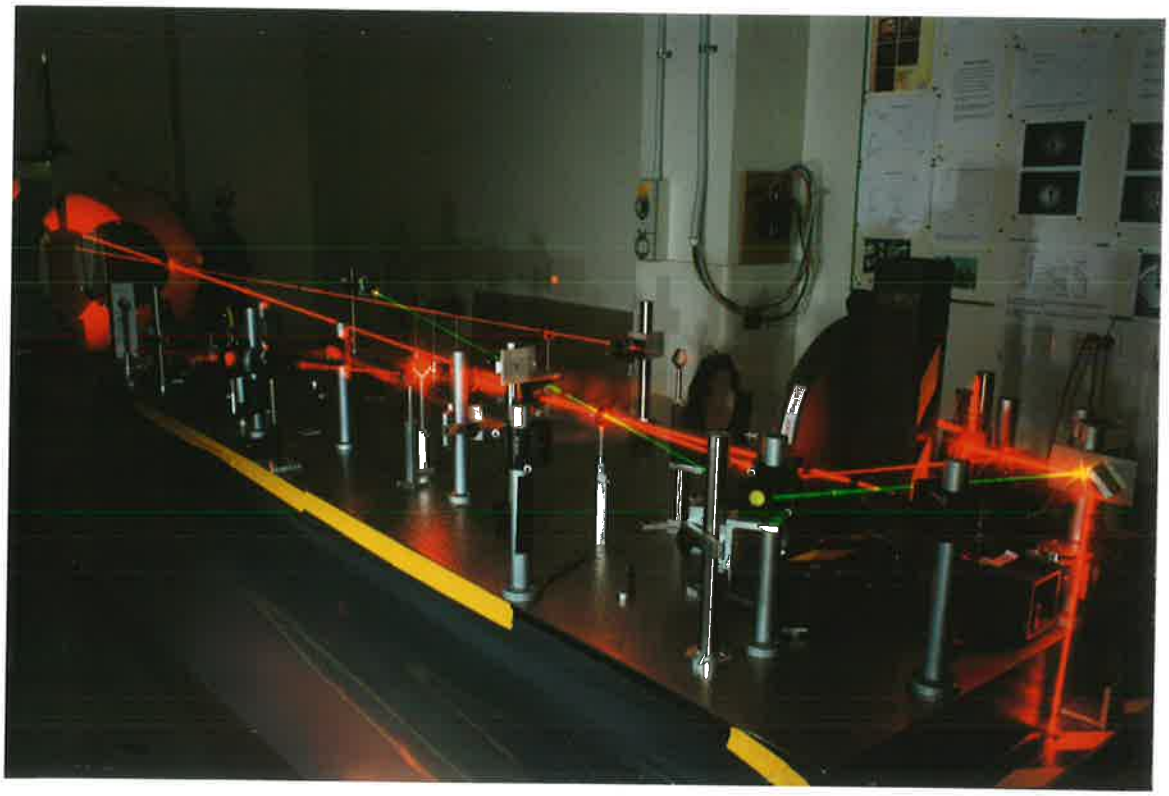

Figure A.2: Two photos of the set-up used in the holographic correction of the large slumped-glass mirror. The parabolic collimator is in the foreground (facing away) and the large aberrated mirror is in the background.

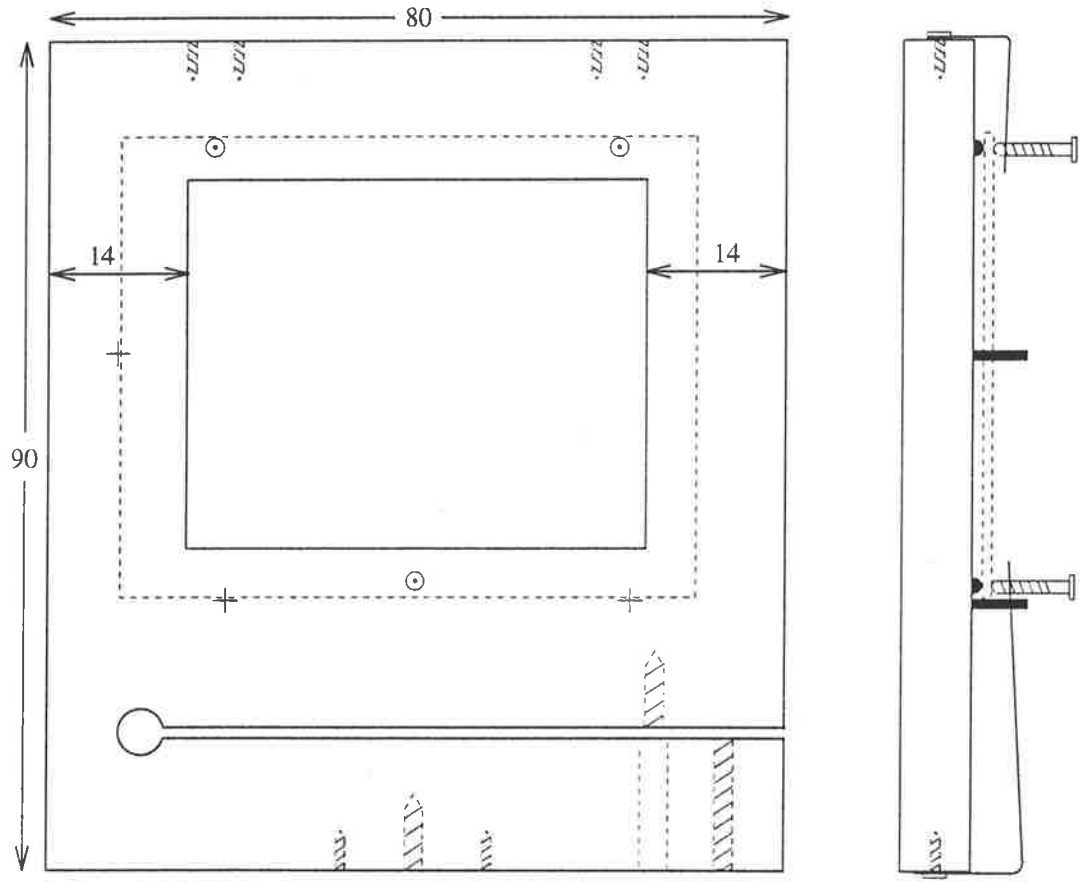

Figure A.3: The design of the holder (to scale). The large dashed rectangle indicates the size and position of the hologram when in place. The dotted circles represent ball-bearings and the crosses represent stainless steel studs. All dimensions are in millimetres.

orientation between the recording and replay holders, a small amount of tilt could be applied by two screws at the bottom of the mount.

A.3 Exposure and Processing

In all of the experiments discussed in this thesis, the holograms made were transmission phase holograms. Transmission holograms are made with the object and reference beams incident on the plate from the same side. A phase hologram is one in which the recording emulsion is bleached when processing in order to give a grating composed of variations in emulsion refractive index. The procedure for exposure and processing varied greatly over the course of this research in order to improve the diffraction efficiency (η_e - the ratio of the power in the first diffracted order to the input power).

The holograms were recorded on Agfa 10E75 plate film cut to $2'' \times 2.5''$. The path-matched reference and object beams were adjusted to have equal power at the plate. The angle between them was minimised in order to reduce the spatial frequency of the fringes at the plate (with $2\sin\theta/\lambda$ fringes per unit length for a recording angle of θ between the beams). The exposure energy was usually about 100-200μJ which is much more than required (and specified) for an intensity hologram. The processing of the holographic plate followed the following recipe;

1. Develop in Agfa Refinal or Kodak D-19 to O.D. ~ 2.
2. Wash in warm water ($\sim 50°$C) for 5-10 mins.
3. Fix (if desired) in non-hardening fixer 40°C for 1 min.
4. Bleach for 1 min in bleach at 30°C (see recipe below).
5. Wash in flowing water (20°C) for 10 minutes.
6. Rinse in 50% iso-propanol (propan-2-ol) for 3 mins.
7. Rinse in 75% iso-propanol for 3 mins.
8. Rinse in 100% iso-propanol for 3 mins.
9. Allow to dry in air.

Bleach Recipe (courtesy Australian Holographics Inc.);

Sodium Hydrogen Sulphate	.....	80g
Potassium Dichromate	.....	5g
Water	.....	1L

The temperature of the baths is especially important as it affects the efficiency dramatically. The temperature of the wash in Step 2 was found to be critical. If it is too hot, the emulsion will be damaged and cause a gradual fogging to appear after drying. Although this fogging can be removed by breathing on the affected areas, there is some loss of diffraction efficiency. Care should also be taken to ensure that no dramatic changes in temperature occur between one bath and another as this puts strain on the emulsion and results in increased scatter which, it is believed, comes from minute tears and cracks. The rinsing in iso-propanol is designed to expel the water from the emulsion. The successive baths of increasing concentration are designed to do this gradually and not subject the emulsion to a sudden stress. Many agents, such as Agapon (Agfa) and PhotoFlo (Kodak), are available to help dry out negatives without leaving watermarks. These are just detergents which were found to give poorer quality holograms when used instead of the iso-propanol baths. N.B. Grease, naturally present on fingers, will cause spots to appear on the hologram if they come into contact with the plate during processing. These spots increase light scatter and as such reduce the efficiency of the hologram, so gloves were used at all times during processing.

The application of these procedures usually resulted in a low-noise hologram with a diffraction efficiency of 20-40% and a significant reduction in distortion of the emulsion. The best hologram made by this method had a diffraction efficiency of 70%. Additional further information on processing can be found in References [87, 22, 48, 36] and [79]. Two photographs of a hologram reconstructed in white light are shown in Figure A.4.

(a).

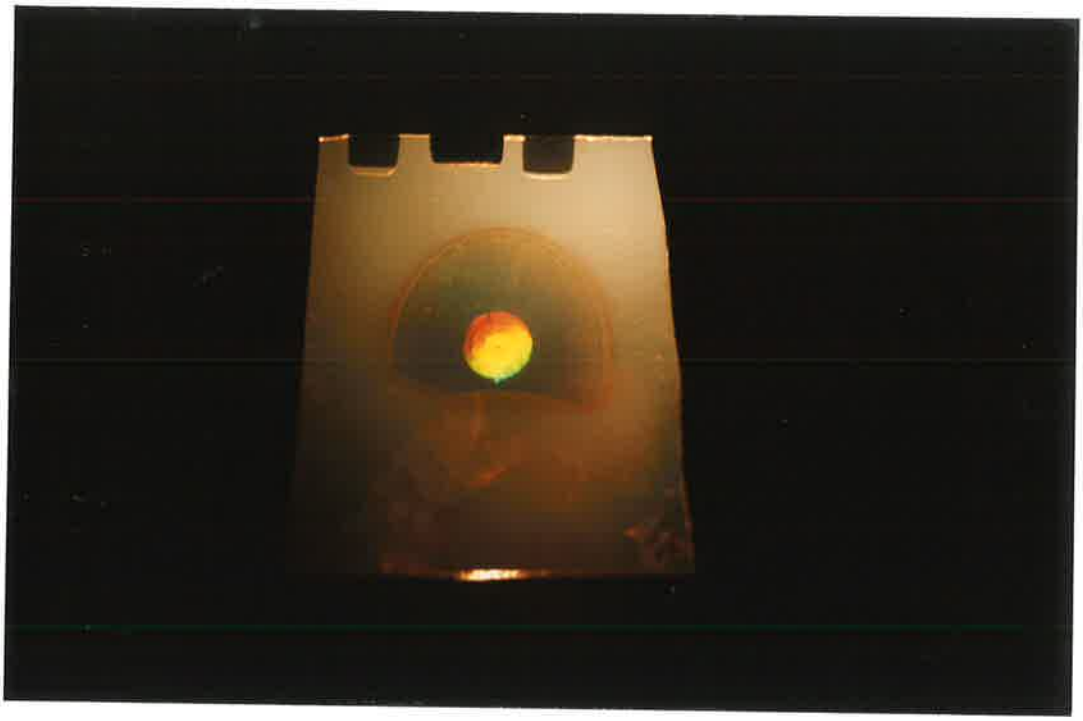

(b).

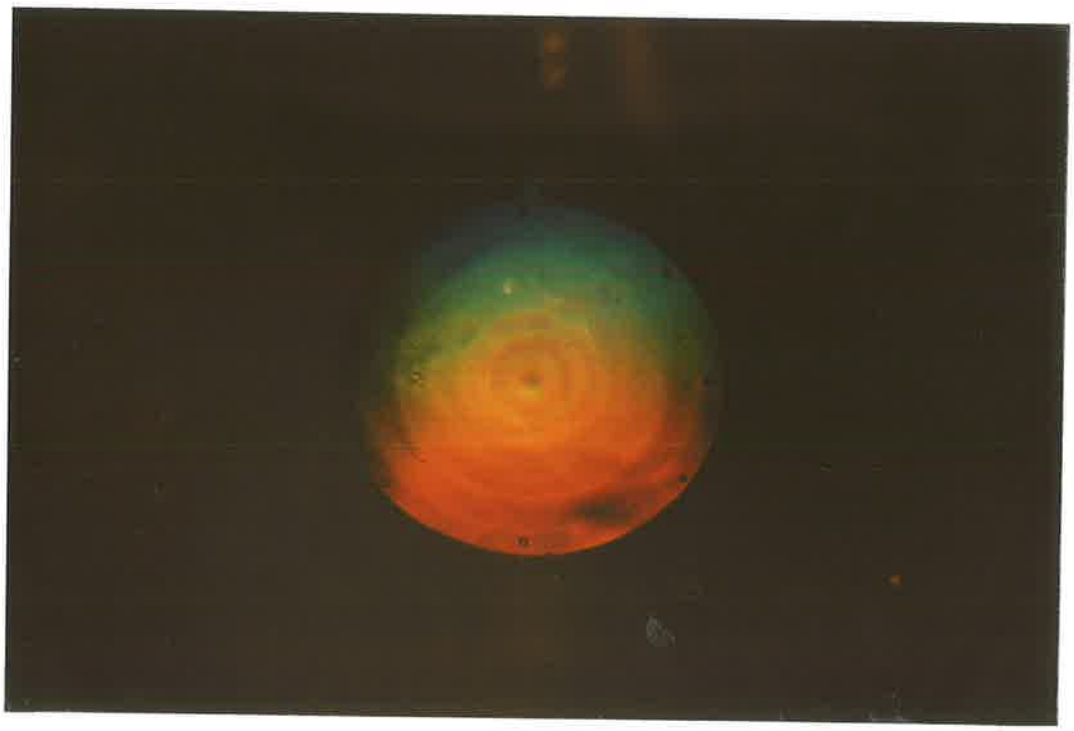

Figure A.4: (a). A typical image hologram ($D = 10$mm), as seen reconstructed by a halogen light. (b). A magnified view. Notice the "rings" present on the image of the mirror surface. The smaller circles located at various points around the edge are fiducials placed on the mirror to allow for accurate relocation at the reconstructing image plane. Note the elliptical appearance due to the tilt of the plate.

Appendix B

The Aberration Correction Factor

This appendix will provide a more detailed description of the derivation of the formulae quoted in Chapter 2. The relative phase difference, Δ, has been defined as;

$$\Delta = \frac{\lambda' \cos\alpha}{\lambda \cos\beta} - 1 \tag{B.1}$$

with the recording and replay geometries as shown in Figures B.1 and B.2.

Beginning with the geometry for writing the hologram, we wish to find $\cos\alpha$;

$$z = R - \sqrt{R^2 - \rho_{uv}^2} \tag{B.2}$$

$$z^2 = 2Rz - \rho_{uv}^2 \tag{B.3}$$

where;

$$\rho_{uv}^2 = u^2 + v^2 \tag{B.4}$$

From ΔOBG:

$$l = \sqrt{y^2 + x^2} \tag{B.5}$$

$$\cos\gamma = \frac{y}{\sqrt{y^2 + x^2}} \tag{B.6}$$

Now looking at an enlarged view of the portion of the mirror inside the mirror;

$$a = \frac{z\sqrt{y^2 + x^2}}{y} \tag{B.7}$$

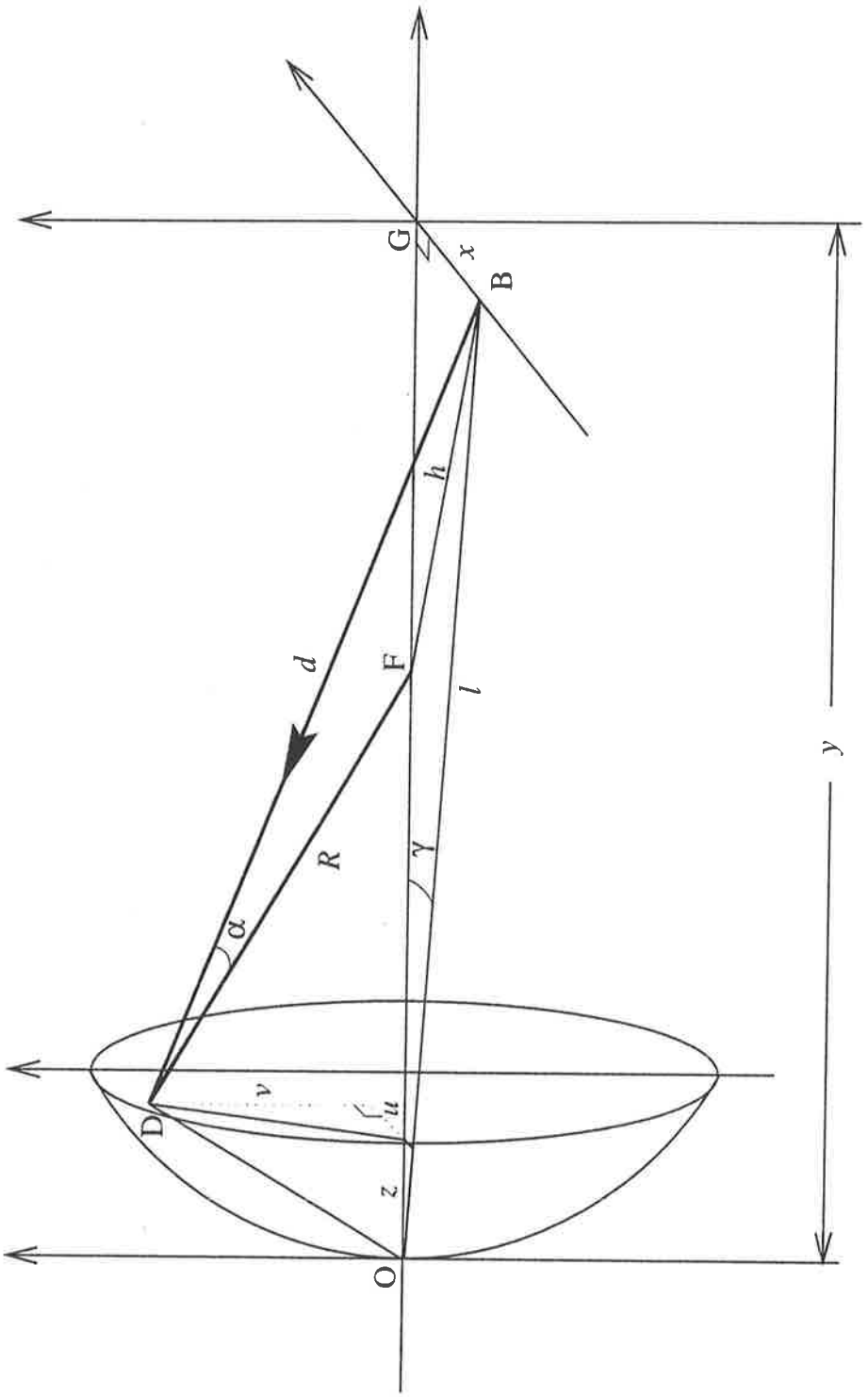

Figure B.1: The beacon illuminates the mirror from point B. A ray from the beacon to a point D on the mirror surface will make an angle of α to the normal at that point. The coordinates of the point D are (u, v).

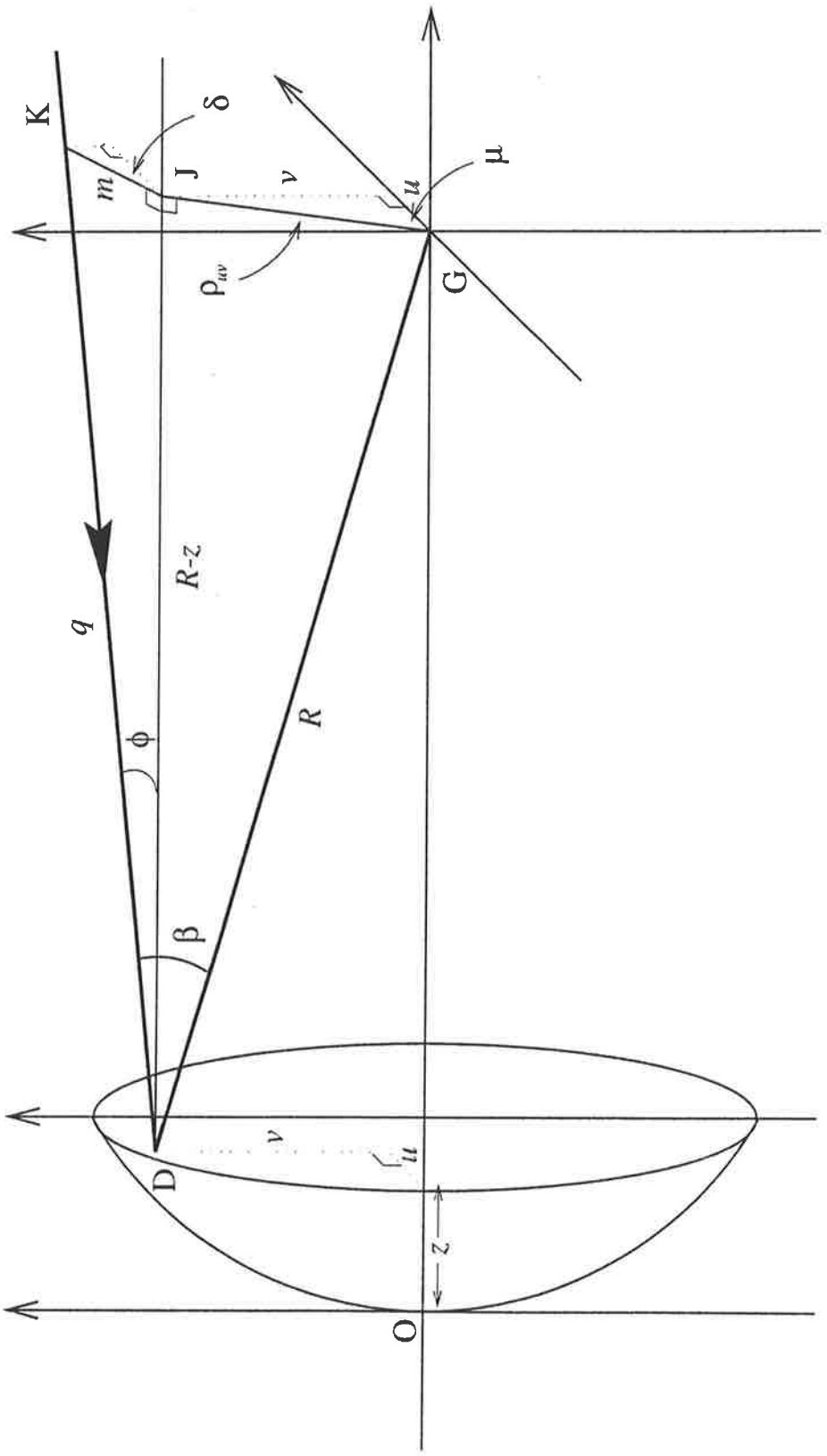

Figure B.2: An incoming ray, off-axis by an angle of magnitude ϕ and direction δ, strikes the mirror at point D and makes an angle of β with the normal at that point.

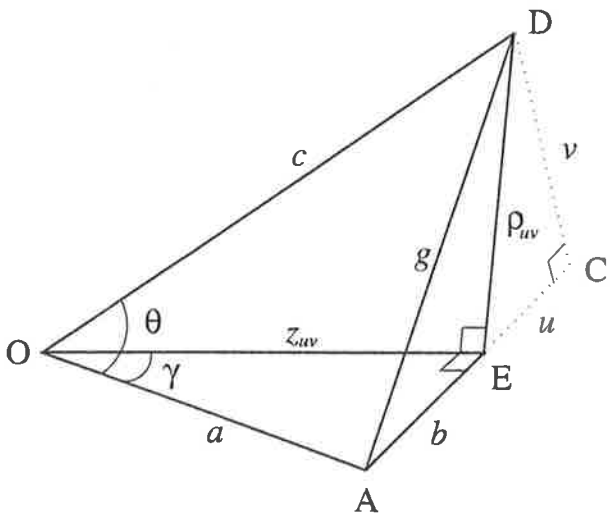

Figure B.3: A more detailed view of the geometry inside the mirror

$$b = \frac{zx}{y} \tag{B.8}$$

$$c = \sqrt{z^2 + \rho_{uv}^2} = \sqrt{2Rz} \tag{B.9}$$

$$g^2 = (b+u)^2 + v^2 \tag{B.10}$$

From ΔACD:

$$g^2 = a^2 + c^2 - 2ac\cos\theta \tag{B.11}$$

$$\Rightarrow \qquad \cos\theta = \frac{a^2 + c^2 - g^2}{2ac} \tag{B.12}$$

From ΔODB:

$$d^2 = c^2 + l^2 - 2cl\cos\theta \tag{B.13}$$

Combining this with Eq. B.12:

$$d^2 = c^2 + l^2 - \frac{l(a^2 + c^2 - g^2)}{a} \tag{B.14}$$

Now a look at ΔDFB/FGB shown in Figure B.4;

$$h^2 = R^2 + d^2 - 2Rd\cos\alpha \tag{B.15}$$

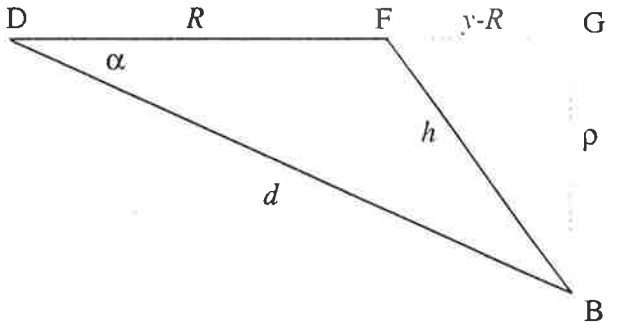

Figure B.4: Depiction of the geometry involved.

$$\Rightarrow \qquad \cos\alpha = \frac{R^2 + d^2 - h^2}{2Rd} \tag{B.16}$$

along with,

$$h^2 = (y - R)^2 + x^2 \tag{B.17}$$

gives;

$$\cos\alpha = \frac{R^2 + d^2 - (y - R)^2 - x^2}{2Rd} \tag{B.18}$$

Combining this with Eqs. B.5, B.7, B.8, B.9. B.10 and B.14 gives;

$$\cos\alpha = \frac{2xu + \frac{u^2 y}{z} + \frac{v^2 y}{z} + 2Rz - yz}{2R\sqrt{x^2 + 2xu - 2Ry + y^2 + \frac{u^2 y}{z} + \frac{v^2 y}{z} + 2Rz - yz}} \tag{B.19}$$

Rearranging Eq. B.3 will show;

$$\frac{u^2 y}{z} + \frac{v^2 y}{z} = 2Ry - zy \tag{B.20}$$

This means that Eq. B.19 becomes;

$$\cos\alpha = \frac{xu + Ry + Rz - yz}{R\sqrt{x^2 + 2xu + y^2 + 2Rz - 2yz}} \tag{B.21}$$

Now we can have a look at the situation for reconstruction (Figure B.2). The

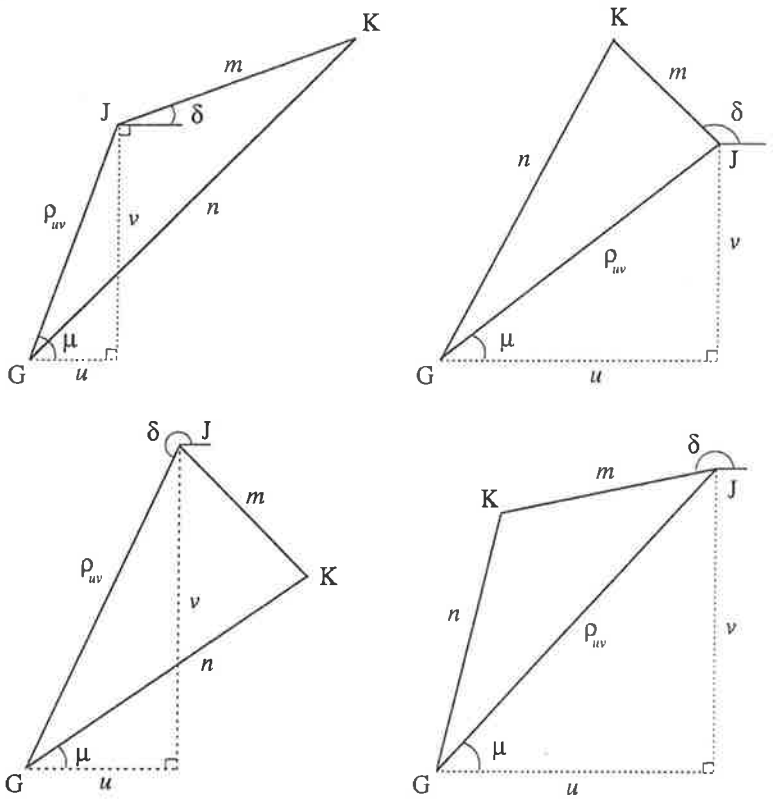

Figure B.5: Possible geometries for different angles δ.

total angle for the incoming ray at any point on the mirror surface with respect to the normal at that point is β. We need to find $\cos\beta$.
Looking at ΔDJK;

$$q = (R-z)/\cos\phi \tag{B.22}$$

$$m = (R-z)\tan\phi \tag{B.23}$$

We need to examine the various possible cases for the off-axis reconstruction. These are shown in the figure above. In each case we can see that $\angle$GJK is either $(180-\mu+\delta)$ or $(180-\delta+\mu)$. As it happens we are only concerned with the cosine of this angle and in both cases the cosine will be the same, so all situations will be

covered by the following formulae. From the diagrams;

$$n^2 = m^2 + \rho_{uv}^2 - 2m\rho_{uv}\cos(180 - \delta - \mu) \quad \text{(B.24)}$$

$$= m^2 + \rho_{uv}^2 - 2m\rho_{uv}\cos(\delta - \mu) \quad \text{(B.25)}$$

$$= m^2 + \rho_{uv}^2 - 2m\rho_{uv}[\cos\delta\cos\mu + \sin\delta\sin\mu] \quad \text{(B.26)}$$

$$= m^2 + \rho_{uv}^2 + 2m[u\cos\delta + v\sin\delta] \quad \text{(B.27)}$$

ΔDGK;

$$n^2 = q^2 + R^2 - 2qR\cos\beta \quad \text{(B.28)}$$

$$\Rightarrow \quad \cos\beta = \frac{q^2 + R^2 - n^2}{2qR} \quad \text{(B.29)}$$

Substituting in values for q and n as calculated previously and reducing;

$$\cos\beta = \frac{R^2 - \rho_{uv}^2 - m[u\cos\delta + v\sin\delta]}{qR} \quad \text{(B.30)}$$

$$= \frac{(R-z)^2 - (R-z)\tan\phi[u\cos\delta + v\sin\delta]}{R(R-z)/\cos\phi} \quad \text{(B.31)}$$

$$= \frac{\cos\phi}{R}(R-z) - \frac{\sin\phi}{R}[u\cos\delta + v\sin\delta] \quad \text{(B.32)}$$

Combining Eqs. B.21 and B.32 in the form of Eq. B.1 we can calculate the total relative path difference to be;

$$\Delta = \frac{\lambda'\,(xu + Ry + Rz - yz)}{\lambda\,((R-z)\cos\phi - [u\cos\delta + v\sin\delta]\sin\phi)\,\sqrt{x^2 + 2xu + y^2 + 2Rz - 2yz}} - 1 \quad \text{(B.33)}$$

where z is the spherical sag as shown previously in Eq. B.2.

Appendix C

Wavefront Analysis of Interferograms

For an analysis of the interferograms in this thesis, a computer program was written to calculate the peak-to-valley (W_{pv}) and root mean squared (W_{rms}) wavefront errors as well as a surface contour of the aberrated wavefront (*e.g.* Figures 3.9(b). & 4.11(b).). The following section aims to outline the theory behind this fringe analysis. Much of this can be found in References [82, 55, 6, 72] and [57].

An arbitrary interference pattern formed between an unknown wavefront and a plane wave reference beam has the form

$$u(x,y) = a(x,y) + b(x,y)\cos[2\pi f_o + \phi(x,y)] \tag{C.1}$$

where $a(x,y)$ is the background intensity, $b(x,y)$ relates to the fringe contrast, f_o is the carrier frequency and $\phi(x,y)$ is the phase information we require. We can rewrite Eq. C.1 as

$$u(x,y) = a(x,y) + c(x,y)e^{2\pi i f_o x} + c^*(x,y)e^{-2\pi i f_o x} \tag{C.2}$$

where

$$c(x,y) = \tfrac{1}{2}b(x,y)e^{i\phi(x,y)} \tag{C.3}$$

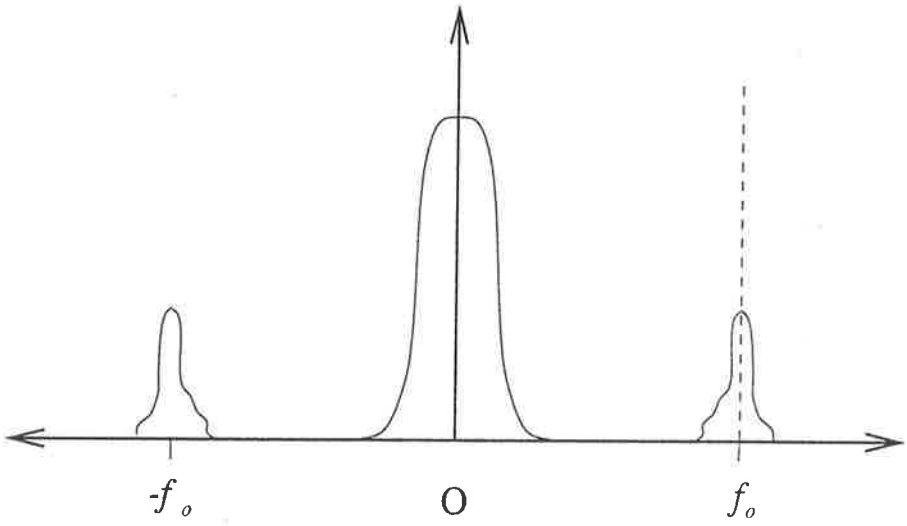

Figure C.1: The Fourier transform of the fringe pattern (simplified to 1-D) will have a central peak with two peaks at $\pm f_\circ$. The two peaks at 0 and $-f_\circ$ are discarded and the remaining peak is moved so that the maximum lies at the origin (dotted).

Taking the Fourier Transform of the image data $u(x, y)$ we get $U(f, y)$;

$$U(f, y) = A(f, y) + C(f - f_\circ, y) + C^*(f + f_\circ, y) \tag{C.4}$$

which is just the central peak $A(f, y)$, along with two first order peaks at $\pm f_\circ$ either side. Since the spatial variations of $a(x, y)$, $b(x, y)$ and $\phi(x, y)$ are assumed to be slow with respect to the carrier frequency, $f_\circ$, it is possible to isolate one of these peaks from the rest of the information in the Fourier domain. The broad peak $C(f - f_\circ, y)$ is chosen and all other information in the Fourier space is discarded. This peak is then translated by $f_\circ$ so that it now lies at the origin (Figure C.1). If we now take the inverse FFT with respect to f we get $c(x, y)$,

$$c(x, y) = \tfrac{1}{2} b(x, y) e^{i\phi(x,y)} \tag{C.5}$$

which is just a DC term multiplied by the phase factor. This indicates that the phase information $\phi(x, y)$ can be retrieved and isolated from the carrier fringe pattern. Once we have the phase factor we can calculate the extent of the deviation

from a plane wave at every point on the image ($s_{ij} = o_{ij}(x, y)$) and hence the wavefront error. Normally, this wavefront error is defined in two ways; Peak-to-Valley (p-v) and Root Mean Squared (r.m.s.)

The p-v error is simply a measure of the maximum departure of the wavefront from a plane wave, at any point on the wavefront. According to the Rayleigh criterion, the maximum allowable p-v error due to spherical aberration for an optical element to still be considered diffraction limited is $\lambda/4$ [7]. This has come to mean that on an interferogram, the maximum allowed deviation of a fringe is 1/4 of the fringe separation. It is now generally accepted that this type of measurement is all but completely useless in determining the imaging capabilities of an optical element. A mirror may produce an almost perfect interferogram but in one small, isolated region the fringes could exceed the 1/4-wave limit. In this case, according to the previous criterion, the mirror will produce images of less than perfect quality. In fact this is not so as the error is only confined to a portion of the mirror surface and so has little effect on the total imaging capability. The r.m.s. measurement seeks to improve the significance of the measured amount of wavefront error on the overall image quality. The phase deviation of the tested wavefront from a best-fit perfect wavefront (s_{ij}) is made at many different points over the aperture, and the r.m.s. error is calculated from the following equation;

$$W_{rms} = \sqrt{\overline{s^2} - \overline{s}^2} \tag{C.6}$$

For the r.m.s. meaurement the diffraction limited condition is an error of $\lambda/14$ or less. Typically the r.m.s. value is about a factor of three to four times smaller than the p-v error.

After calculation of the wavefront error, a surface plot of the reconstructed wavefront can be obtained. A computer program was written according to this basic concept, with minor adjustments made to make it possible to detect wavefront errors greater than $\pm\pi$. The results were compared to a commercial program which uses a Zernike polynomial fit to the image data, and was found to give consistent results.

Appendix D

The Distant Beacon

Although the idea of a beacon at infinity is impractical, a design incorporating a beacon at a large distance is reasonable. Since the recording beacon is an approximation to an object at infinity, this concept has several benefits. Firstly, there will be an increase in correction, allowing for a more aberrated primary. Secondly, an amount of spherical aberration will be recorded which will partly correct for that present on reconstruction from infinity. If the beacon is distant enough, the same optics can be used for recording and replay which eliminates the problem of moving the hologram [63]. If this is the case, a partially aberrated secondary could be used with a minor reduction in field of view[1].

With this basic design there are two possibilities, which I will call the active and the passive beacons. With the active beacon, the light source is separate from the telescope, and situated some distance away. With the passive beacon, the laser is located at the telescope but is reflected from an unresolved source some distance away. The choice of the most appropriate type will depend on the application for the corrected telescope. The recording scheme for the active distant beacon is shown in Figure D.1. The reconstruction set-up at the focal plane is the same as for the proximal beacon.

The correction factor in such a scheme is found using Eq. 2.9. With an on-axis

[1]This distant beacon approach should not confused with a beacon *at* infinity which utilises a collimated recording beam of the same diameter as the mirror. In this scheme, no large perfect optic is required to provide the illuminating beacon.

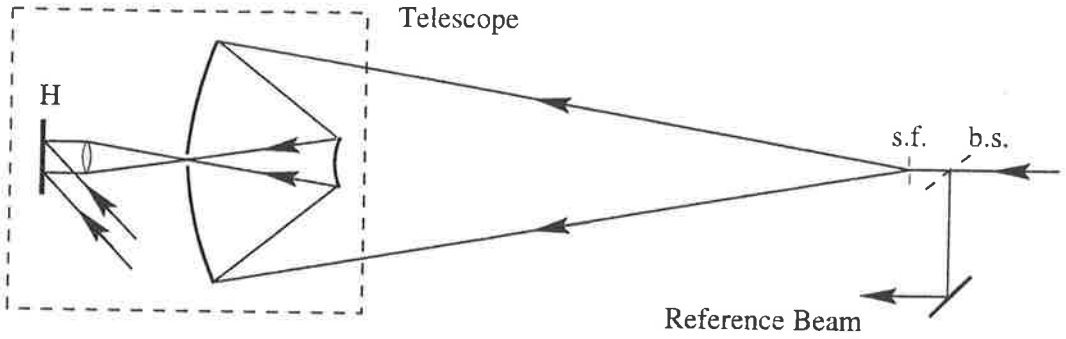

Figure D.1: Active Distant Beacon: A laser beacon (spatial filter) illuminates the aberrated primary from a distant location. A small portion of the laser beacon is split off to be used for the reference beam.

beacon ($x = 0$) located at some distance y, and on-axis reconstruction;

$$\Delta = \frac{\lambda' \left[y(R-z) + Rz\right]}{\lambda \left(R-z\right) \sqrt{y^2 + 2Rz - 2yz}} - 1 \tag{D.1}$$

As demonstrated previously in this thesis, the correction factor provided by a beacon at the centre of curvature is sufficiently large to allow correction of heavily aberrated mirror. As the beacon distance increases further, so will the correction factor. As an example, the minimum correction factor for beacon distances of $y = R = 5.2$m, $y = 10R$ and $y = 100R$ with a 0.86m aperture are $\Delta = 292$, $\Delta = 1534$ and $\Delta = 14647$ respectively.

With a beacon located at a distance other than the radius of curvature there will be some amount spherical aberration recorded. This will then cancel out part of the spherical aberration present when viewing an object at infinity. The amount of spherical aberration recorded is found using Eq. 2.27, or the fifth order expansion, Eq. 2.28;

$$W_{rec} = \frac{(R-y)^2\rho^4}{4R^3y^2} + \frac{(R-y)^2(3y-2R)\rho^6}{8R^5y^3} \tag{D.2}$$

On replay, the remaining spherical aberration will be

$$W_{rep} = \frac{\rho^4}{4R^3} + \frac{3\rho^6}{8R^5} \tag{D.3}$$

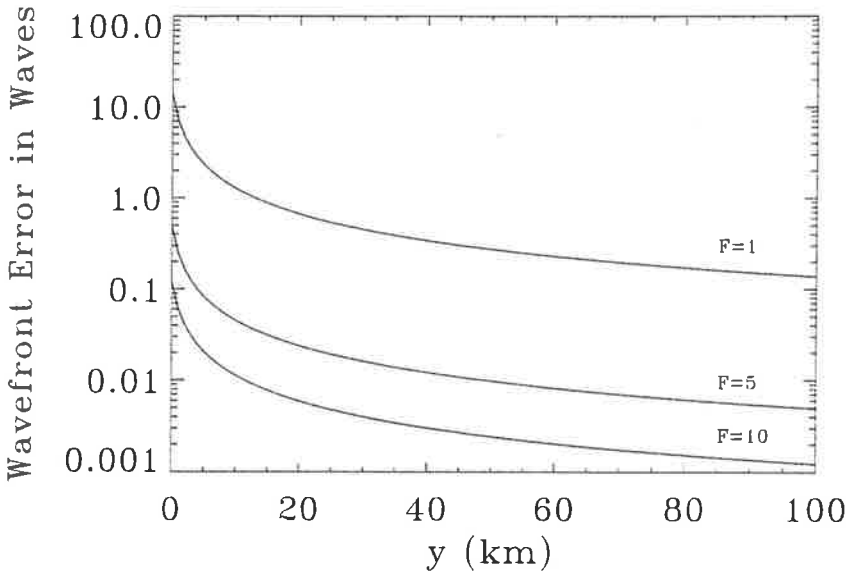

Figure D.2: A plot of the remaining spherical aberration error vs beacon distance, y, for three different mirror speeds (D = 1m in each case).

The difference between these two quantities ($\Delta W = W_{rep} - W_{rec}$) will be the amount of spherical aberration remaining;

$$\Delta W = \frac{\rho^4(2y - R)}{4R^2y^2} + \frac{\rho^6(8y^2 - 7Ry + 2R^2)}{8R^4y^3} \tag{D.4}$$

Obviously, $\Delta W \to 0$ as $y \to \infty$. As for finite values of y, the amount of spherical aberration correction will depend heavily on the mirror dimensions. Figure D.2 shows the amount of spherical aberration (in waves) remaining as a function of beacon distance for several different mirrors, all 1m in diameter. It is obvious from this plot that for the diffraction limited correction of spherical aberration, the beacon distance involved is quite large. At a distance of even 100m over ground, light from a beacon will become severely distorted by turbulence. It is for this reason that this scheme was not tested experimentally. For a space telescope, however, where there is no atmospheric turbulence to overcome, this approach may be practical.

As a further extension of this scheme, the distant beacon needn't be on-axis. In

fact, with several distant beacons, over a large area, the telescope could be corrected over a large field of view in much the same way as guide stars are used in adaptive optics. Because the distance is large, the off-axis aberrations recorded by the hologram are a close approximation to those which will appear on reconstruction in exactly the same way as the spherical aberration. Now, however, the aberrations introduced by the beacon can be used in order to increase the field of view. Given a large enough beacon distance, there should be no real limit to the field of view achievable with this scheme.

If the beacon is at a large enough distance from the primary, the imaging optics could remain in place for reconstruction. This would also permit the secondary to be partially aberrated as well. This is a return to the thick aberrator problem discussed previously in Chapter 2. In this case however, the recorded wavefront is almost identical to the reconstructing wavefront, so the recording and reconstructing rays will follow nearly the same path. If the primary and secondary mirrors are not too heavily aberrated, there will only be a small deviation of rays from two adjacent field points, so the field of view will not be reduced significantly.

Even if the secondary is diffraction limited, the distant beacon approach would allow the length of the instrument (minus the beacon) to be reduced to less than the focal distance of the primary. For a space telescope, where large thermal gradients will produce large expansions in both the primary and the framework around it, the shorter the telescope, the less often a hologram will have to be recorded. In fact, with the recording and replay optics as one, photo-refractive media might be used for real-time holographic correction.

D.1 Summary

A distant beacon could be used to give an increased correction both for the inherent random aberrations of the mirror and geometrical aberrations. Although this idea would be impractical for producing diffraction limited ground-based telescopes, due to the effect of atmospheric turbulence on the beacon light, it may be practical for a space telescope or for ground-based lidar.

Appendix E

Microscopes

Throughout this thesis, an evaluation of the imaging performance of a corrected telescope was made using a resolution chart. The fact that the telescope has, in that particular arrangement, produced high quality images of microscopic objects seems to suggest that the correction of large mirrors could be applied to microscope objectives. While the magnification provided by the reconstruction arrangements was low, the following section will introduce several designs with both high magnification/resolution and large working distances.

E.1 Microscopy

The angular resolution limit of a single optic is $\alpha = 1.22\lambda/D$ and the smallest resolvable feature has a diameter $d = 1.22\lambda l/D$ where l is the working distance (or distance from the sample to the objective). To increase the resolution, a faster optic must be used, which would suggest that we increase D and decrease l. In most microscopes the objective is very fast and, in order to reduce spherical aberration, generally quite small in diameter. These means that the working distances are very small. In order to increase the working distance, a large diameter, diffraction limited optic would have to be made which has no geometric aberrations, even if only over a small field of view [77].

Several different methods have been used to overcome these limitations. A confocal microscope (CM), increases resolution (and contrast) at the expense of field of

view [66, 76]. This is achieved by limiting the illuminating source and viewing region by a circular or annular aperture (typically in the order of $1-10\mu$m in diameter). A magnified image is constructed by a raster scan of the sample beneath this point of high (sub-micron) resolution. The working distance in a CM, however, is still quite small and good-quality objectives are still required.

A second major type of instrument is the scanning near-field optical microscope (SNOM) [70]. The SNOM uses a very small aperture/antenna as the source or detector of radiation over a point on the sample. There are many variations on the theme, but one basic design has a transparent object back-lit with the transmitted light picked up by a fine-tipped, aluminium-coated fibre, and funnelled to a photodetector. By raster-scanning the tip close to the surface, an image can be constructed with a resolution exceeding 10Å. The working distance in this case is of the order of $0.1-1\mu$m with an aperture size of $< 1\mu$m.

Such instruments provide ultra-high resolution but access to the sample is limited due to the small working distances and true real-time observation over any extent of the object is impossible. A useful instrument would be one in which a moderate field of view can be directly viewed with high magnification and a large working distance allowing access to the sample. In this appendix I will present a few possibilities for a holographically corrected microscope which incorporate one or more of these features, and have the benefit of using low-quality optical components[1].

E.2 The Basic Concept

Holographic microscopy in a refracting system is not new [13, 39, 93, 69]; the basic idea is shown in Figure E.1. A point source of laser light (smaller than the resolution limit of the objective) illuminates the objective and the transmitted light is collected to form a hologram with a diffraction limited reference beam (Figure E.1(a).). This scheme operates in almost precisely the same way as for the correction of a telescope objective.

[1] *N.B.* While holography has been used in optical microscopy before, most of the applications involve recording a hologram *of the object*, either for its high object information content [13, 39, 93, 69] or for optical filtering [29]. Most holographic correction schemes have concentrated only on

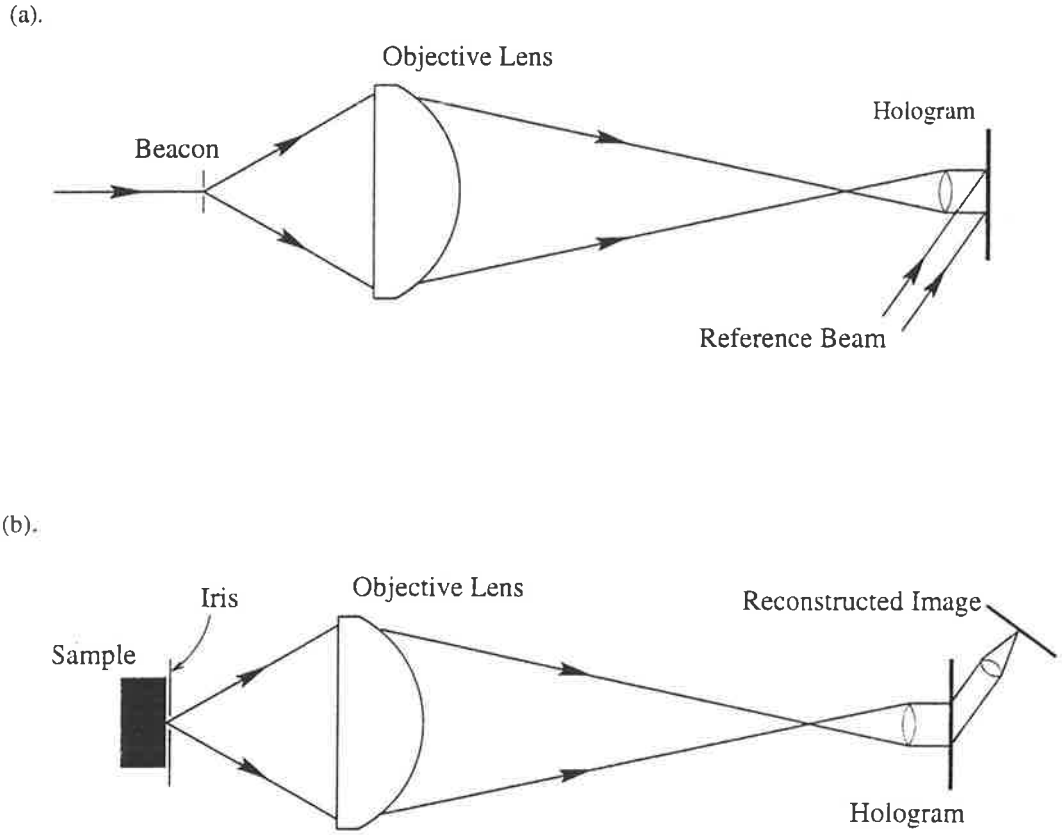

Figure E.1: (a). Recording: A beacon (spatial filter) illuminates the objective with the transmitted, aberrated light gathered by a secondary lens to form a hologram with a diffraction limited, plane wave reference beam. (b). Reconstruction: The beacon is replaced by an object. Light from a point on the object coinciding with the previous position of the beacon will reconstruct the reference beam at the hologram. An image of the object is formed by focussing this diffracted beam. An iris may be required at the object plane to prevent light from other field points reaching the hologram.

On replay, the beacon is replaced by the object we wish to observe. This object is illuminated with diffuse laser light, and the reflected light, from the previous position of the beacon will be transmitted through the system to reconstruct the reference beam. The object information is retained and this diffracted beam can be focussed to form an image of the object (Figure E.1(b).). It is important to note that the objective can have random aberrations of its own, though the holographic correction is mostly aimed at correcting for the geometrical aberrations which presently limit the size of current high magnification objectives.

The reconstruction set-up remains exactly the same as the recording set-up, with the beacon replaced by the object. In this case, the reconstructing object wave will be exactly the same as the recording wave. As a result, there is no real need for a secondary lens to image the objective onto the hologram. The lens is retained, however, as it still provides a demagnified image and removes the problem of speckle.

The hologram perfectly corrects for the aberrations in the image of the object *only at the point where the beacon was located.* Once again, however, if the field of view is too small, conventional raster-scanning can be used in the same way as for a confocal microscope.

E.3 A Reflecting Microscope

The refracting microscope has appeal as it closely resembles the appearance and operation of a conventional microscope. A holographically corrected, reflecting microscope has the advantage over a refractor, in that good-quality, inexpensive mirrors can be fabricated with larger F-numbers and with less material than lenses. With conventional microscopes, a reflecting primary can be used, but the obscuration of the reflected light by the on-axis object will degrade the image quality, while off-axis aberrations prevent the use of even a small off-axis angle. In a holographically corrected microscope, however, these off-axis aberrations can be recorded and removed since they remain the same on reconstruction. The basic scheme is shown in Figure E.2. Note that in this case the mirror is quite fast and so the diffraction

---

the spherical aberration in the microscope optics.

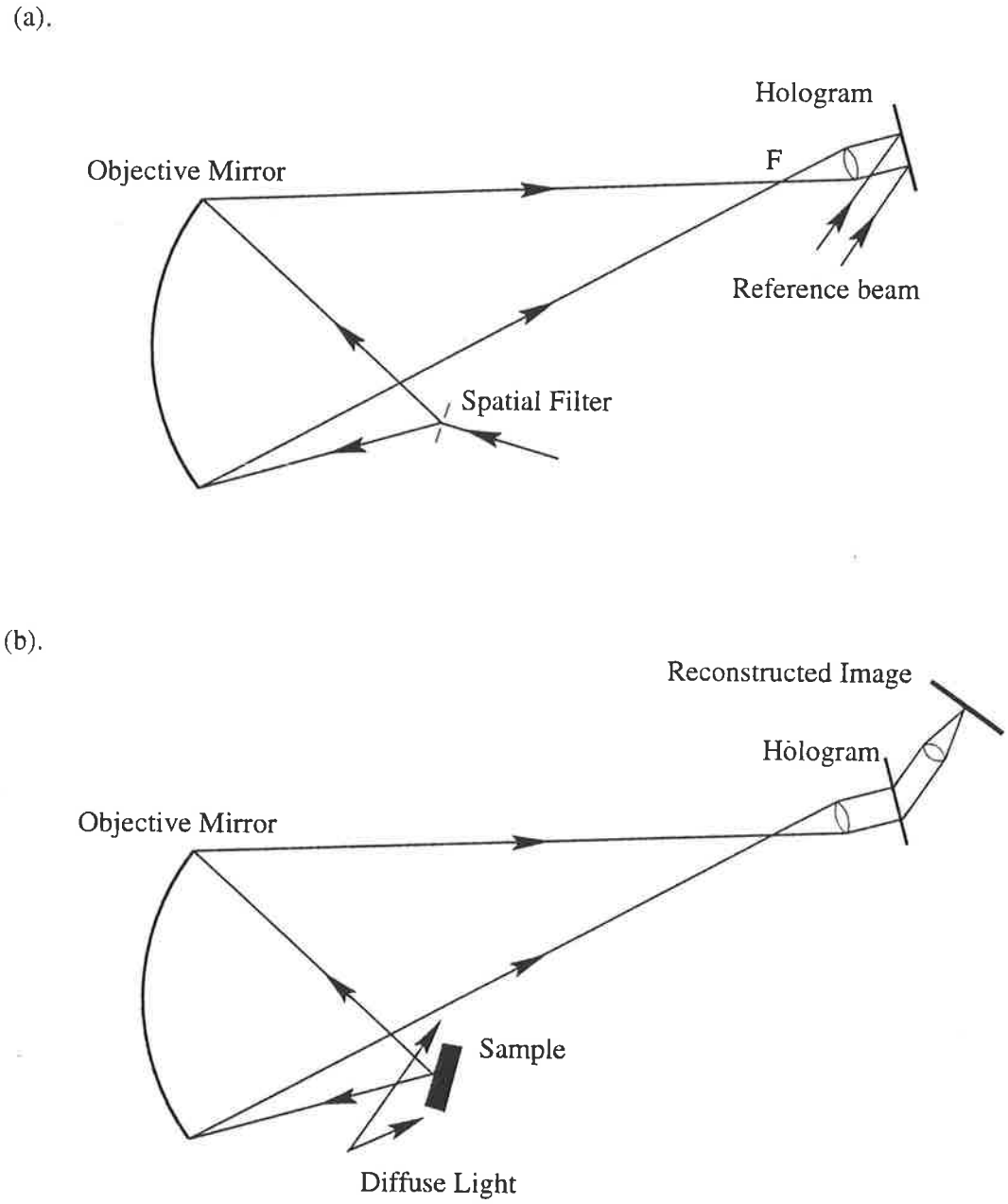

Figure E.2: (a). Recording: The off-axis beacon illuminates the mirror and the reflected light is gathered to form a hologram. Note that the focus (F) will be severely aberrated. (b). Reconstruction: The beacon is replaced by an object (illuminated with diffuse laser light), and light from a point coinciding with the beacon position will reconstruct the reference beam at the hologram as before.

limited pinhole required will have to be very small (of the order of the wavelength of the light used). An alternative to a pinhole would be to use an optical fibre drawn out to have this diameter exit aperture. Such fibres are available for use in SNOMs.

This microscope has several advantages over other techniques such as confocal microscopy. A large working distance has been retained, along with a high resolution. Furthermore, the cost of fabrication has been reduced as the microscope uses a reflecting objective which can not only be spherical, but can also have a poor surface quality. The one drawback (as with most microscopes) is the limited field of view.

E.4 Increasing the Field of View

To increase the field of view, it would be necessary to record the hologram of an infinite number of point sources over the extent of the object field desired. Recording different holograms for different field points on the one photographic plate poses the problem of multiple images on reconstruction. A solution to this is to record an infinite array of point sources over the entire object field simultaneously. This could be achieved using a particular type of holey film which is currently becoming available [83, 60, 67]. If the diameter and separation of the point sources is below the resolution limit of the objective, it will "see" what appears to be a large, coherently illuminated field. The light will be focussed by the mirror as before, and a hologram can be written (Figure E.3). On reconstruction, the holey film can be replaced by the sample to be magnified. In this case however, since the hologram has already recorded a wave from the entire field, the reconstructed image will also be corrected over the same large field.

There are several important factors to consider with this concept. Firstly, if the holey film is made optically flat (which would be ideal), then the object would not be allowed much of a departure from this flatness since the correction of the aberrations in such a fast system would be limited to a small depth of field. However, even if this is a limiting factor, the microscope would still have a great potential in large scale silicon chip manufacture, where a magnified view of a large portion of a chip simplify defect detection [29].

(a).

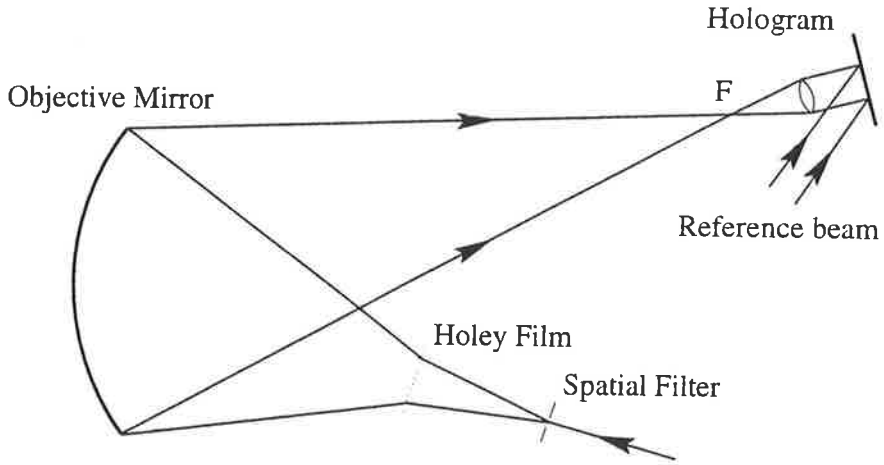

(b).

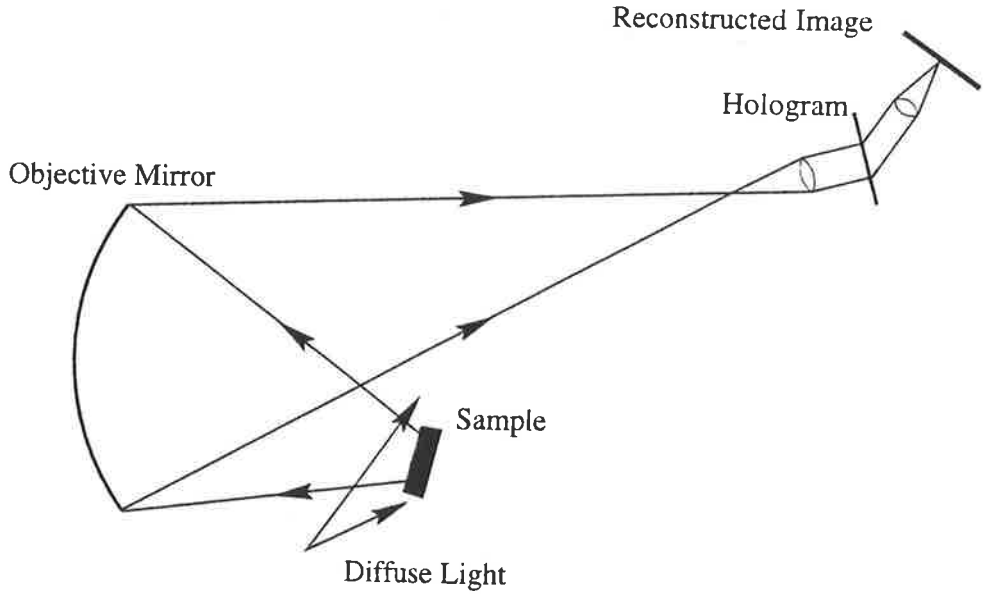

Figure E.3: (a). Recording: A spatial filter illuminates the holey film. The point sources each diffract to illuminate the entire mirror. The reflected light is gathered to form a hologram. (b). Reconstruction: The sample is placed where the film was. The diffuse light reflected off the object will reflect off the mirror and reconstruct the object - with full field of view.

One benefit of holographic correction, however is that height information can be obtained simply by keeping the reference beam present on reconstruction. The result will be that the reconstructed reference beam (with the added object information) will interfere with the reference beam proper. When these combined beams are focussed to form an image of the object, the interference pattern will be present, producing a fringe pattern over the image, with the fringes shifted laterally with changes in height of the object. By a small movement of the sample towards or away from the mirror the movement of the fringes can be observed and using phase shifting interferometric techniques, a relief map of the surface can be determined to a high precision (at least to $\lambda/10$).

Finally, it is worth mentioning that this holographic scheme could be used for an inexpensive, high magnification, large field of view photolithographic copier. This idea has been tried by Ross et. al. [75], where an inexpensive off-axis reflective arrangement was used for one-to-one copying of chips from a recorded mask pattern. The results indicated that elements 1μm in size could be faithfully reproduced with an F/2 mirror, proving that holographic correction of this sort can be used over large fields. It seems from these experiments, and those detailed in this thesis, that the holographically corrected microscope would be feasible.

E.5 Summary

As a further demonstration of the usefulness of holographic correction of aberrated optics in general, I have outlined a scheme for a microscope. The technique is basically the same as for the correction of a telescope but in this case the recording and reconstruction arrangements are identical. The possible increase in field of view and working distances which could be gained using this technique, along with the large resolution while using inexpensive optical components, could prove to be useful for many applications in microscopy.

Appendix F

Publications

Holographic correction of large telescope primaries by proximal, off-axis beacons

Geoff Andersen, Jesper Munch and Peter Veitch

Applied Optics - in press (Vol 35, No. 4 pp 603 - 608, Feb 1 1996)

Abstract

Compact telescope configurations incorporating holographic correction of large, low-quality primary collectors are demonstrated. Aberration correction is demonstrated with an off-axis laser beacon located close to the primary. This arrangement results in a compact telescope with minimum obscuration. The reduction of additional off-axis aberrations introduced by the method is also demonstrated.

Introduction

Holographic correction of optical aberrations in very large, low cost, light weight collectors is an attractive approach for applications ranging from space and lunar telescopes to ground based lidar receivers. This approach may even permit the use of structures such as inflatable balloons[1] as diffraction-limited optical elements in telescopes and will thus extend the range of possibilities available to optical designers for space experiments.

In earlier research[2,3], it was shown that a hologram can be used to correct for large optical aberrations in an imperfect primary element of a telescope. In that work, a distant laser source (the beacon) was used to record an image hologram of the primary. This hologram was subsequently used as an optical element to remove the aberrations, resulting in diffraction limited performance over a limited range of wavelengths. One drawback which rendered the design somewhat impractical, was the use of a distant laser beacon. The present paper concentrates on demonstrating practical design approaches for bringing the laser beacon close to the telescope.

The basic concept of holographic correction of telescopes is an extension of the work by Upatnieks et. al.[4] and Kogelnik and Pennington[5] and is described in detail in reference 2. For completeness, we shall briefly describe the concept as illustrated for a refracting telescope in Fig. 1. An image hologram of the aberrated objective is recorded using a beacon at infinity and a diffraction limited reference beam [Fig. 1a]. If the beacon is used to reconstruct this hologram, the original diffraction limited reference beam is recreated with the hologram effectively subtracting the aberrations on the incoming beam [Fig. 1b]. If instead the incident light comes from a distant object, the hologram will still subtract the aberrations but not the object information, resulting in a reconstructed beam from which a diffraction limited image of the object can be produced [Fig. 1c]. This concept was successfully demonstrated by correcting for large aberrations of up to 1000 waves, resulting in diffraction limited performance with a useful field of view, for both refracting and reflecting telescopes[2]. Broad-band operation, by the addition of an appropriate dispersive optical element, was also demonstrated[3]. In the latter case, the range of useful wavelengths was found to be limited by the amount of correction required, rather than the distortion commonly encountered when reconstructing a hologram with a wavelength different from that used in the recording phase.

Although the distant beacon can be retained in certain applications, it is usually desirable to minimise the length of the overall instrument. This can be accomplished using several approaches. The particular solution employed depends on whether the telescope is a refractor or reflector, on the severity of the aberrations to be corrected and on design specific issues such as the F-number of the primary, obscuration and

the location of the holograms. In all cases there will be limitations to the degree of correction achievable since there will be an increasing difference between the angle of incidence of the light from a distant object and that from a point beacon as it approaches the primary. This will result in an Optical Path Difference (OPD) between the rays used to record the aberration and the rays from an object at infinity that reconstruct the hologram. In addition, Seidel aberrations will appear. For example, spherical aberration is not present in a hologram recorded using a beacon placed at the radius of curvature of a spherical mirror. but will appear when light from a distant object is imaged by the spherical mirror. These additional aberrations need not detract from the advantages of holographic correction. They can be completely avoided by using a beacon at infinity[2], but this is not considered a scalable or practical approach. Alternatively, they can be minimised by careful positioning of the beacon, and, in the case of Seidel aberrations, they are known and can be compensated for by using an appropriate computer generated hologram or specially fabricated optical components.

In this paper we shall demonstrate the principle of an off-axis proximal beacon. In order to better understand the optical system, we have chosen to used conventional optics to correct for the induced aberrations. The advantage of the off-axis concept will be shown to be lack of obscuration of the primary and better correction of the useful part of the mirror, while the disadvantage is the introduction of correctable off-axis aberrations.

Refracting Telescope

In the early work[2] we moved the beacon from infinity to a point closer to the telescope, while keeping it on-axis and retaining common secondary optics for recording and reconstruction. With this approach the proximity of the beacon was limited by the magnification of the system, and the speed of the secondary optics. Furthermore, distortions were eventually encountered because the divergences of the beams used to record and reconstruct the hologram were different. In this section we shall discuss an experiment to overcome these limitations in a refractor design.

The experimental arrangement to investigate the off-axis concept for a refracting

telescope is illustrated in Fig. 2. The primary was a simple, plano-convex lens with focal length $f = 1$m and diameter $D = 0.37$m. When used to image a distant point source, it produced a minimum spot about 14mm in diameter, dominated by spherical aberration. It was this aberration which was to be removed by the holographic method. The beacon was placed off-axis to avoid obscuration of the primary and to record and reconstruct the hologram without moving any optics. The latter is a useful feature for future designs which may incorporate real-time holographic correction. The small, diffraction limited, secondary lenses were chosen to image the surface of the large aberrated primary lens onto the hologram with equal magnification, and also to collimate the light incident on the hologram. Due to the simultaneous magnification and imaging requirements, and a limited choice of available lenses for use as secondaries, the distance to the beacon was 10m. The distant object (a resolution chart) was located at infinity by using a 0.35m (14-inch) diameter astronomical telescope as a collimator.

The image of the resolution chart, when observed by the uncorrected telescope, was severely degraded by spherical aberration [Fig. 3a]. Using the hologram to correct the aberrations of the primary lens, an image degraded only by astigmatism was obtained. This astigmatism arose from the off-axis beacon used to record the hologram. It was found that the astigmatism could be partially corrected by passing the reconstructed beam through a cylindrical lens, that was located near the image plane of the primary, as shown in Fig. 2. With this arrangement we achieved diffraction limited performance of the corrected telescope, using a primary aperture of 200mm in diameter, as shown in Fig. 3b. With larger apertures no improvement in resolution was obtained and the image began to suffer from decreased contrast. Although we did not investigate this limitation in detail, we attribute it to uncompensated, higher order off-axis aberrations and inevitable differences in the recording and reconstructing optical trains.

The experiment thus demonstrated that the introduction and subsequent subtraction of off-axis aberrations is possible, but the concept was not pursued further due to the scaling limitations of refractors.

The Proximal Beacon in Reflecting Telescopes

In most reflecting telescopes, some obscuration will occur due to the secondary optics. Additional obscuration due to the components required for holographic correction can be avoided entirely if the beacon is placed off-axis. A further advantage of the off-axis scheme, as we shall show below, is that it provides the maximum degree of correction over the largest area of the mirror, including perfect correction at the edge of the mirror where maximum resolution is obtained. However, as with the refracting telescope discussed above, the scheme introduces off-axis aberrations which must be removed separately.

The off-axis reflector concept is shown in Fig. 4. The recording beacon is placed at one edge of the primary aperture and at a distance approximately equal to the radius of curvature of the mirror [Fig. 4a]. The hologram is located on the other side of the mirror aperture. Subsequent reconstruction is on-axis, as shown in Fig. 4b. This was accomplished in the lab by physically moving the hologram from the position of recording to that of reconstruction, whereas in a real telescope an optical image relay system would be used.

This approach introduces new aberrations in addition to those of the low quality mirror that the method seeks to correct. Since the hologram is recorded using an off-axis beacon, it will contain off-axis aberrations, dominated by astigmatism, which are not present in the on-axis reconstruction. Also, uncompensated spherical aberration will be introduced during reconstruction, which is not recorded on the hologram in this geometry. However, as these aberrations are known they can, in principle, be removed.

The limit of the achievable correction of a surface defect is determined by the OPD between the recording and reconstructing rays at the defect position. Fig. 5 shows the geometry used to calculate the OPD for two rays incident on a surface bump of height h. The path difference (d) of a ray reflected from a perfect mirror surface and one from the top of the bump is $d = a + b = 2h\cos\alpha$. Thus the total OPD between the recording ray (angle α) and the reconstructing ray (angle β) is

$$OPD = 2h(\cos\beta - \cos\alpha) \qquad \text{(F.1)}$$

For our off-axis scheme at the recording wavelength, with the recording beacon in the $x-z$ plane, the OPD at any position (u, v) on the mirror is given by

$$OPD = \frac{2h}{R}\left[\frac{xu + Ry + Rz - yz}{\sqrt{x^2 + 2xu + y^2 + 2Rz - 2yz}} - (R - z)\right] \tag{F.2}$$

where R is the radius of curvature and $z = R - \sqrt{R^2 - u^2 - v^2}$ is the sag of the spherical mirror. When the beacon is placed at a distance $y = R$ from the mirror and at the edge of the aperture ($x = \rho$), this equation simplifies to

$$OPD = \frac{2h}{R}\left[\frac{\rho u + R^2}{\sqrt{\rho^2 + 2\rho u + R^2}} - \sqrt{R^2 - u^2 - v^2}\right] \tag{F.3}$$

A plot of the relative path difference (OPD/h) is shown in Fig. 6 for a mirror $x = \rho = 0.25$m, $R = 5.2$m. The reciprocal, h/OPD, represents the correction factor by which the height of a bump can be reduced using this method. Notice that there is zero path difference around the edge of the mirror (correction factor is infinite). This means that perfect correction occurs in the region of the mirror which does the most work, while the minimum correction occurs at the centre, which, in most telescope designs, will be partly obscured by the secondary optics. This minimum correction depends heavily on the F-number ($F = R/4\rho$) of the mirror. Better correction can be obtained for a slower mirror (large F-number) as the angular difference between recording and reconstructing beams decreases. However, in order to reduce the size of a telescope, faster mirrors are generally used. Thus, for a compact telescope, a compromise must be made between the severity of aberrations initially present in the primary and the final surface accuracy desired. For a lidar receiver, for example, a more imperfect, fast mirror could be employed as diffraction limited performance over the whole aperture may not be required.

Large reflector experiment

The purpose of this experiment was to investigate the off-axis recording scheme with a large, severely aberrated mirror to be used in high resolution applications where the field of view is small. The experimental set-up was similar to that shown in Fig. 4. The 0.9m diameter, F/3 mirror was made by slumping a flat sheet of glass,

12mm thick, over a spherical mould in an oven. In the present experiment, where precise interferometric diagnosis was required, we restricted the useful aperture to 0.5m to match the diameter of the perfect parabolic collimator available. The central section of the mirror used may thus be described as an aberrated 0.5m diameter, F/5 aperture, which focuses a plane wave to an irregular spot about 8mm in diameter. An interferogram [Fig. 7a] shows that the deviations from an ideal surface ranged from 150 to 250 waves across the aperture.

An image hologram was made using bleached Agfa 10E75 plate film, to produce a phase grating with high diffraction efficiency ($\eta \sim 40\%$). The plate was placed in a kinematic mount which allowed it to be replaced after processing to within $\sim 1\mu$m of its original position. For reconstruction, the hologram was moved to an identical on-axis mount at the focal plane of the mirror and was positioned using fiducials on the mirror.

The light reflected by the aberrated mirror was directed through imaging lenses onto the hologram. High quality camera lenses were used for imaging, producing a near aberration-free, flat-field image on the plate. Due to the lack of depth of focus of the lenses, the plate was placed perpendicular to the object beam. The imaging lenses were chosen to image the mirror with the same magnification for both recording and reconstruction. With this arrangement, the object beam reconstructed the initial reference beam and perfect correction should result in a plane wave. Departure from perfect correction was detected by interfering the reconstructed beam with the original plane wave reference beam. The astigmatism present in the reconstructed beam was removed by two cylindrical lenses and an off-axis, tilted 10cm focal length achromat, chosen experimentally to minimise the spot size of the focussed, reconstructed beam. This was done on the assumption that the hologram had successfully removed the intrinsic aberrations of the mirror, leaving only spherical aberration and astigmatism. The result was a beam with elliptical cross-section and nearly all of the astigmatism removed. The circular interferometric pattern was produced by passing the beam through a prism to correct the aspect ratio.

An interferogram of the corrected beam, [Fig 7b], shows that the surface aberrations of the mirror have been greatly reduced, but there remains a residual error

of 7-8 waves, in a pattern consistent with spherical aberration. We have calculated that there should be 7.7 waves of uncorrected spherical aberration introduced during reconstruction. In addition the theory predicts the remaining uncorrected, random mirror aberration to be less than one wave. The results shown in Fig. 7b are thus consistent with the theoretical predictions. The spherical aberration was apparent in the focus of the reconstructed beam which consisted of a bright central spot ($\sim 14\mu$m diameter) surrounded by a diffuse circular halo, 0.8mm in diameter as compared to the diffraction limited spot diameter of 9μm.

The spherical aberration cannot be corrected by using an appropriate secondary mirror because the irregular way in which the rays reflect off the aberrated primary requires that this correction be performed in the image plane of the primary. Several other schemes were investigated to remove the spherical aberration from the reconstructed beam. In one scheme, we placed a negative lens after the cylindrical lens train, but this was not completely successful because the beam was elliptical and thus the amount of spherical aberration removed in one axis was different to the other. The best result achieved using this method was a reduction of the wavefront error to 4-5 waves. An alternative method involved introducing the correct amount of negative spherical aberration in the reference beam during recording. We have shown this method to work perfectly in a small on-axis experiment, where the diffracted beam was free of off-axis aberrations from the recording beacon. This method is not readily adaptable for an aberrated mirror due to additional constraints: In a two-beam hologram, with the plate perpendicular to the object beam, the reference beam is incident on the hologram at an angle producing an elliptical spot. This is not a problem for a plane wave reference beam, as the wavefront is everywhere the same. However, when the negative spherical aberration is introduced, the reference beam must overlap perfectly the almost circular image of the mirror, so that the spherical aberration is correctly recorded. To do this with the beam at an angle, the aspect ratio of the reference beam must be adjusted using either a prism or a diffraction grating. When this is done, however, astigmatism is introduced, which added to the astigmatism in the object beam, makes this aberration all but impossible to remove from the reconstructed beam.

We also attempted to remove the astigmatism directly by introducing the appropriate amount in either the object or reference beams. One approach was to place the spatial filter at the centre of curvature of a smaller, perfect spherical mirror at an off-axis angle which would give the amount of astigmatism necessary to cancel out that from the large mirror. However, for a smaller diameter mirror, a much larger angle is required, which gives rise to higher order aberrations. It should be possible to remove completely the off-axis aberrations in the recording process if a mirror of the exact dimensions of the aberrated mirror were used as the reflective null. This would make sense only if a large number of aberrated mirrors required correction at the cost of just one perfect mirror. A second possibility would be to pass the reference beam through cylindrical lenses during recording. This was not attempted since the only lenses available were simple lenses which give rise to other aberrations. Alternatively, as previously mentioned, computer generated holograms could be used to modify the reference beam in such a way that the correct amount of off-axis aberration is introduced into the system. We are currently investigating the practicality of such a scheme.

Conclusion

By analysis and experiment we have demonstrated the practicality and limitations of holographic correction of an aberrated primary mirror in a scheme using an off-axis, proximally located laser beacon. The off-axis arrangement has the benefits of leaving a clear aperture as well as giving the most desirable correction, but adds large amounts of astigmatism which must be corrected separately. We have shown that the method reduces the mirror defects by the amount predicted by simple theory and we have also shown that the induced aberrations can be reduced using simple optical components. Although the correction achieved was not perfect, the system as demonstrated would be useful in applications such as lidar receivers where a few waves of error can be tolerated. For diffraction limited designs we conclude that although the removal of the mirror aberrations is possible, the subsequent correction of induced aberrations is not readily practical for small F-numbers using simple optical components. However, since the aberrations introduced are known in

principle, it should be possible to produce a small, exotically shaped reflective null or computer generated, diffractive optical component[6] to correct for these aberrations. Since these components are small and predictable, this added requirement does not negate the benefits attainable from using a very large, low quality primary.

Acknowledgments

We gratefully acknowledge the help of D. Fotheringham and P. Foster with early experiments. This research was supported in part by TRW Inc., the University of Adelaide and by a grant from the Australian Research Council.

References

1. L. Schroeder, M. Bailey, R. Harrington, B. Kendall and T. Campbell, "Design Studies of Large Aperture, High-Resolution Earth Science Microwave Radiometers Compatible With Small Launch vehicles", NASA Tech. Paper 3469 (1994).

2. J. Munch and R. Wuerker, "Holographic Technique for Correcting Aberrations in a Telescope", Appl. Opt. **28**, 1312-1317 (1989).

3. J. Munch, R. Wuerker and L. Heflinger, "Wideband Holographic Correction of an Aberrated Telescope Objective", Appl. Opt. **29**, 2440-2445 (1990).

4. J. Upatnieks, A. Vander Lugt and E. Leith, "Correction of Lens Aberrations by Means of Holograms", Appl. Opt. **5**, 589-593 (1966).

5. H. Kogelnik and K. S. Pennington, "Holographic Imaging Through a Random Medium", J. Opt. Soc. Am. **58**, 273-274 (1968).

6. G. Lemelin, R. A. Lessard and E. F. Borra, "An Investigation of Holographic Correctors for Astronomical Telescopes," Astron. Astrophys. **274**, 983-992 (1993).

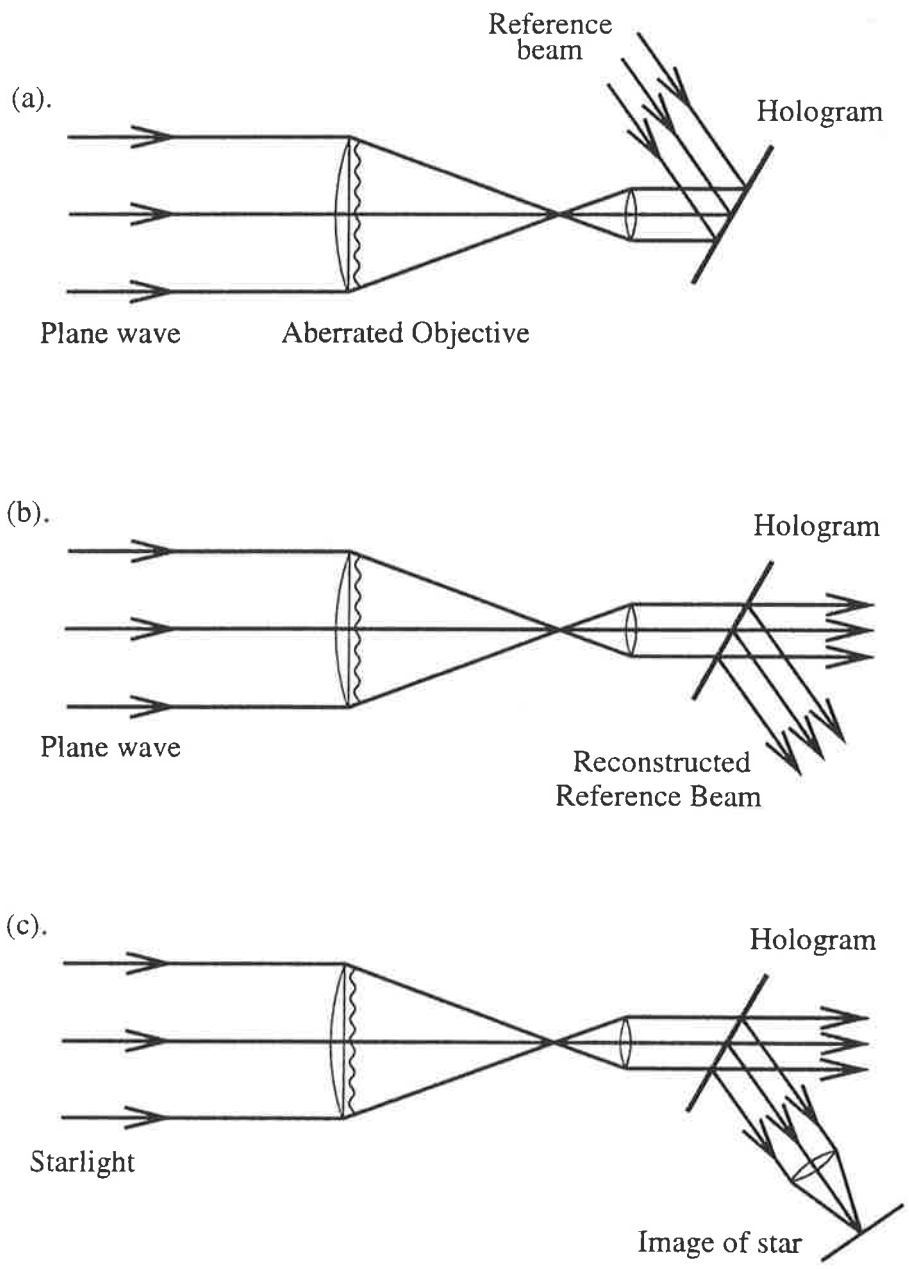

Figure F.1: The basic concept of holographic correction for a refractor: (a) A diffraction limited, collimated beam passes through the aberrated lens and a secondary lens images the primary onto the plane of the hologram. A reference beam interferes with this first beam to produce the image hologram. (b) The original diffraction limited, collimated beam is aberrated by the lens before reconstructing the original reference beam from the hologram. Since the object beam is the same as the one used to write the hologram initially, the reconstructed reference beam will be diffraction limited and aberration free. (c) If a distant object were used instead, then the diffracted light at the hologram can be used to produce an aberration free image of the object.

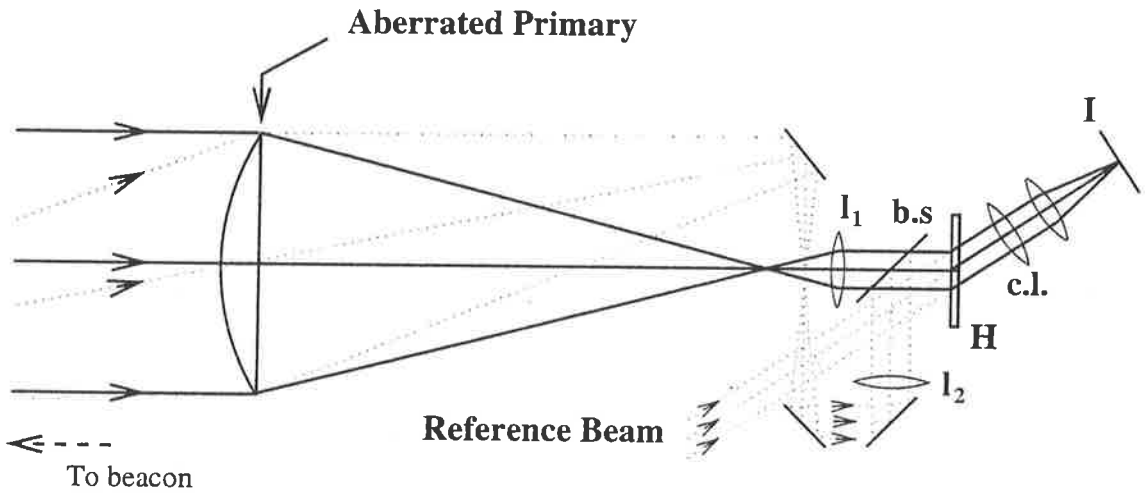

Figure F.2: (a). Recording: The beacon illuminates the mirror from the centre of curvature. The reflected light is collimated and the mirror is imaged by camera lens L1 onto the plate were a hologram is recorded. The off-axis angle has been exaggerated for clarity. (b). Reconstruction: Collimated light from the parabolic mirror is focussed by the aberrated mirror and collimated by the second camera lens, L2, to reconstruct the reference beam.

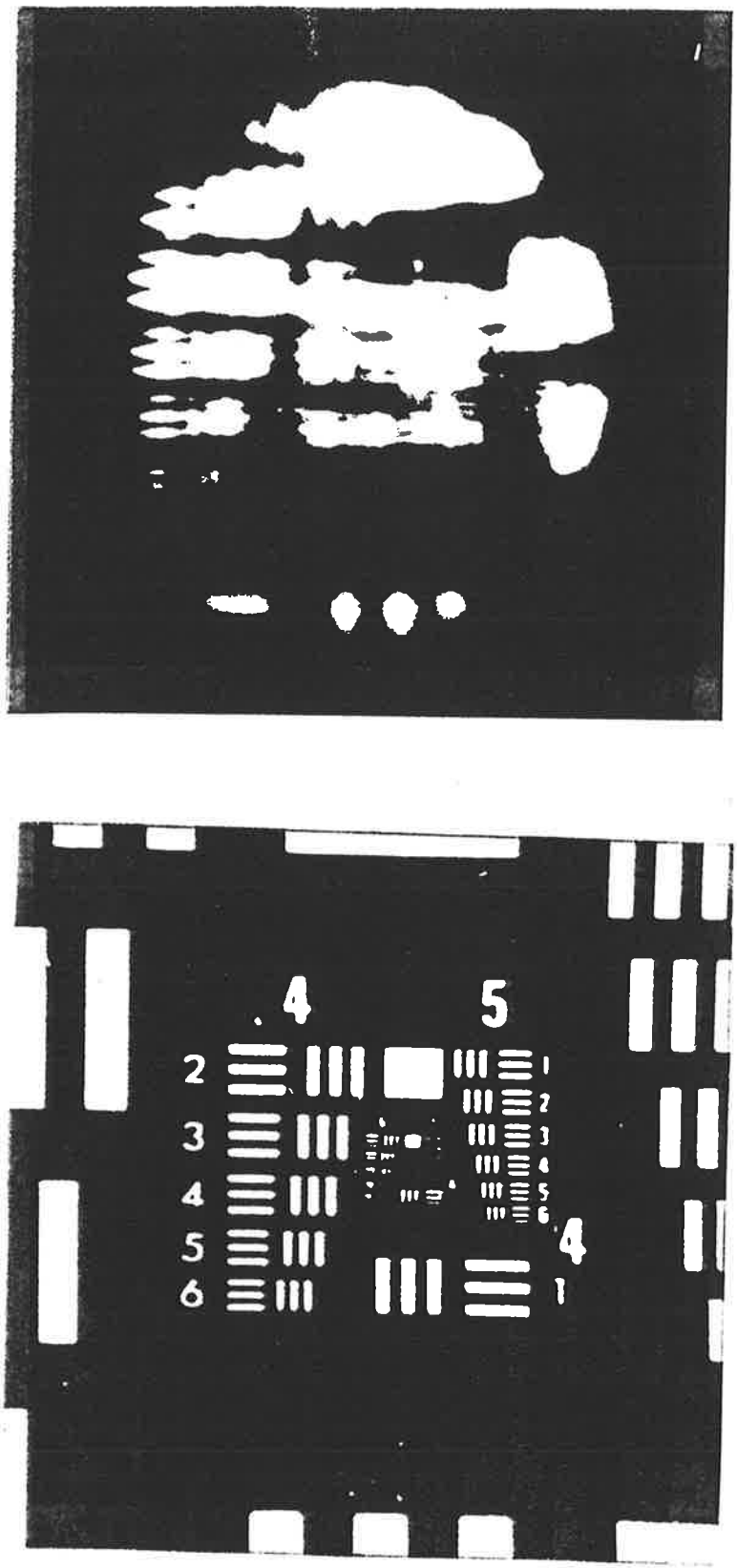

Figure F.3: Results of the holographic correction applied to an aberrated 200mm diameter, f/5 refracting lens: (a) The resolution chart as imaged on-axis by the aberrated telescope, without correction. This scene includes column 2. (b) Magnified central portion of the resolution chart after holographic correction and using a cylindrical lens to correct for astigmatism.

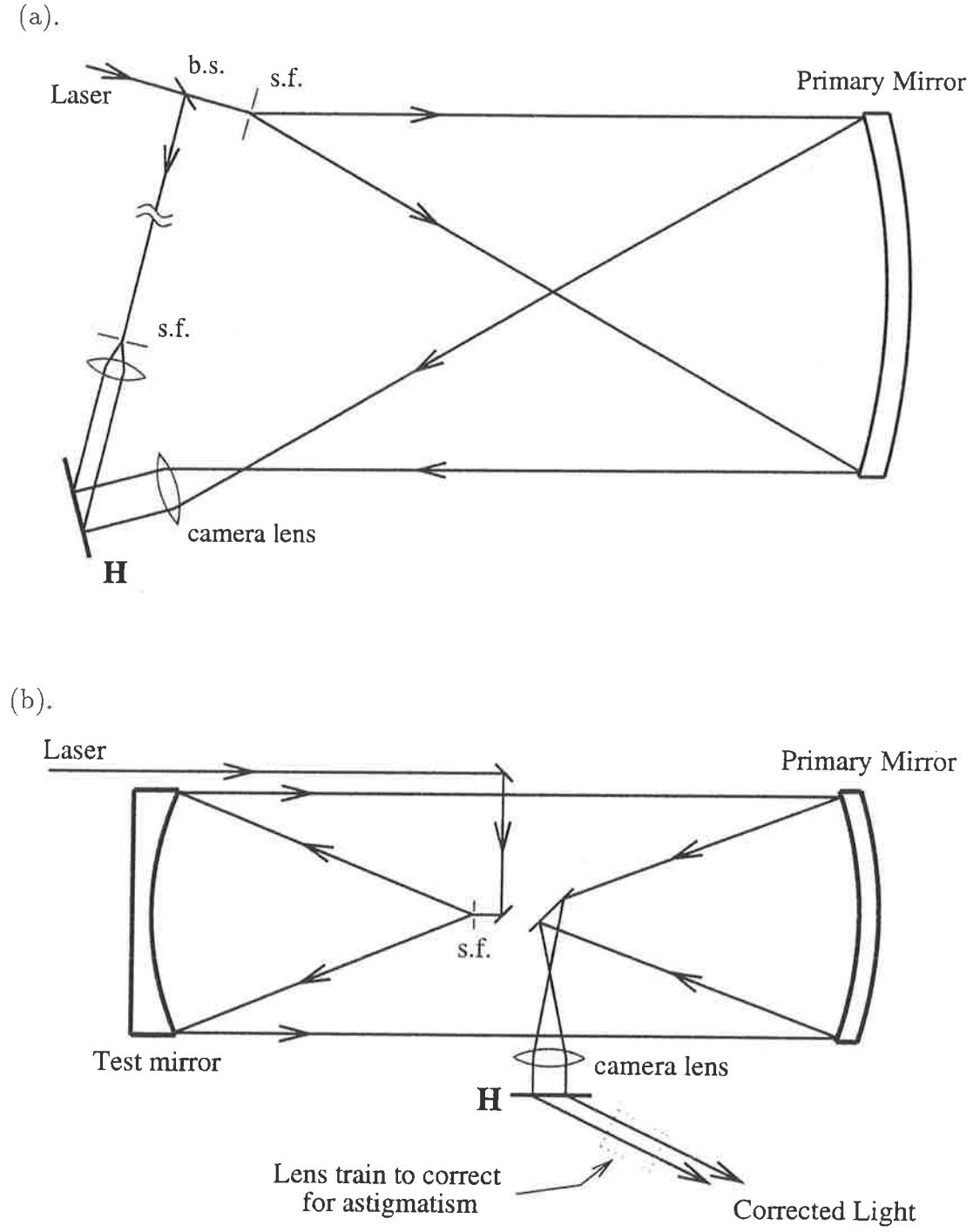

Figure F.4: The off-axis scheme for holographic correction of a reflector: (a) A spatially filtered beacon, placed at the off-axis position shown, illuminates the mirror. A camera lens collimates the reflected light and images the mirror onto the holographic plate (H). The path-matched reference beam interferes with the object beam to form the image hologram. (b) On-axis reconstruction using a parabolic mirror collimator to place the test beacon (spatial filter) at infinity. Off-axis astigmatism is removed from the reconstructed beacon using a lens train as shown.

(a).

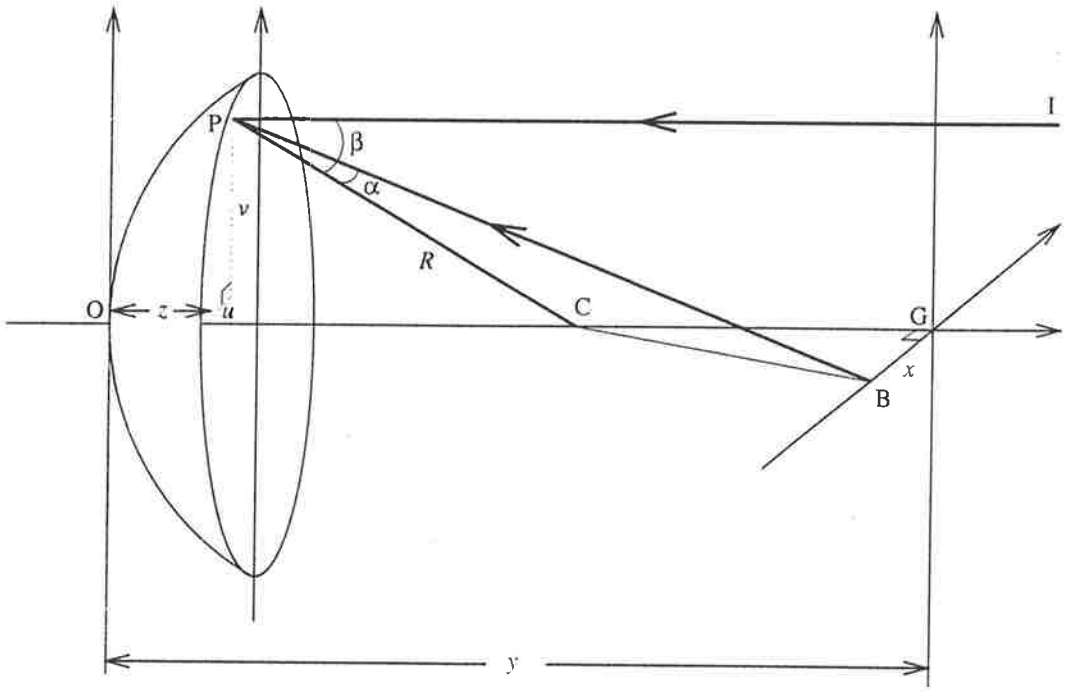

(b).

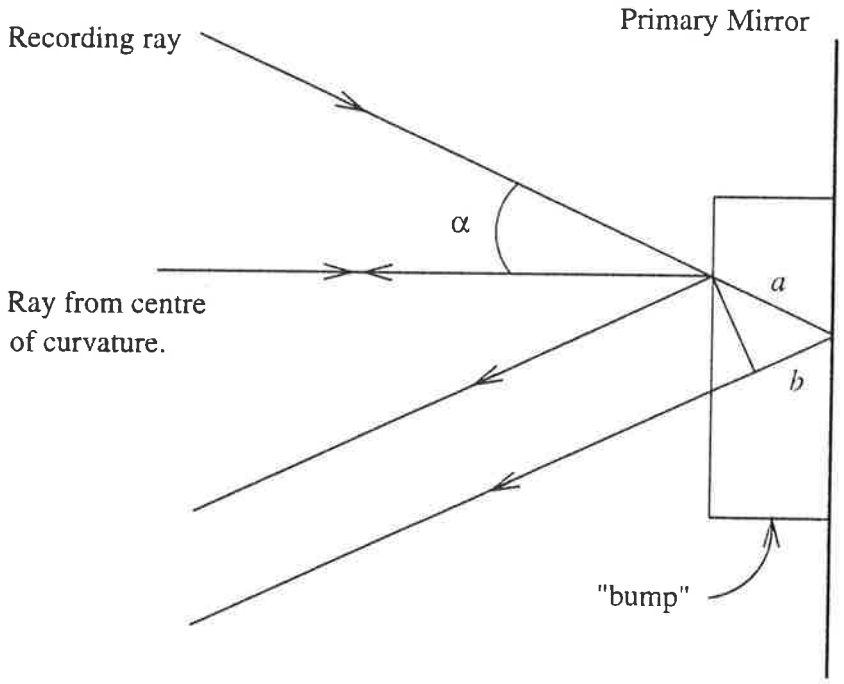

Figure F.5: Geometry used in the analysis of the correction of surface defect: (a) The off-axis ray from the beacon (B) strikes the mirror surface at P(u.v). at an angle α to the normal (a ray from the radius of curvature). The on-axis reconstructing ray from infinity (I) forms an angle β with the normal at the same point. (b) A ray from the recording beacon is shown reflecting off a bump on the primary mirror.

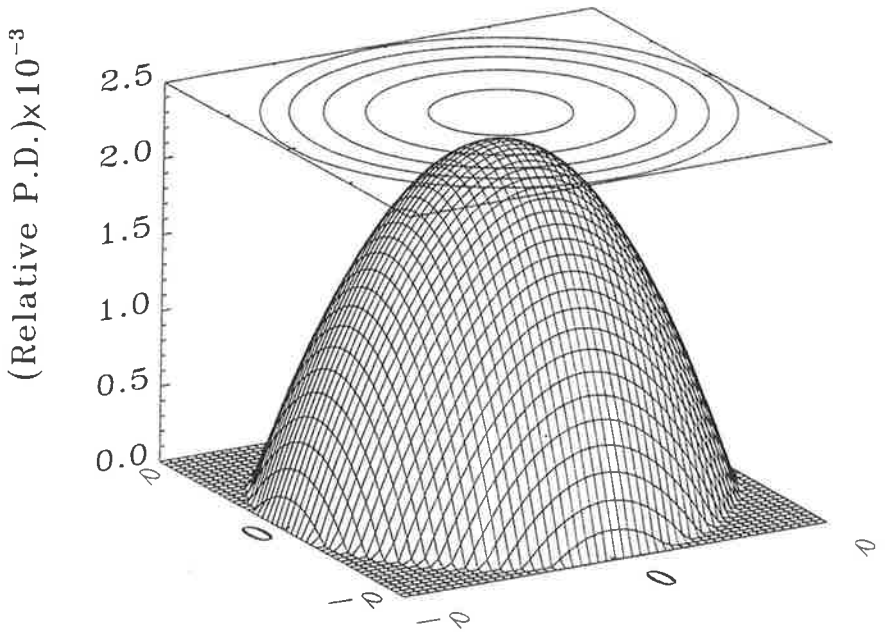

Figure F.6: Calculations of the expected correction from the off-axis scheme for a reflector: The Relative Path Difference (OPD/h) is plotted over the mirror surface for a mirror with $x = \rho = 0.25$m and $R = 5.2$m. The correction will be perfect at the edge of the mirror where the OPD is always zero. The correction is a minimum at the centre with a value of 0.0023. Thus a bump can be reduced in size by a factor of $(0.0023)^{-1} = 433$.

(a).

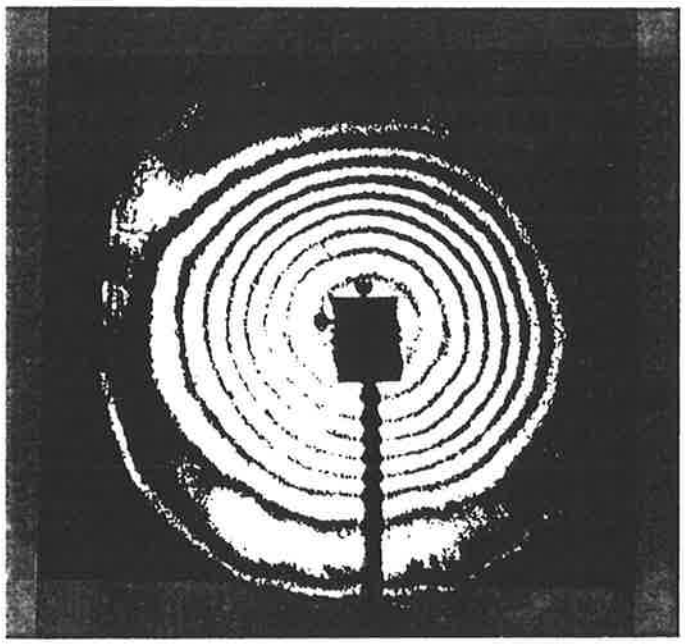

(b).

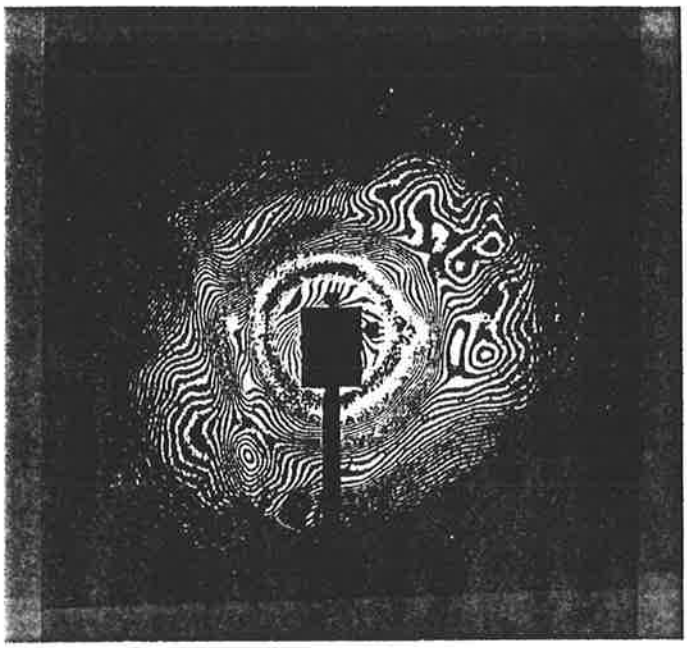

Figure F.7: Results for large scale aberrated reflector: (a) Interferogram shows the surface aberration before correction. (b) After the correction the remaining error is 7-8 waves.

Compact holographic correction of large diameter aberrated telescopes

Geoff Andersen, Jesper Munch and Peter Veitch

Submitted to Applied Optics

Abstract

We demonstrate a compact reflector telescope design incorporating the holographic correction of a large, low quality primary spherical mirror using a laser beacon located at the centre of curvature. The simple design makes use of conventional optics and is easily scalable to much larger apertures. Experimental results indicate diffraction limited performance from a heavily aberrated 0.5m diameter spherical mirror.

Introduction

In recent publications[1-3] we have described and demonstrated practical concepts for using holographic optical elements to correct aberrations in large, low-quality telescope primaries, for applications ranging from space or moon based telescopes to ground based lidar. We have shown that a hologram recorded using a laser beacon located in the far field of a telescope can correct a primary element with hundreds of waves of aberrations to diffraction limited performance over a useful but limited bandwidth[1,2]. More recently[3] we have shown that an off-axis proximal beacon can result in a useful compact design with no obscuration of the primary. The latter approach suffered however, from a large amount of introduced astigmatism which was difficult to remove with conventional optical components. While computer generated holograms could be used to remove the astigmatism, we have chosen to concentrate on a simpler on-axis configuration suitable for the correction of large spherical surfaces. This approach is advantageous because it does not introduce any

unnecessary additional aberrations, and can produce diffraction limited performance from an inexpensive, low quality primary using simple, readily available optical components.

The basic concept of holographic correction of a refractor telescope is reproduced from Ref. 1 in Fig. 1. An image hologram of the aberrated objective is recorded using a coherent light source (beacon) at infinity and a diffraction limited reference beam [Fig. 1(a)]. If the beacon is used to reconstruct this hologram, the original diffraction limited reference beam is recreated with the hologram effectively subtracting the aberrations on the incoming beam [Fig. 1(b)]. If instead the incident light comes from a distant object, the hologram will still subtract the aberrations but not the object information, resulting in a reconstructed beam from which a diffraction limited image of the object can be produced [Fig. 1(c)]. In this paper, we will demonstrate for the first time, a compact adaptation of this concept which uses a spherical reflector and a beacon located at the centre of curvature.

The Proximal On-Axis Beacon

The On-Axis Design

The most compact configuration for recording an image hologram of a spherical mirror using a point-source beacon is shown in Fig. 2(a). The beacon is a diffraction limited spatial filter located at the centre of curvature of the aberrated mirror. A high quality camera lens (L1) is used to form a demagnified, flat-field image of the mirror on the hologram. A hologram is recorded with this object wave and a diffraction limited, plane wave reference beam.

In a telescope, light from a distant object is brought to a focus at half the radius of curvature of the mirror. In order to use the hologram as an optical element to correct the mirror, the hologram must either be moved to the focal plane or, in the case of modest aberrations, an image relay system could be employed. Due to the heavily aberrated mirror used, we chose the former solution in this experiment. In Fig. 2(b), collimated light is focussed by the aberrated mirror, then re-collimated by a second camera lens (L2) which also images the mirror on the plane of the

hologram. The camera lenses must be chosen to give the same image magnification on the hologram during recording and reconstruction and the hologram must be accurately relocated so that its recorded image is congruent to the image in the new location.

The reconstructing object beam will differ from the recording object beam in two ways: spherical aberration is not present during recording but is present on reconstruction, and the angular difference between the reflected recording and reconstructing rays over the mirror surface will result in a difference in the perceived height of a mirror deformation. Both of these factors will affect the fidelity of the reconstructed reference beam, and will be discussed below.

Mirror Aberrations

When the recording and reconstructing rays differ in their wavelengths and angles of incidence, the phase change caused by the reflection from an aberration will differ, resulting in imperfect aberration correction. This effect has been calculated for a completely general geometry[4], but for the present case, with the beacon on-axis, it can be accomplished using the simplified arrangement of Fig. 3. An aberration is assumed to be a bump of height h above the unaberrated surface. The angle of incidence and wavelength of the recording ray are α and λ respectively, and the corresponding quantities for the reconstructing ray incident on the same point are α' and λ'. Assuming perfect imaging properties of the secondary optics, it is easily shown that if the phase error due to the aberration recorded on the hologram is ϕ, and if the phase error experienced by the reconstructing ray from a distant object is ϕ', then the error in the resulting phase correction is

$$\delta\phi = \phi - \phi' = \frac{h}{\pi}\left(\frac{\cos\alpha}{\lambda} - \frac{\cos\alpha'}{\lambda'}\right) \tag{F.4}$$

If the aberrated telescope was used to observe a distant object without aberration correction, the phase error introduced would be ϕ'. The factor K by which the error

on the reconstructing ray is reduced by the hologram is thus

$$K^{-1} = \frac{\delta\phi}{\phi'} = \left[\frac{\lambda'}{\lambda}\frac{\cos\alpha}{\cos\alpha'} - 1\right] \tag{F.5}$$

In the case of a spherical mirror used to observe a point at infinity, and a laser beacon located at the radius of curvature of the spherical mirror, the expression for the correction factor can be calculated to be,

$$K^{-1} = \left[\frac{\lambda'}{\lambda}\frac{x}{[x^2-1]^{1/2}} - 1\right] \tag{F.6}$$

where R is the radius of curvature of the mirror, r is the distance from the centre of the mirror to the aberration and $x = R/r$. Assuming an identical wavelength for recording and reconstruction, the correction factor is infinite at the centre and decreases towards the rim of the mirror. This is shown in Fig. 4. where the minimum correction factor is shown as a function of mirror speed ($F = x/4$). As an example, the minimum correction factor at the edge of a spherical mirror with dimensions, $R = 5.2$m and $r = 0.225$m, is 1067 which means that an aberration will be reduced by at least a factor of 1000 anywhere on the mirror.

Spherical Aberration

With the beacon at the centre of curvature of the spherical mirror, there will be no spherical aberration recorded. However, when reconstructing with a distant object, spherical aberration will be present. A successful telescope configuration must provide for the removal of this aberration. We have previously considered a variety of possible options for the removal of spherical aberration[3], and choose here the simplest and most promising approach when the required amount of spherical aberration is included in the object beam during recording, resulting in a reconstructed object beam which is aberration free. The recording scheme used is shown in Fig. 5. The beacon light produced by a diffraction limited spatial filter is passed through a simple lens which introduces the spherical aberration and refocuses the light to form a new, aberrated beacon. The positions of the lens and the spatial filter aperture used are optimised with an optical ray tracing code to produce the

spherical aberration required. From this point onwards the scheme is exactly as before.

Results

We used a 0.9m diameter, 5.2m radius of curvature spherical mirror, made by slumping 12mm thick plate glass. The wavefront error is up to 100 waves and the uncorrected focal spot is 8mm in diameter. In this experiment we tested only the central 0.45m diameter portion of the mirror, as this was the diameter of the diffraction limited parabolic mirror available as a collimator. An interferogram of this central portion is shown in Fig. 6(a).

The spherical aberration was added to the object beam using a plano-convex singlet (d = 30mm, f = 100mm) as described above. The optimised distance between the lens and the spatial filter was 179.9mm which resulted in a residual peak-to-valley error of $\lambda/10$ over the entire aperture. This limit is due to the mismatch between the spherical aberration from a lens and a mirror. It was also calculated that a positioning error of $\pm$1mm would increase the residual error by only $\lambda/10$ and an error of $\pm$5mm would give an increase of λ. The mirror was imaged with a 100mm camera lens and the hologram was constructed with a diffraction limited, collimated reference beam. The bleached hologram was recorded on Agfa 10E75 plate film using a HeNe laser (λ = 632.8nm) and was $\sim$ 10mm in diameter. The typical diffraction efficiency was 40%.

The hologram was reconstructed using a collimated beam produced by a spatial filter at the focus of a parabolic mirror (f = 2m, d = 450mm). The aberrated mirror was imaged with a high quality zoom lens, adjusted to give the correct image size at collimation. The reconstructed beam emerged from the circular hologram at an angle, and therefore had an elliptical cross-section. The aspect ratio was corrected, when necessary, by passing the beam through a prism or by simple digital image processing.

The reconstructed beam was compared interferometrically to the original reference beam used in recording. The results are shown in Fig. 6. and indicate a final wavefront error of $\lambda/2$ peak-to-valley and 0.11λ rms. The residual wavefront error

was limited by several factors. Firstly, errors introduced by non-common optical elements used in either recording or reconstruction, including the parabolic mirror, increased the error of the final wavefront. The parabolic mirror was tested by the manufacturers and specified to have an error of 0.23λ peak-to-valley (0.04λ rms) with an overall figure similar to that of our reconstructed wavefront. A further 0.03λ rms wavefront error was expected to remain due to the uncorrected spherical aberration.

The calculated correction factor for this experiment has a minimum value of 1067 [Fig. 4] at the mirror edge. From the interferogram in Fig. 6(a), we can see that the maximum error of the mirror close to the edge is $\sim 100\lambda$, implying that the maximum uncorrected surface error will amount to $\lambda/10$ or less at the edge.

The telescope was also tested as an imaging instrument by placing a resolution chart at the focus of the parabolic collimator and illuminating it with diffused laser light [Fig. 7]. The first image shows the imaging before correction with Columns 2 and 3 heavily blurred. After correction, the image of the chart is resolved to Column 7 Line 3, which corresponds to diffraction limited performance for the mirror in this configuration. The field of view is difficult to assess due to the small field of view of the collimator itself, but the resolution chart does maintain a sharp image quality over the whole pattern.

As demonstrated previously[2], the holographic concept has a bandwidth limited by the magnitude of the surface errors to be corrected. From Eq. F.6 we can predict the correction for different wavelengths. For a hologram written in the red (λ = 632.8nm) and reconstructed in the green (λ' = 532nm), the calculated correction factor is ~6.3. Although this would not result in a high resolution telescope at this wavelength we present experimental data to further verify the theory. We used a CW, doubled-YAG laser to reconstruct the hologram, giving the results shown in Fig. 8. The correction factor suggests that for every six fringes on the interference pattern of the uncorrected mirror [Fig. 6(a)] there should be one fringe on the corrected pattern at this wavelength [Fig. 8(a)]. This indeed seems to be the case. The resolution is indicated by the image in Fig. 8(b). Column 3 Row 6 (14.3 lines/mm) can be resolved in the vertical direction and Column 4 Row 3 (20.1

lines/mm) in the horizontal.

Conclusion

We have presented a compact design for the holographic correction of a spherical reflector telescope. The design included a method of incorporating spherical aberration correction during the recording of the hologram to cancel out that which is present when imaging a distant object. We have demonstrated the successful application of this scheme in correcting a large diameter, heavily aberrated telescope. Diffraction limited correction is implied, with the remaining error consistent with the limited quality of non-common optical components used. The correction scheme was purposefully designed using conventional optical components with a view to scalability. These experimental results indicate no limit to the size of an aperture which could be corrected by this method.

References

1. J. Munch and R. Wuerker, "Holographic technique for correcting aberrations in a telescope", Appl. Opt. **28**, 1312-1317 (1989).

2. J. Munch, R. Wuerker and L. Heflinger, "Wideband holographic correction of an aberrated telescope objective", Appl. Opt. **29**, 2440-2445 (1990).

3. G. Andersen, J. Munch and P. Veitch, "Holographic correction of large telescope primaries using proximal, off-axis beacons", Appl. Opt. in press.

4. G. Andersen, PhD Thesis, University of Adelaide (1996).

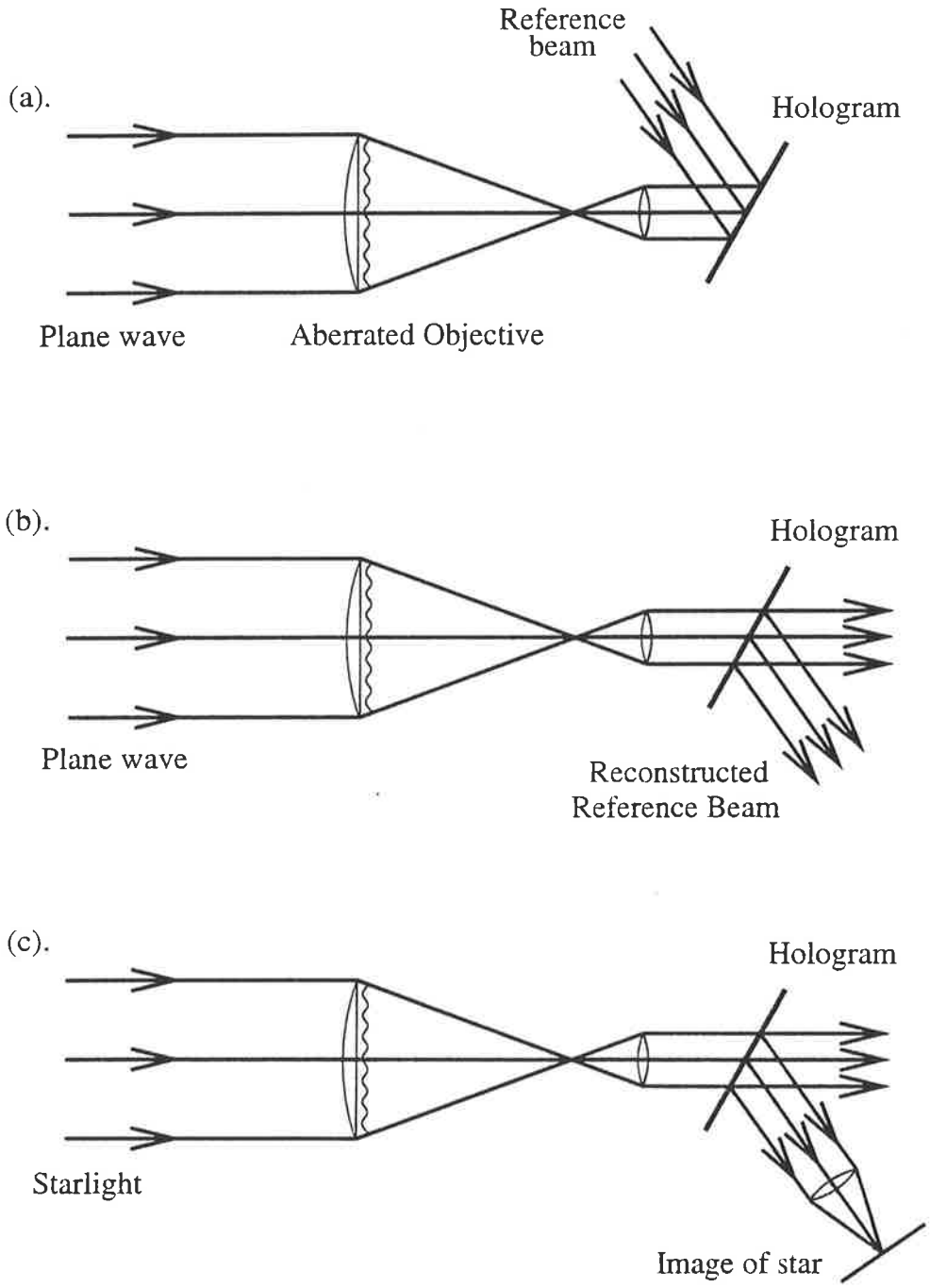

Figure F.8: (a). Recording: A plane wave is focussed by the aberrated primary. The light is collimated and an image hologram is constructed. (b). Reconstruction: Collimated light passes through the telescope making an object wave identical to that used in writing the hologram. This object wave reconstructs the original reference beam. (c). Imaging: Instead of collimated light, a distant object is viewed with the telescope. The additional object wave information is retained in the reconstructed reference beam.

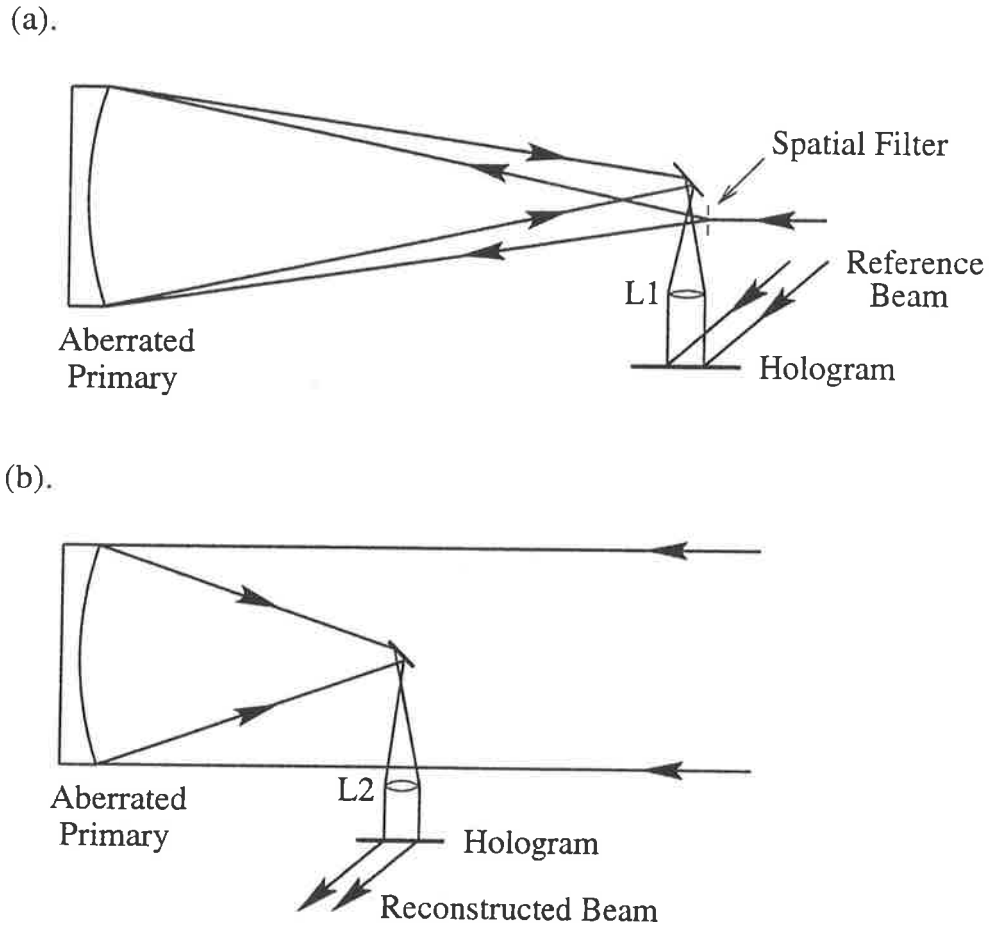

Figure F.9: (a). Recording: The beacon illuminates the mirror from the centre of curvature. The reflected light is collimated and the mirror is imaged by the camera lens on the plate where a hologram is recorded. The off-axis angle has been exaggerated for clarity. (b). Reconstruction: Collimated light from the parabolic mirror is focussed by the aberrated mirror and collimated by the second camera lens, L2, to reconstruct the reference beam.

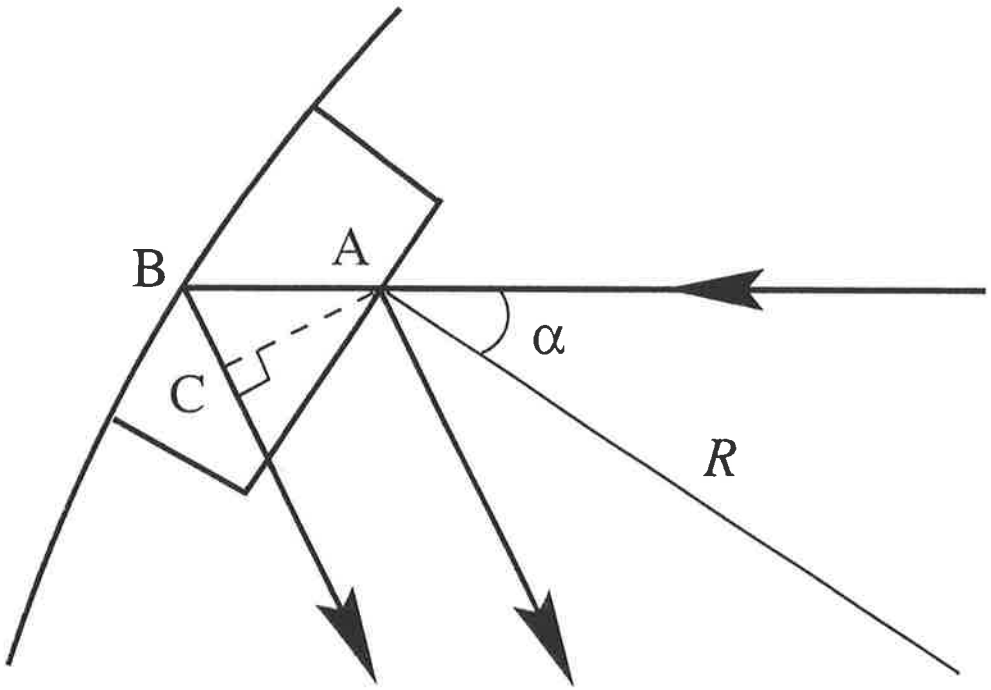

Figure F.10: A ray from the recording beacon is shown reflecting off a bump on the mirror surface (at A) at an angle α to the mirror normal (R). The phase difference between this ray and one which would have reflected off an unaberrated mirror (at B) is $\phi = (AB + BC)/2\pi\lambda = h\cos\alpha/\pi\lambda$. A ray on reconstruction will make an angle α' to the normal at the same point A.

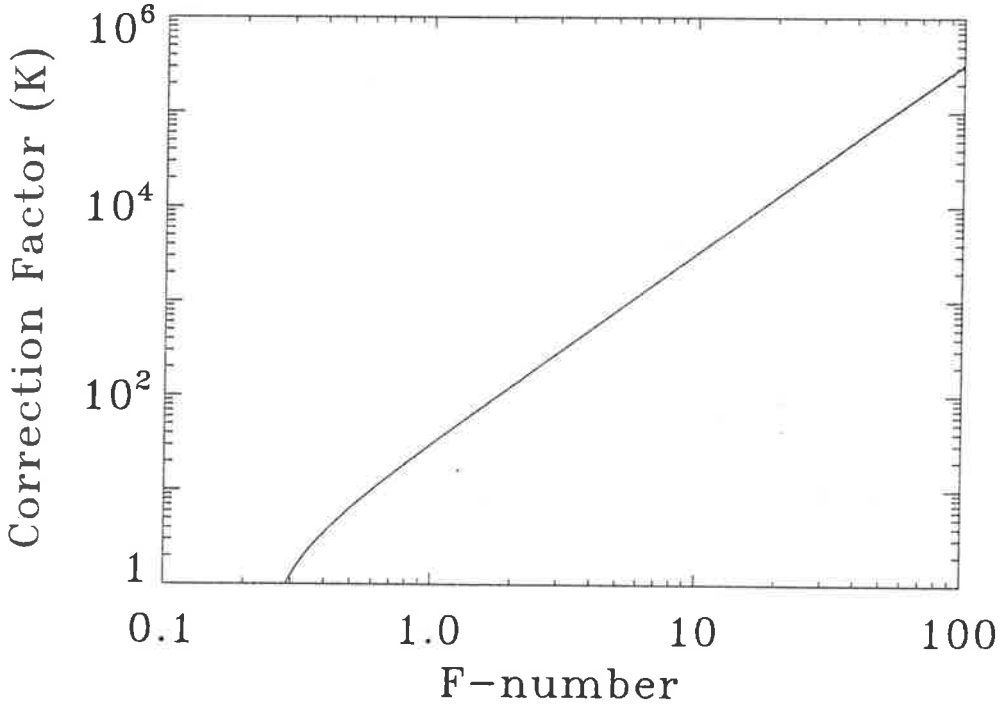

Figure F.11: The minimum correction factor (K) is plotted as a function of mirror speed, $F = x/4$. For example, with an F/5.8 mirror, the minimum correction (which is at the edge) will be 1067. As we move towards the centre of the mirror, the effective speed decreases and the correction factor will increase until it reaches an infinite value at the centre.

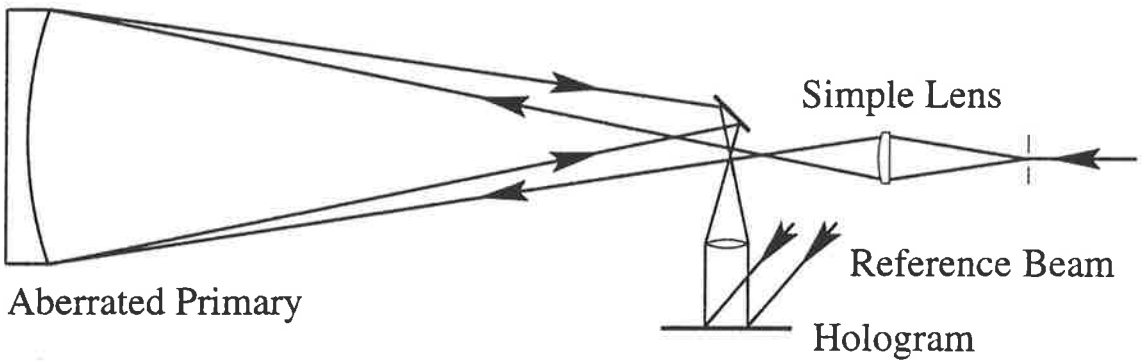

Figure F.12: Recording: The beacon light is spherically aberrated using a simple plano concave lens. The focussed light then continues on to illuminate the mirror as per usual. The off-axis angle has been exaggerated for clarity.

(a).

Figure 4.9, page 96

(b).

Figure 4.10, page 97

Figure F.13: (a). Before correction. The interference pattern shows the wavefront error over the 0.45m aperture. (b). After correction.

(a).

Figure 4.13, page 101

(b).

Figure 4.14, page 102

Figure F.14: (a). USAF resolution chart before correction - showing Columns 2 and 3. (b). After correction showing the bars resolved to Column 7 Line 3.

(a).

Figures 4.15 (a) & (b), page 104

(b).

Figure F.15: (a). The interference pattern for reconstruction at $\lambda' = 532$nm. (b). The resolution chart image at the same wavelength.

Bibliography

[1] Various Authors, "Special Edition - Space Optics", Applied Optics **32** (1993), No. 10.

[2] K. Avicola et al., "Sodium-Layer Laser-Guide-Star Experimental Results", J. Opt. Soc. Am. A **11** (1994), No. 2, 825–831.

[3] J. M. Beckers, "Adaptive Optics for Astronomy: Principles, Performance and Applications", Annual Review of Astronomy and Astrophysics, Annual Review, 1993, pp. 13–62.

[4] E. E. Becklin, "Ground-Based Infrared Astronomy", Frontiers of Space and Ground-Based Astronomy (W. Wamsteker et. al., ed.), Kluwer Academic, 1994, pp. 129–132.

[5] S. N. Bezdid'ko, "The Use of Zernike Polynomials in Optics", Sov. J. Opt. Tech. **41** (1974), No. 9, 425–429.

[6] D. Bone et al., "Fringe-Pattern Analysis Using a 2-D Fourier Transform", Appl. Opt. **25** (1986), No. 10, 1653–1660.

[7] M. Born and E. Wolf, "Principles of Optics", Pergamon Press, 1959.

[8] E. F. Borra, "The Case for Liquid Mirrors in Orbiting Telescopes", ApJ **392** (1992), 375–383.

[9] E. F. Borra, "On the Correction of the Aberrations of a Liquid-Mirror Telescope Observing at Large Zenith Angles", Astron. Astrophys. **278** (1993), 665–668.

[10] E. F. Borra et al., "Liquid Mirrors: Optical Shop Tests and Contributions to the Technology", Ap. J. **393** (1992), 829–847.

[11] E. F. Borra, G. Moretto, and M. Wang, "An Optical Corrector Design that Allows a Fixed Telescope to Access a Large Region of Sky", Astron. Astrophys. **109** (1995), 563–570.

[12] G. B. Brandt, "Image Plane Holography", Appl. Opt. **8** (1969), No. 7, 1421–1429.

[13] R. A. Briones, L. O. Heflinger, and R. F. Wuerker, "Holographic Microscopy", Appl. Opt. **17** (1978), No. 6, 944–950.

[14] E. B. Champagne and N. G. Massey, "Resolution in Holography", Appl. Opt. **8** (1969), No. 9, 1879–1885.

[15] R. A. Chipman et al., "Wavefront Correcting Properties of Corner-Cube Arrays", Appl. Opt. **27** (1988), No. 15, 3203–3209.

[16] R. W. Clay et al., "The Design and Construction of the University of Adelaide Bicentennial Gamma-Ray Telescope", Proc. ASA **8** (1989), No. 1, 41–45.

[17] C. E. Coulman, "Fundamental and Applied Aspects of Astronomical Seeing", Annual Review of Astronomy and Astrophysics, Annual Reviews, 1985, pp. 19–57.

[18] P. Dierickx, "Optical Performance of Large Ground-Based Telescopes", J. Mod. Opt. **39** (1992), No. 3, 569–588.

[19] B. L. Ellerbroek, "First-Order Performance Evaluation of Adaptive-Optics Systems for Atmospheric-Turbulence Compensation in Extended-Field-of-View Astronomical Telescopes", J. Opt. Soc. Am. A **11** (1994), No. 2, 783–805.

[20] J. Feinberg, "Imaging Through a Distorting Medium With and Without Phase Conjugation", Appl. Phys. Lett. **42** (1983), No. 1, 30–32.

[21] R. T. Fienberg, "Hubble's Road to Recovery", Sky and Telescope (1993), 16–22.

[22] A. Fimia, A. Belendez, and I. Pascual, "Silver Halide (Sensitized) Gelatine in Agfa-Gevaert Plates: The Optimized Procedure", J. Mod. Opt. **38** (1991), No. 10, 2043–2051.

[23] B. Fischer et al., "Real-Time Phase Conjugate Window for One-Way Optical Field Imaging Through a Distortion", Appl. Phys. Lett. **41** (1982), No. 2, 141–142.

[24] D. Fotheringham, "Collimated Beams from Large Holographically Corrected Imperfect Mirrors", Honours Thesis, 1991.

[25] R. G. Frehlich and M. J. Kavaya, "Coherent Laser Radar Performance for General Atmospheric Refractive Turbulence", Appl. Opt. **30** (1991), No. 36, 5325–5351.

[26] D. L. Fried, "Statistics of a Geometric Representation of Wavefront Distortion", J. Opt. Soc. Am. **55** (1965), No. 11, 1427–1435.

[27] D. L. Fried, "Limiting Resolution Looking Down Through the Atmosphere", J. Opt. Soc. Am. **56** (1966), No. 10, 1380–1384.

[28] D. L. Fried, "Optical Resolution Through a Randomly Inhomogeneous Medium for Very Long and Very Short Exposures", J. Opt. Soc. Am. **56** (1966), No. 10, 1372–1379.

[29] R. L. Fusek, L. H. Lin, K. Harding, and S. Gustafson, "Holographic optical Processing For Submicrometer Defect Detection", Opt. Eng. **24** (1985), No. 5, 731–734.

[30] D. Gabor, "A New Microscopic Principle", Nature **161** (1948), No. 4098, 777–778.

[31] D. Gabor, "Microscopy by Reconstructed Wavefronts", Proc. Roy. Soc. **A197** (1949), 454–487.

[32] J. D. Gaskill, "Imaging Through a Randomly Inhomogeneous Medium by Wavefront Reconstruction", J. Opt. Soc. Am. **58** (1968), No. 5, 600–608.

[33] J. W. Goodman et al., "Wavefront-Reconstruction Imaging Through Random Media", Appl. Phys. Lett. **8** (1966), No. 12, 311–313.

[34] J. W. Goodman et al., "Experiments in Long-Distance Holographic Imagery", Appl. Opt. **8** (1969), No. 8, 1581–1586.

[35] J. Grygar, "The Role of Space-Based Observations in Astrophysical Research,", Basic Space Science - AIP Conference Proceedings No. 245, AIP, AIP, 1992, pp. 219–229.

[36] C. S. Guo and L. Z. Cai, "Postheat Treatment of Silver Halide Holograms", Opt. Lett. **16** (1991), No. 22, 1777–1779.

[37] P. Hariharan, "Optical Holography", Cambridge University Press, 1984.

[38] J. G. Hawley et al., "Coherent Launch-Site Atmospheric Wind Sounder: Theory and Experiment", Appl. Opt. **32** (1993), No. 24, 4557–4568.

[39] L. O. Heflinger, G. L. Stewart, and C. R. Booth, "Holographic Motion Pictures of Microscopic Plankton", Appl. Opt. **17** (1978), No. 8, 951–954.

[40] P. Hickson, B. K. Gibson, and D. W. Hogg, "Large Astronomical Liquid Mirrors, ", Pub. Astr. Soc. Pac. **105** (1993), 501–508.

[41] H. W. Hoeness et al., "Spin-Cast Zerodur Mirror Substrates of the 8m Class and Lightweight Substrates for Secondary Mirrors", Astrophysics and Space Science **160** (1989), 193–197.

[42] N. Hubin and L. Noethe, "Active Optics, Adaptive Optics and Laser Guide Stars, ", Science **262** (1993), 1390–1394.

[43] M. P. Jelonek et al., "Characterisation of Artificial Guide Stars Generated in the Mesospheric Sodium Layer With a Sum-Frequency Laser", J. Opt. Soc. Am. A **11** (1994), No. 2, 806–812.

[44] C. Karaguleff and Sr. G. L. Clark, "Optical Aberration Correction by Real-Time Holography in Liquid Crystals", Opt. Lett. **15** (1990), No. 4, 820–822.

[45] H. Kogelnik, "Holographic Image Projection Through Inhomogeneous Media", Bell Syst. Tech J. **44** (1965), 2451–2455.

[46] H. Kogelnik, "Coupled Wave Theory for Thick Hologram Gratings", Bell Syst. Tech. J. **48** (1969), No. 9, 2909–2947.

[47] H. Kogelnik and K. S. Pennington, "Holographic Imaging Through a Random Medium", J. Opt. Soc. Am. **58** (1968), 273–274.

[48] S. Kumar and K. Singh, "Bleached Phase Holograms Exposed on Agfa-Gevaert 10E75 NAH Plates", Optics and Laser Technology **23** (1991), No. 1, 37–41.

[49] H. S. Lee and H. Fenichel, "One-Way Image Transmission Through a Distorting Medium Using Two Holograms", Appl. Phys. lett. **55** (1989), No. 6, 543–544.

[50] E. N. Leith and J. Upatnieks, "Reconstructed Wavefronts and Communication Theory", J. Opt. Soc. Am. **52** (1962), No. 10, 1123–1130.

[51] E. N. Leith and J. Upatnieks, "Wavefront Reconstruction With Diffused Illumination and Three-Dimensional Objects", J. Opt. Soc. Am. **54** (1964), No. 11, 1295–1301.

[52] E. N. Leith and J. Upatnieks, "Holographic Imagery Through Diffuse Media", J. Opt. Soc. Am. **56** (1966), No. 4, 523.

[53] G. R. Lemaitre and M. Wang, "Active Mirrors Warped Using Zernike Polynomials for Correcting Off-Axis Aberrations of Fixed Primary Mirrors - 1. Theory and Elasticity Design", Astron. Astrophys. Sippl. Ser. **114** (1995), 373–378.

[54] G. Lemelin, R. A. Lessard, and E. F. Borra, "An Investigation of Holographic Correctors For Astronomical Telescopes", Astronomy and Astrophysics **274** (1993), 983–992.

[55] W. W. Macy, Jr., "Two-Dimensional Fringe-Pattern Analysis", Appl. Opt. **22** (1983), No. 23, 3898–3901.

[56] V. N. Mahajan, "Aberration Theory Made Simple", Tutorial Texts in Optical Engineering, Vol. TT6, SPIE Optical Engineering Press, 1990.

[57] D. Malacara, "Optical Shop Testing (2nd Edition)", Wiley-Interscience, 1992.

[58] B. Martin, J. M. Hill, and R. Angel, "The New Ground-Based Optical Telescopes, ", Physics Today (1991), 22–30.

[59] C. R. Masson, "Seeing", Very High Angular Resolution Imaging (J. G. Robertson and W. J. Tango, eds.), Kluwer Academic, 1994, pp. 1–10.

[60] H. Masuda and K. Fukuda, "Ordered Metal Nanohole Arrays Made by a Two-Step Replication of Honeycomb Structures of Anodic Alumina", Science **268** (1995), 1466–1468.

[61] A. B. Meinel and M. P. Meinel, "Two-Stage Optics: High Acuity Performance From Low-Acuity Optical Systems", Opt. Eng. **31** (1992), No. 11, 2271–2281.

[62] G. Moretto et al., "Active Mirrors Warped Using Zernike Polynomials for Correcting Off-Axis Aberrations of Fixed Primary Mirrors - 2. Optical Testing and Performance Evaluation", Astron. Astrophys. Suppl. Ser. **114** (1995), 379–386.

[63] J. Munch and R. Wuerker, "Holographic Technique for Correcting Aberrations in a Telescope", Appl. Opt. **28** (1989), No. 7, 1312–1317.

[64] J. Munch, R. Wuerker, and L. Heflinger, "Wideband Holographic Correction of an Aberrated Telescope Objective", Appl. Opt. **29** (1990), No. 16, 2440–2445.

[65] J. Nelson, "The Keck Telescope", American Scientist **77** (1989), 170–176.

[66] J. B. Pawley (ed.), "Hanbook of Biological Confocal Microscopy", Plenum Press, 1990.

[67] D. H. Pearson and R. J. Tonucci, "Nanochannel Glass Replica Membranes", Science **270** (1995), 68–69.

[68] F. J. Pedrotti and L. S. Pedrotti, "Introduction To Optics (2nd Edition)", 2 ed., Prentice Hall, 1993.

[69] M. Pluta, Advances in Optical and Electron Microscopy, Vol. 10, 99–213, Academic Press, 1987, pp. 99–213.

[70] D. W. Pohl, Advances in Optical and Electron Microscopy, Vol. 12, 243–312, Academic Press, 1991, pp. 243–312.

[71] J. L. Rayces, "Exact Relation Between Wave Aberration and Ray Aberration", Opt. Acta **11** (1964), 85–88.

[72] C. Roddier and F. Roddier, "Interferogram Analysis Using Fourier Transform Techniques", Appl. Opt. **26** (1987), No. 9, 1668–1673.

[73] C. Roddier and F. Roddier, "Combined Approach to the Hubble Space Telescope Wave-Front Distortion Analysis", Appl. Opt. **32** (1993), No. 16, 2992–3008.

[74] F. Roddier, "Adaptive Optics: Performance and Limitations", Very High Angular Resolution Imaging (J.G. Robertson and W.J. Tango, eds.). Kluwer Academic, 1993, pp. 273–281.

[75] I. N. Ross, G. M. Davis, and D. Klemitz, "High-resolution Holographic Image Projection at Visible and Ultraviolet Wavelengths", Appl. Opt. **27** (1988), No. 5, 967–972.

[76] C. J. R. Sheppard, Advances in Optical and Electron Microscopy, Vol. 10, 1–98, Academic Press, 1987, pp. 1–98.

[77] Y. Shimizu and H. Takenaka, Advances in Optical and Electron Microscopy, Vol. 14, 249–334, Academic Press, 1994, pp. 249–334.

[78] R. J. Sica et al., "Lidar Measurements Taken With a Large-Aperture Liquid Mirror - 1. Rayleigh Scatter System", Appl. Opt. **34** (1995), No. 30, 6925–6936.

[79] E. S. Simova and M. Kavehrad, "Silver-Halide Sensitized Gelatin Derived From Agfa-Gevaert Holographic Plates", Appl. Opt. **33** (1994), No. 10, 1875–1879.

[80] H. J. Smith, "A Decade Of Cost-Reduction In Very Large Telescopes", Astrophysics and Space Science **160** (1989), 123–134.

[81] Y. Sun and M. G. Moharam, "Real-Time Image Transmission and Interferometry Through a Distorting Medium Using Two Phase Conjugators", Appl. Opt. **32** (1993), No. 11, 1954–1957.

[82] M. Takeda et al., "Fourier-Transform Method of Fringe-Pattern Analysis for Computer-Based Topography and Interferometry", J. Opt. Soc. Am. **72** (1982), No. 1, 156–160.

[83] R. J. Tonucci et al., "Nanochannel Array Glass", Science **258** (1992), 783–785.

[84] I. R. Tuohy, "Space Telescopes: an International Perspective", Proc. ASA **8** (1989), No. 1, 2–24.

[85] J. Upatnieks, A. Vander Lugt, and E. Leith, "Correction of Lens Aberrations by Means of Holograms", Applied Optics **5** (1966), No. 4, 589–593.

[86] J. Y. Wang and D. E. Silva, "Wave-front Interpretation with Zernike Polynomials", Appl. Opt. **19** (1980), No. 9, 1510–1518.

[87] A. A. Ward and L. Solymar, "Diffraction Efficiency Limitations of Holograms Recorded in Silver-Halide Emulsions", Appl. Opt. **28** (1989), No. 10, 1850–1855.

[88] B. M. Welsh, "Imaging Performance Analysis of Adaptive Optical Telescopes Using Laser Guide Stars", Appl. Opt. **30** (1991), No. 34, 5021–5030.

[89] J. P. Wetzel and S. W. Johnson, "Engineering Technologies For Lunar-Based Astronomy", Adv. Space Res. **14** (1994), No. 6, (6)253–(6)257.

[90] J. P. Woerdman, "Formation of a Transient Free Carrier Hologram in Si", Opt. Com. **2** (1970), No. 5, 212–214.

[91] L. Woltjer, "Large Ground-Based Telescopes", Frontiers of Space and Ground-Based Astronomy (W. Wamsteker et. al., ed.), Kluwer Academic, 1994, pp. 123–127.

[92] N.J. Woolf, "High Resolution Imaging From the Ground", Annual Review of Astronomy and Astrophysics, Annual Reviews, 1982, pp. 367–398.

[93] R. F. Wuerker and D. A. Hill, "Holographic Microscopy", Opt. Eng. **24** (1985), No. 3, 480–484.